PHOTODYNAMICS OF EXTENDED POLYATOMIC SYSTEMS

By

DEEPAK SRIVASTAVA

TO MY WIFE

ACKNOWLEDGEMENTS

TABLE OF CONTENTS

PHOTODYNAMICS OF EXTENDED POLYATOMIC SYSTEMS

by

DEEPAK SRIVASTAVA

December 1988

Chairman: Prof. David A. Micha
Major Department: Physics

A general time-dependent quantum mechanical approach to the interaction
of visible and UV light with extended polyatomic systems is presented in this
work. The interaction of light with a large polyatomic system is treated as a
two-step process: a photon absorption excites electronic transitions in the target
system, and this is followed by a dynamical evolution of the system on the excited
potential energy surface. Transition rates for photon-molecule interaction processes
are described in terms of time-correlation functions (TCF) of transition operators.
These are written as a product of TCFs of the target and of the light source. The
time evolutions in these two TCFs are carried out independently, and the statistical
properties of the light source are explicitly incorporated in the formalism. The
procedure is developed for resonance absorption-emission and for scattering of
thermal, chaotic and coherent light.

The time evolution in a large polyatomic system is treated within a molecular
TCF approach. For a general two-surface electronic excitation problem, a trans-
formation of these molecular TCFs from the real arguments to complex time is

described so that their computation by a numerical path-integral method become feasible. The complex time dependence in these TCFs is described by the dynamical evolution of an amplitude under the influence of a frequency operator. A time-dependent self-consistent field (TDSCF) approximation is used for large polyatomic system to factor the molecular TCFs into primary and secondary region TCFs. The primary and secondary regions are modeled by considering general primary motion coupled to many harmonic degrees of freedom in the secondary region. The strong coupling between the primary and the secondary regions has a general dependence on the variables of the primary region, whereas it has linear and bilinear terms in the variables of the secondary region. The weak coupling limit is considered by dropping the bilinear terms in the coupling. The complex time propagators for the secondary region dynamics for both of these cases are constructed analytically, while an efficient path-integral method is developed for the dynamics of the primary region.

As applications, the path-integral method for the primary region dynamics is used for computing the electronic absorption spectra of a model two-potential problem, and the TDSCF approach to the dynamics of large systems is used for studying the photodissociation dynamics of CH_3I from ground and excited vibrational states of the ground potential energy surface. The cross-sections for both of these cases are compared with other available works with good results. Extensions of the method to the other extended systems, with many degrees of freedom, and involving tunneling and barrier crossing in the primary region dynamics, are briefly discussed.

CHAPTER 1
INTRODUCTION

Theories of light absorption-emission, elastic and Raman scattering are described by time-dependent perturbation expressions in terms of transition dipole moments, and polarizability tensors [Kramers and Heisenberg, 25], respectively. The interaction of atoms and molecules with quantized radiation field was first introduced by Dirac [Dirac, 27]. Since then many developments have been made along the same lines and have included higher order corrections in these theories to increase accuracies [Herzberg, 50]. The basic approach of these developments is to concentrate on small atoms, accurately compute all of their eigenvalues and eigenstates, and use them in a summation according to the Fermi Golden Rule [Messiah, 62] for computing the total cross-section for the required photointeraction process. In case of polyatomics, using the Born-Oppenheimer approximation [Balint-Kurti, 75], the electronic part of the Schrodinger equation is first solved for fixed nuclear positions to obtain electronic potential energy surfaces; these are then used for the nuclear part of the problem. Given electronic potential energy surfaces for a small polyatomic system, one can still obtain all the low-lying vibrational and rotational eigenstates and eigenvalues to calculate cross-section. However, cross-sections processes which involve rearrangement in the molecule due to the absorption of light are not easily described by the method of summing over all the accessible quantum states of the system. This is mainly because one needs exact scattering wavefunctions of many channels in the excited state of the system, and the number of such available channels can be very large even for small polyatomics. Still, the time-

1

independent quantum mechanical method, based on summation over all the state to state information, and known as the stationary coupled channel (CC) approach, has been used successfully to produce total cross-sections for light-molecule interaction processes involving rearrangement in the target [Balint-Kurti and Shapiro, 81; Heather and Light, 83]. However, as the size of the system starts to increase, methods such as these involve a larger and larger number of available quantum states of the system, and therefore soon become too cumbersome to be of any practical use.

Alternatively, efforts have been made to change the approach from the time-independent quantum mechanical theories, which involve summations over all of the stationary states of the system, to the time-dependent quantum mechanical descriptions which are based on the dynamical evolution of the system from given initial conditions to the required final conditions [Lee and Heller, 79; Berens and Wilson, 81; Thirumalai and Berne, 83; Mukamel et al., 85; Srivastava and Micha, 87; Coalson, 87]. These methods do not require summations over all the states of the system, and therefore are better suited for dealing with large molecular systems. The basic feature of these approaches is to start from the expression for the total cross-section in the energy domain, use the Fourier transform definition of the energy conserving delta function to make a transformation to the time domain, and use the time-dependent Schrodinger equation for the dynamical evolution of the system between given initial and required final conditions. In recent years, many advances have been made in solving the time-dependent Schrodinger equation for nuclear vibrational and rotational motion with given initial conditions for an arbitrary general potential in many dimensions [Kosloff, 88 for a recent review]. They can be catagorized into the following broad groups: (a) semi-classical methods [Marcus, 72; Miller, 74; Mukamel and Jortner, 76; Micha, 83; Billing and Jolicard,

84; Gray and Child, 84; Henriksen, 85] are generally based on running classical trajectories for the nuclear motions, whereas the electronic transitions are treated quantum mechanically; (b) approximate quantum mechanical approaches based on wavepacket dynamics [Heller, 75, 81; Agrawal and Raff, 82; Mowrey and Kouri 85; Sawada and Metiu, 86], where the mean position and the spread of the wavepacket follow a canonical set of equations which are derived from a time-dependent variational principle [Heller, 81]; (c) straightforward integration of the time-dependent Schrodinger equation by discretizing the phase space and using a Fast Fourier Transform (FFT) algorithm [Feit, Fleck and Steiger, 82; Kosloff and Kosloff, 83; Hellsing, Nitzan and Metiu, 86; Kosloff, 88]; and (d) path integral approaches [Thirumalai and Berne, 83; Miller, Schwartz and Tromp, 83; Behrman et al., 83; Coalson, Freeman and Doll, 85] which provide complex time propagators between given initial and final positions in the coordinate space.

The present developments in the time-dependent descriptions still have the following problems which must be addressed.

1. By restricting the radiation field part of the interaction Hamiltonian to simple monochromatic circular wave forms, these approaches do not explicitly incorporate the statistical and dynamical properties of the light source in the formalism.

2. Semiclassical methods for solving the time-dependent Schrodinger equation are based on classical trajectories which do not sample the non-classical regions of the potential energy surfaces.

3. Approximate quantum mechanical techniques based on wavepacket dynamics require local quadratic forms for potentials, hence they exclude extensive delocalization of wavepackets.

4. The numerical path-integral methods, for a potential of arbitrary functional form, are not useful in the calculation of the required real time dynamics because of the oscillatory nature of the real time propagator.

5. Straightforward integration of the time-dependent Schrodinger equation by discretizing the phase space and using FFT for propagation are practical only for problems with few spatial dimensions.

The time-correlation function approach to thermodynamic and electromagnetic response properties of extended molecular systems is well known in statistical mechanics [Forster, 75; McQuarrie, 76; Lovesey, 80]. Recently, there have also been efforts to describe molecular processes occuring in a target following its collision with a projectile, using a collisional time-correlation function (TCF) approach [Micha, 77, 79, 81, 86]. Since, as before, this approach does not require summations over all the states of the target, it is useful in dealing with many degrees of freedom in extended molecular targets [Vilallonga and Micha, 87; Micha and Parra, 88]. In this work we present a formalism and applications of a time-dependent quantum mechanical approach to light-molecule interactions in large systems with the following desirable features.

1. We treat the radiation field and the molecular target of the interaction Hamiltonian on equal footing so that, at any stage in the formalism, explicit statistical and dynamical properties of the light source are easily incorporated.

2. Within a mean field approximation, we separate the degrees of freedom of an extended molecular system into a primary region (containing a few important degrees of freedom along which all significant dynamical events take place) and a secondary region (with all of the remaining degrees of freedom).

3. For a general potential of arbitrary functional form in the primary region, we use

a complex time path-integral method which can incorporate important quantum effects such as tunneling and barrier crossing in this region.

4. The computational efforts for the method do not increase quadratically with an increase in the range and the dimensionality of the potential.

In chapter 2 we describe transition rates for general light-molecule interaction processes in terms of the TCF of the Lippman-Schwinger $\hat{T}$ operator. In the dipole approximation to the light molecule interaction, the $\hat{T}$ operator is expanded into terms containing factors for the radiation field and the molecular target. The transition rates for all first order processes such as resonance absorption and emission are written in terms of the molecular dipole TCF of the target, and the electric field TCF of the light source. For all second order processes, such as multiphoton absorption-emission, elastic and Raman scattering, the transition rates are written in terms of the TCFs of the molecular polarizability tensors. The statistical properties of the light source are incorporated in the formalism, and specific cases of thermal, chaotic and coherent light are discussed.

In chapter 3 we introduce electronic potential energy surfaces by using the Born-Oppenheimer approximation to separate electronic and nuclear motions in a molecular target, and write a general molecular TCF in the electronic adiabatic representation. We describe a transformation from real to complex time of these TCFs, and discuss some of their general properties. The complex time dependence in the TCF, for a general light-molecule interaction process involving electronic transitions in the target, is shown to be equivalent to the dynamical evolution of an amplitude (equal to the initial eigenstate times the transition dipole) induced by a frequency operator (an operator depends upon the energy difference between the upper and the lower potential energy surfaces divided by $\hbar$).

In chapter 4 we describe the time evolution of the amplitude introduced in the previous chapter through a norm conserving time-dependent variational principle (TDVP). Considering fast and localized electronic tranisitions in a large molecular target, we use a time-dependent self-consistent field (TDSCF) approximation to factor the molecular dipole TCF of the target into self-consistent primary and secondary region TCFs.

In chapter 5 we describe time-dependent effective frequency operators for many intra- and intermolecular photointeraction processes by considering an arbitrary general motion in the primary region dynamics coupled linearly and bilinearly to many degrees of freedom in a secondary region dynamics undergoing harmonic motions. We show a direct relationship between our TDSCF approach and the phenomenological Generalised Langevin Equation (GLE) [Mori, 65] approach to the stochastic dynamics in large systems. We explicitly prove a Fluctuation-Dissipation Relationship (FDR) between the fluctuation force and the memory kernel in our TDSCF approach for linearly coupled primary and secondary region dynamics. We also develop the formalism for many degrees of freedom in the primary region dynamics coupled linearly and bilinearly to many harmonic degrees of freedom in the secondary region dynamics.

In chapter 6, we describe details of an efficient path-integral method for the primary region dynamics. Using a discretized coordinate space, the computational method does not depend upon any specific functional form of the primary region potential and also avoids problems of other methods which scale quadratically with respect to the range and the dimensionality of the potential.

In chapter 7 we describe applications and results of the TCF approach to the interaction of visible and UV light with extended molecular systems. We first de-

scribe an application to the electronic absorption spectra of a model one-dimensional problem for two-potential energy surfaces. The complex time computations for the TCF in a single spatial dimension, using the complex time numerical path-integral method, are performed so as to provide a check of the accuracy of the numerical method for the primary region dynamics. We study the photodissociation dynamics of a realistic polyatomic system (CH_3I) in an electronically excited state within a TDSCF approximation by factoring the TCF for the process into self-consistent primary and secondary region TCFs. The resulting total TCF has been used to compute the total cross-sections for the photodissociation of CH_3I, which are then compared with results from other methods with good results. We have also extended the method to the computations of total cross-sections for many vibrationally excited states of CH_3I on the ground potential energy surface.

Finally, in chapter 8 we discuss advantages and distinctive features of our approach and mention possibilities for further improvements and future extensions of our work.

CHAPTER 2
COLLISIONAL TIME-CORRELATION FUNCTION APPROACH
TO LIGHT-MOLECULE INTERACTIONS

We treat the interaction of light with a molecular system as a photon scattering

process through a collisional TCF approach [Srivastava and Micha, 87]. Starting

from the transition rates for a collision process in terms of the Lippmann-Schwinger

transition operator $\hat{T}$ [Messiah, 62] in section 2.1, we derive the transition rates

for the interaction of light with a molecular system in terms of the TCF of these

$\hat{T}$ operators. In the dipole approximation to the light-molecule interaction, the

$\hat{T}$ operator is written as an expansion with terms containing radiation field and

molecular system factors. For first order processes such as resonance absorption and

emission, transition rates are derived in terms of molecular dipole TCF of the target

and the electric field dipole TCF of the light source. For second order processes

such as elastic and inelastic (Raman) scattering due to polarization fluctuations in

the target, transition rates are written in terms of the polarizability tensor TCFs

of the molecular system and the polarizability tensor TCFs of the light source.

In section 2.2 we treat the interaction of molecules with thermal light, which

is given in the photon number representation by a Bose-Einstein distribution of

the initial number of photons in a particular mode. Section 2.3 considers the

interaction of a molecule with a single mode laser. The laser light source is treated

by considering the radiation field to be in the coherent state representation. The first

order transition rates for laser-molecule interaction processes are derived when a)

the laser is operating below the threshold (chaotic light with a poisson distribution

8

for the mean number of photons), and b) the laser is operating above the threshold (coherent light with a statistical distribution for the phase and the mean number of photons given by the experimental conditions).

2.1. Transition Rates from Time-Correlation Functions

We consider the interaction of visible and UV light with a molecular system. The treatment is general so that the molecular system can be as large as a protein molecule, a polymer chain, an adsorbate on a surface, or a solid surface. We denote with $\hat{H}_M$, $\hat{H}_R$, and $\hat{H}_I$ the Hamiltonians of the molecular system, the radiation field, and their interaction, respectively. The total Hamiltonian is expressed as

$$\hat{H} = \hat{H}_M + \hat{H}_R + \hat{H}_I. \tag{2.1}$$

Eigenstates $| j \rangle$ and $| r \rangle$, corresponding to the noninteracting molecular system Hamiltonian $\hat{H}_M$ and the radiation field Hamiltonian $\hat{H}_R$, respectively, are given by

$$\hat{H}_M|j\rangle = E_j|j\rangle$$
$$\hat{H}_R|r\rangle = E_r|r\rangle. \tag{2.2}$$

We treat the interaction of light with a molecular system as photon scattering, during which the radiation field goes from an initial state $| r \rangle$ to a final state $| r\prime \rangle$. Later on we shall describe various processes like absorption or Raman scattering by specifying $| r \rangle$ and $| r\prime \rangle$. Transition operators $\hat{T}^+$ describing the scattering satisfy the Lippmann-Schwinger equation [Messiah, 62]

$$\hat{T}^+ = \hat{H}_I + \hat{H}_I \frac{1}{E + i\epsilon - \hat{H}_M - \hat{H}_R}\hat{T}^+, \tag{2.3}$$

where $\epsilon \to 0$ is a limit to be taken after matrix elements of these operators have been calculated. Rates of transition R, averaged over the statistical distribution w_j

of the initial target states, w_r of the initial radiation states, and summed over final states of the target and the radiation, $|j'\rangle$ and $|r'\rangle$, respectively, are expressed as

$$R = \frac{2\pi}{\hbar} \sum_{jj'} w_j \sum_{rr'} w_r |\langle r'j'| \hat{T}^+ |rj\rangle|^2 \delta(E - E') \qquad (2.4)$$

where $E = E_r + E_j$ is the total energy, and the Dirac δ function imposes energy conservation. By using the Fourier transform of the $\delta-$ function

$$\delta(E - E') = \frac{1}{2\pi\hbar} \int_{-\infty}^{+\infty} e^{\frac{i}{\hbar}(E-E')t} \, dt, \qquad (2.5)$$

and the completeness relation

$$\sum_{j'} \sum_{r'} |j'r'\rangle \langle j'r'| = 1, \qquad (2.6)$$

Eq.(2.3) can be written as [Micha, 81]

$$R = \frac{1}{\hbar} \int_{-\infty}^{+\infty} dt \; \langle\langle \hat{T}^+(t)^\dagger \hat{T}^+(0) \rangle\rangle_{M,R} \qquad (2.7)$$

where the time-dependence in the $\hat{T}^+$ is given by

$$\hat{T}^+ = \exp\left(-\frac{i}{\hbar}\hat{H}_0 t\right) \hat{T}^+ \exp\left(+\frac{i}{\hbar}\hat{H}_0 t\right) \qquad (2.8)$$

and $\hat{H}_0 = \hat{H}_M + \hat{H}_R$, is the total Hamiltonian for the molecular system and the radiation field without interaction. The double bracket $\ll \dots \gg_{M,R}$ indicates the quantal average over the initial state $|j\rangle$ of the molecular system with a statistical distribution w_j, and over the initial state $|r\rangle$ of the radiation field with a statistical distribution w_r. So far we have not specified the interaction or the coupling Hamiltonian $\hat{H}_I$. Treating the interaction Hamiltonian in the electric dipole approximation,

$$\hat{H}_I = -\vec{E}.\vec{D} \qquad (2.9)$$

where $\vec{D}$ is the dipole vector of the molecular system, and $\vec{E}$ is the electric field vector of the light source. The transition operator $\hat{T}$ of Eq.(2.2) is written up to the second order, with an implicit + sign, as

$$\hat{T} = -\sum_{\xi} \hat{E}_{\xi}\hat{D}_{\xi} + \sum_{\eta\zeta} \hat{E}_{\eta}\hat{D}_{\eta} \frac{1}{E + i\epsilon - \hat{H}_M - \hat{H}_R}\hat{E}_{\zeta}\hat{D}_{\zeta} \qquad (2.10)$$

where (ξ, η, ζ) = (x, y, z), and the time-dependence of the $\hat{T}$ operator is given by Eq.(2.8). Since $\hat{H}_M$ and $\hat{H}_R$ commute with each other, it is straightforward to take matrix elements of the first term in Eq.(2.10) and to separate them into radiation field and molecular system factors. In the second term we use the following expression

$$\frac{1}{a + b} = \frac{1}{\pi} \int_{-\infty}^{+\infty} d\lambda \, \frac{a}{a^2 + \lambda^2} \frac{b}{b^2 + \lambda^2} \, , \qquad (2.11)$$

valid also for complex values of a and b to write

$$\frac{1}{E + i\epsilon - \hat{H}_M - \hat{H}_R} = \frac{i\hbar}{\pi} \int_{-\infty}^{+\infty} du \, \frac{\hat{M}_M}{\hat{M}_M^2 - \hbar^2 u^2} \frac{\hat{M}_R}{\hat{M}_R^2 - \hbar^2 u^2} \qquad (2.12)$$

where

$$\hat{M}_M = E^M + i\epsilon^M - \hat{H}_M \qquad (2.13a)$$

$$\hat{M}_R = E^R + i\epsilon^M - \hat{H}_R \qquad (2.13b)$$

$$E = E^M + E^R \qquad (2.13c)$$

$$\epsilon = \epsilon^M + \epsilon^R \, , \qquad (2.13d)$$

and we have replaced $\lambda = i\hbar u$. Using these expressions in the second term of Eq.(2.10), to factor it into a radiation field part and a molecular system part, and the result in Eq.(2.6), we write the transition rates R up to the second order as

$$R = \sum_{\xi\xi'} \int_{-\infty}^{+\infty} dt \; \langle\langle \hat{D}_{\xi'}^{\dagger}(t)\hat{D}_{\xi}(0)\rangle\rangle_M \; \langle\langle \hat{E}_{\xi'}^{\dagger}(t)\hat{E}_{\xi}(0)\rangle\rangle_R$$

$$- \frac{i\hbar}{\pi} \sum_{\xi'} \sum_{\eta\zeta} \int_{-\infty}^{+\infty} du \int_{-\infty}^{+\infty} dt \; \langle\langle \hat{D}_{\xi'}^{\dagger}(t)\hat{\chi}_{\eta\zeta}(u,0)\rangle\rangle_M$$

$$\langle\langle \hat{E}_{\xi'}^{\dagger}(t)\hat{\phi}_{\eta\zeta}(u,0)\rangle\rangle_R$$

$$- \frac{i\hbar}{\pi} \sum_{\xi'} \sum_{\eta\zeta} \int_{-\infty}^{+\infty} du' \int_{-\infty}^{+\infty} dt \; \langle\langle \hat{\chi}_{\eta'\zeta'}^{\dagger}(u',t)\hat{D}_{\xi}(0)\rangle\rangle_M \qquad (2.14)$$

$$\langle\langle \hat{\phi}_{\eta'\zeta'}^{\dagger}(u',t)\hat{E}_{\xi}(0)\rangle\rangle_R$$

$$+ \frac{\hbar^2}{\pi^2} \sum_{\eta\zeta} \sum_{\eta'\zeta'} \int_{-\infty}^{+\infty} du \int_{-\infty}^{+\infty} du' \int_{-\infty}^{+\infty} dt$$

$$\langle\langle \hat{\chi}_{\eta'\zeta'}^{\dagger}(u',t)\hat{\chi}_{\eta\zeta}(u,0)\rangle\rangle_M$$

$$\langle\langle \hat{\phi}_{\eta'\zeta'}^{\dagger}(u',t)\hat{\phi}_{\eta\zeta}(u,0)\rangle\rangle_R$$

where the polarizability tensor operator for the molecular system is defined by

$$\hat{\chi}_{\eta\zeta}(u,0) = \hat{D}_{\eta} \frac{\hat{M}_M}{\hat{M}_M^2 - \hbar^2 u^2} \hat{D}_{\zeta} \qquad (2.15a)$$

the polarizability tensor operator for the radiation field is defined by

$$\hat{\phi}_{\eta\zeta}(u,0) = \hat{E}_{\eta} \frac{\hat{M}_R}{\hat{M}_R^2 - \hbar^2 u^2} \hat{E}_{\zeta} \quad , \qquad (2.15b)$$

and the time-dependence in these operators are given for example by

$$\hat{\chi}_{\eta\zeta}(u,t) = e^{-\frac{i}{\hbar}\hat{H}_M t} \hat{\chi}_{\eta\zeta}(u,0) \; e^{+\frac{i}{\hbar}\hat{H}_M t} \qquad (2.16)$$

The expression for R has four terms, each of them corresponding to different photointeraction processes. The first term describes first order processes such as resonance dipolar absorption and emission of light. The second and the third terms are cross-terms the contribution of which will depend upon the statistical properties

of the light source used in the experiment. For thermal light in the photon number representation, they become zero and do not contribute to the overall transition rates. In the later sections, we shall, however, see that the contribution of these terms cannot be ignored if the light source used is a coherent light. The fourth term describes second order processes such as elastic and Raman scattering mediated by polarization fluctuations in the target.

The transition rates R expressed in Eq.(2.14), as opposed to the standard expressions [Dirac, 47; Heitler, 54], are specially useful for the treatment of light-molecule interactions in large systems because they do not involve summations over excited states of the molecular system. Furthermore, Eq.(2.10), which is used to separate in the transition operator the radiation field and molecular system variables, can also be used to derive a similar separation of the transition operator to order higher than the second. Thus, a similar formulation of the transition rates for higher order photointeraction processes can be systematically derived.

Lastly, the main purpose of separating the TCF of the $\hat{T}$ operator into the TCF of the radiation field and the TCF of the molecular system is to uncouple the time evolution of the molecular system from that of the radiation field. This has a twofold advantage: firstly, one can use time-dependent quantum mechanical techniques to describe the time evolution of the molecular system without referring to the time evolution of the radiation field, and secondly, we can easily incorporate the statistical properties of the light source into the dynamics.

2.2. Radiation Field TCFs For Thermal Light

When the light source is maintained at a temperature T, it is described by the Bose-Einstein statistical distribution function $W_s(\omega_s, T)$, of the number of photons

in a mode s with energy $\hbar\omega_s$. Then it is easier to work in the photon number representation of the radiation field. The electric field operator in Eq.(2.14) is decomposed as

$$\hat{E}_\xi(t) = \hat{E}_\xi^{(+)}(t) + \hat{E}_\xi^{(-)}(t) \tag{2.17}$$

where

$$\hat{E}_\xi^{(+)}(t) = i \sum_{\vec{k}} \left(\frac{\hbar\omega_{\vec{k}}}{2\epsilon_0 V} \right)^{\frac{1}{2}} \epsilon_\xi \, \hat{a}_{\vec{k}\xi} e^{-i\omega_{\vec{k}} t} \tag{2.18}$$

and

$$\hat{E}_\xi^{(-)}(t) = \left(\hat{E}_\xi^{(+)}(t) \right)^\dagger \tag{2.19}$$

where $\vec{k}$ is the photon wavevector, ϵ_ξ is the ξ component of the polarization vector, and $\hat{a}_{\vec{k}\xi}$ the annihilation operator of a photon of energy $\hbar\omega_{\vec{k}} = \hbar kc$ and polarization ξ. In the photon number representation, a general radiation field state with several modes s is written as $|\{(\vec{k}_s\xi_s)^{N_s}\}\rangle$ where N_s is the number of photons in mode s; then

$$\hat{E}_\xi^{(+)}(t) \, |\{(\vec{k}_s\xi_s)^{N_s}\}\rangle = i \sum_{\vec{k}_s} \left(\frac{\hbar\omega_{\vec{k}_s}}{2\epsilon_0 V} \right)^{\frac{1}{2}} \epsilon_\xi \, \delta_{\xi\xi_s}$$
$$e^{-i\omega_{\vec{k}_s} t} N_s \, |\{...(\vec{k}_s\xi_s)^{N_s-1}...\}\rangle \tag{2.20}$$

Using Eqs.(2.17–2.20) in Eq.(2.14), one can write the transition rates for first and second order processes. In the photon number representation, the second and third terms of Eq.(2.14) do not contribute, because they do not conserve the number of photons in the initial and the final radiation state. Therefore the transition rate is written as

$$R = R_{11} + R_{22} \tag{2.21}$$

where R_{11} is the transition rate for the first order processes, in which a single electric field operator at an initial time $t = 0$, is correlated to its adjoint at a later time t. Similarly, R_{22} is the transition rate for second order processes, where the time-dependent polarization tensor operator, $\hat{\phi}_{\eta\zeta}(u, 0)$, which is second order in the electric field operators of Eq.(2.17), is correlated to its adjoint at a later time t. In the same notation R_{12} and R_{21} are the cross-terms, the contributions of which are zero in the photon number representation. The transition rates R_{11} for first order processes are given by

$$R_{11} = \sum_{\xi\xi'} \int\limits_{-\infty}^{+\infty} dt \ f_{\xi\xi'}^M(t) \ f_{\xi\xi'}^R(t) \ , \tag{2.22}$$

where

$$f_{\xi\xi'}^M(t) = \left\langle \left\langle \hat{D}_{\xi'}(t)^\dagger \, \hat{D}_\xi(0) \right\rangle \right\rangle_M \tag{2.23}$$

is the molecular dipole TCF of the extended system, and

$$f_{\xi\xi'}^R(t) = \left\langle \left\langle \hat{E}_{\xi'}^{(-)}(t) \, \hat{E}_\xi^{(+)}(0) \right\rangle \right\rangle_R + \left\langle \left\langle \hat{E}_{\xi'}^{(+)}(t) \, \hat{E}_\xi^{(-)}(0) \right\rangle \right\rangle_R \tag{2.24}$$

is the electric field TCF of the light source. The first term in Eq.(2.24) corresponds to resonance absorption, whereas the second term corresponds to spontaneous and stimulated emissions. Other cross-terms in R_{11} do not contribute because they do not conserve the number of photons. Using Eqs.(2.18–2.20) in the above equation we write

$$f_{\xi\xi'}^{R}(t) = \frac{\hbar}{2\epsilon_0 V} \, \epsilon_\xi^2 \delta_{\xi\xi'} \sum_s \sum_{\vec{k}_s} W_s [N_s \omega_{\vec{k}_s} e^{i\omega_{\vec{k}_s} t}$$
$$+ (N_s + 1) \omega_{\vec{k}_s} e^{-i\omega_{\vec{k}_s} t}] \qquad (2.25)$$

and the transition rate R_{11} is given by

$$R_{11} = \frac{\hbar}{2\epsilon_0 V} \, \sum_s W_s \sum_{\vec{k}_s} \sum_\xi \epsilon_\xi^2 \omega_{\vec{k}_s} \int\limits_0^\infty dt \, [N_s \cos(\omega_{\vec{k}_s} t) \qquad (2.26)$$
$$2Re\langle\langle \hat{D}_\xi(t)^\dagger \, \hat{D}_\xi(0)\rangle\rangle_M + Re\{e^{-i\omega_{\vec{k}_s} t} \langle\langle \hat{D}_\xi(t)^\dagger \, \hat{D}_\xi(0)\rangle\rangle_M\}]$$

where the statistical probability distribution function for a thermal light W_s is the Bose-Einstein distribution for N_s photons with wavevector $\vec{k}_s$ and frequency $\omega_{\vec{k}_s}$, and the summation in Eq.(2.26) over the number of photons can be carried out analytically. We have also used in Eq.(2.26); $\langle\langle \hat{D}_\xi^+(-t)\hat{D}_\xi(0)\rangle\rangle_M = \langle\langle \hat{D}_\xi^+(t)\hat{D}_\xi(0)\rangle\rangle^*$, to ensure that the transition rate R_{11} remains real. For the second order processes, we write the transition rates R_{22} as

$$R_{22} = \frac{\hbar^2}{\pi^2} \sum_{\eta\zeta} \sum_{\eta'\zeta'} \int\limits_{-\infty}^{+\infty} du' \int\limits_{-\infty}^{+\infty} du \int\limits_{-\infty}^{+\infty} dt$$
$$f_{\eta'\zeta'\eta\zeta}^{M}(u',u,t) \quad f_{\eta'\zeta'\eta\zeta}^{R}(u',u,t) \qquad (2.27)$$

where

$$f_{\eta'\zeta'\eta\zeta}^{M}(u',u,t) = \left\langle \left\langle \hat{x}_{\eta'\zeta'}(u',t)^\dagger \, \hat{x}_{\eta\zeta}(u,0) \right\rangle \right\rangle_M \qquad (2.28)$$

is the molecular polarizability tensor TCF of the target, and

$$f_{\eta'\zeta'\eta\zeta}^{R}(u',u,t) = \left\langle \left\langle \hat{\phi}_{\eta'\zeta'}(u',t)^\dagger \, \hat{\phi}_{\eta\zeta}(u,0) \right\rangle \right\rangle_R \qquad (2.29)$$

is the electric field polarizability tensor TCF of the light source. Using Eqs.(2.17–2.20) in Eq.(2.29), the electric field polarizability tensor TCF of the light source can also be further decomposed into terms representing elastic and Raman scattering [Appendix A]. These terms when substituted back in Eq.(2.27), will give transition rates for second order processes when thermal light is interacting with a large molecular system.

Equations (2.22) and (2.27) for the transition rates R_{11} and R_{22} are computationally useful, because they do not involve the summations over the excited states of the target, and the corresponding molecular TCF can be evaluated by time-dependent techniques.

2.3. Radiation Field TCFs For Laser Light

When the light source is a laser, the statistical distribution of its electric field factorizes into a distribution for the electric field amplitude, times a distribution for its phase [Louisell, 73; Sargent, Scully and Lamb, 74; Loudon, 83]. If the laser is operated below the threshold for coherent emission, the amplitude fluctuations of a given mode, which are proportional to the mean number of photons in that mode, have an exponentially decaying distribution about the most probable amplitude (which occurs at zero), whereas fluctuations in the phase, caused by spontaneous emissions, are quite large and therefore the phase can have any value between 0 and 2π. If the laser is operated above the threshold, both the amplitude and the phase have sharply peaked distribution about their most probable values, which are given by experimental conditions. For such a light source it is necessary to include in the description the statistical distributions of both the amplitude and the phase of the electric field, and it is advantageous to work in the coherent state representation

[Klauder and Sudarshan, 68; Loudon, 83]. A general radiation state in the coherent state representation is written as $|\{\alpha_s\}\rangle$, with $\hat{a}_{\vec{k}\xi}|\{\alpha_s\}\rangle = \alpha_s |\{\alpha_s\}\rangle \delta_{\xi\xi}$, where the eigenvalue α_s is a complex number whose square modulus gives the mean number of photons in the s mode of the laser. Using equations (2.17–2.20) for the creation and annihilation terms of the electric field operator, and using a single mode coherent states $|\alpha_s\rangle$, we write

$$\hat{E}_\xi^{(+)}(t)|\alpha_s\rangle = i\left(\frac{\hbar\omega_{\vec{k}_s}}{2\epsilon_0 V}\right)^{\frac{1}{2}} \epsilon_\xi\, \delta_{\xi\xi}\, e^{-i\omega_{\vec{k}_s}t}\alpha_s|\alpha_s\rangle \qquad (2.30)$$

The radiation field TCF of Eq.(2.22), in the coherent state representation, can be written as

$$f_{\xi'\xi}^R(t) = \left\langle\left\langle \hat{E}_{\xi'}^{(-)}(t)\,\hat{E}_\xi^{(+)}(0)\right\rangle\right\rangle_R + \left\langle\left\langle \hat{E}_{\xi'}^{(+)}(t)\,\hat{E}_\xi^{(-)}(0)\right\rangle\right\rangle_R$$
$$+ \left\langle\left\langle \hat{E}_{\xi'}^{(-)}(t)\,\hat{E}_\xi^{(-)}(0)\right\rangle\right\rangle_R + \left\langle\left\langle \hat{E}_{\xi'}^{(+)}(t)\,\hat{E}_\xi^{(+)}(0)\right\rangle\right\rangle_R \qquad (2.31)$$

Unlike $f_{\xi'\xi}^R(t)$ in the photon number representation, cross-terms in Eq.(2.31) are not zero, because we do not need to conserve the number of photons in the initial and the final radiation states $|r\rangle$ and $|r'\rangle$, respectively. As we shall see very shortly, however, it is still possible to have a laser in which the statistical distribution of the phase is such that it again can make the contributions of these cross-terms equal to zero. Using equations (2.18), (2.19) and (2.30) in Eq.(2.31), we write $f_{\xi'\xi}^R(t)$ in a single mode coherent state representation as

$$f_{\xi\xi'}^R(t) = \frac{\hbar\omega_{\vec{k}_s}}{2\epsilon_0 V}\, \epsilon_\xi^2\, \delta_{\xi\xi'} \int d^2\alpha_s P(\alpha_s)$$
$$\times\, [-\alpha_s^2\, e^{-i\omega_{\vec{k}_s}t} + (|\alpha_s^2| + 1)e^{-i\omega_{\vec{k}_s}t}$$
$$+ |\alpha_s^2|e^{+i\omega_{\vec{k}_s}t} - \alpha_s^{*2}\, e^{+i\omega_{\vec{k}_s}t}] \qquad (2.32)$$

where $P(\alpha_s)$, a real statistical weight for the complex amplitude α_s, is given by experimental conditions. The two dimensional integral $\int d^2\alpha_s[...]$ extends over the entire complex plane of α_s. Light sources of experimental significance have different statistical weights $P(\alpha_s)$. In the first and the fourth terms of Eq.(2.32), we have checked that the statistical averages of α_s^2, and $\alpha_s^{*^2}$ are real for several weight factors $P(\alpha_s)$ given in the literature [Schubert and Wilhelmi, 86]. Therefore, the radiation field TCF $f_{\xi\xi'}^R(t)$ in Eq.(2.32) satisfies the relation $f_{\xi\xi'}^R(t)^* = f_{\xi\xi'}^R(-t)$, and hence, the resulting transition rates of experimental significance, are real from Eq.(2.32). As examples of laser sources, with given statistical weights, we consider the radiation field TCFs for chaotic and coherent light. To compare Eq.(2.32) with the equivalant expression in the photon number representation in Eq.(2.25), we have first considered the case of chaotic light, which is the same as that of a laser operating below the threshold. In this case the phase of the light source is randomly distributed between 0 and 2π, therefore the weight factor $P(\alpha_s)$ does not depend on the phase of α_s, and hence, the contributions from the first and the fourth terms of the integrand in Eq.(2.32) are zero. Thus, below the threshold $f_{\xi\xi'}^R(t)$ takes a simpler form

$$f_{\xi'\xi}^R(t) = \frac{\hbar\omega_{\vec{k}_s}}{2\epsilon_0 V}\epsilon_\xi^2 \delta_{\xi\xi'}[\langle N_s\rangle e^{i\omega_{\vec{k}_s}t} + (\langle N_s\rangle + 1)e^{-i\omega_{\vec{k}_s}t}] \qquad (2.33)$$

which agrees with Eq.(2.25) for a single mode, insofar as the average is

$$\langle N_s\rangle = \int\limits_0^\infty d|\alpha_s| \ |\alpha_s|^3 \ P(|\alpha_s|) \qquad (2.34)$$

Substituting Eqs.(2.32) and (2.33) in Eq.(2.21), we can write the first order transition rate R_{11} for the interaction of a single mode laser with a molecular system, when the laser is operating below the threshold, as

$$
R_{11}^{chaotic} = \frac{\omega_{\vec{k}_s}}{\hbar\epsilon_0 V} \sum_\xi \epsilon_\xi^2 \int\limits_0^\infty dt [\langle N_s \rangle \cos(\omega_{\vec{k}_s}t)
$$
$$
\times 2Re(\langle \langle \hat{D}_\xi(t)^\dagger \hat{D}_\xi(0) \rangle \rangle_M) \qquad (2.35)
$$
$$
Re(e^{-i\omega_{\vec{k}_s}t} \langle \langle \hat{D}_\xi(t)^\dagger \hat{D}_\xi(0) \rangle \rangle_M)]
$$

If the laser is operating above the threshold, the rate of transition involves instead the statistical distribution $P(\alpha_s)$, which depends on the amplitude $\mid \alpha_s \mid$, as well on the phase $\varphi_s = Arg(\alpha_s)$, and is given by

$$
R_{11}^{Coherent} = \frac{\omega_{\vec{k}_s}}{2\hbar\epsilon_0 V} \sum_\xi \epsilon_\xi^2 \int\limits_{-\infty}^{+\infty} dt \int d^2\alpha_s \ P(\alpha_s)
$$
$$
\times [2|\alpha_s|^2 \{\cos(\omega_{\vec{k}_s}t)\} - \cos(\omega_{\vec{k}_s}t - 2\varphi_s)
$$
$$
\times \langle \langle \hat{D}_\xi(t)^\dagger \hat{D}_\xi(0) \rangle \rangle_M \qquad (2.36)
$$
$$
+ e^{-i\omega_{\vec{k}_s}t} \langle \langle \hat{D}_\xi(t)^\dagger \hat{D}_\xi(0) \rangle \rangle_M]
$$

This can be rewritten as

$$
R_{11}^{Coherent} = R_{11}^{Chaotic} - \frac{2\omega_{\vec{k}_s}}{2\epsilon_0 V} \sum_\xi \epsilon_\xi^2 \int\limits_0^\infty dt
$$
$$
\times [A_s \cos(\omega_{\vec{k}_s}t)Re\{\langle \langle \hat{D}_\xi(t)^\dagger \hat{D}_\xi(0) \rangle \rangle_M\} \qquad (2.37a)
$$
$$
+ iB_s \sin(\omega_{\vec{k}_s}t)Im\{\langle \langle \hat{D}_\xi(t)^\dagger \hat{D}_\xi(0) \rangle \rangle_M\}]
$$

with

$$A_s = \int d^2\alpha_s \ P(\alpha_s) |\alpha_s|^2 \cos(2\varphi_s) \qquad (2.37b)$$

$$B_s = \int d^2\alpha_s \ P(\alpha_s) |\alpha_s|^2 \sin(2\varphi_s) \qquad (2.37c)$$

showing an additional rate due to coherence. The term containing B_s can be shown to be zero for statistical distributions of experimental interests [Schubert and Wilhelmi, 86].

CHAPTER 3
MOLECULAR TCFs IN THE
ELECTRONIC ADIABATIC REPRESENTATION

In the previous chapter, transition rates for all first and second order pho-
tointeraction processes are expressed as integrals over time of the product of the
molecular TCFs of the target and the radiation field TCFs of the light source. The
time-dependence in the radiation field TCFs is expressed for many physically in-
teresting light sources in terms of exponentials, oscillating with the frequency of
the light source used. Therefore, most of the transition rates are finally written as
the Fourier transforms of the molecular TCFs of the target. In this chapter, we
describe general features of these molecular TCFs and their Fourier transforms.
Indeed, the task of a general formalism should normally include describing a light
source within a frequency range that extends from the far infrared region on one
side, to the ultravoilet region on the other. A complete discussion of such an ex-
tended frequency range, however, is beyond the scope of this work, and we will
describe mainly the interaction of visible or UV light with large molecular systems.
As shown in table 3–1, the light source in this frequency range excites nuclear
vibrations, accompanied by electronic transitions between different states of the
system [McQuarrie, 83]. Thus, our work involves mainly the electronic excitations
of the molecular system, followed by a time-dependent evolution according to the
upper potential energy surface, which in some cases can also cause the dissociation
of the system. We have also considered nuclear motions in the ground electronic
state, which occur generally when the molecule is in a thermal bath.

22

Table 3–1
The Electromagnetic Spectrum And The Corresponding Molecular Processes

Region	Wave # (/cm)	Process
Microwave	0.033 - 3.300	Rotations of Polyatomic Molecules
Far Infrared	3.30 -330	Rotations of small molecules
Infrared	330 - 3300	Vibrations of flexible bonds
Visible and Ultravoilet	3300 - 330000	Electronic transitions with vibrations of flexible bonds

[From, "Quantum Chemistry" by D. A. McQuarrie; 83, pp.438]

In section 3.1, we introduce electronic potential energy surfaces for the motion of the nuclei, and write a general molecular TCF of the target in the adiabatic representation. Due to the difficulty involved in computing a real time propagator with realistic potential energy surfaces, we describe a transformation to complex time TCFs in section 3.2. Section 3.3 discusses general features of these complex time TCFs, and writes them in a form which is used in the later part of this work.

3.1. Electronic Adiabatic Representation for Molecular TCFs

We consider the evaluation of a general positive time TCF for two different operators $\hat{A}$ and $\hat{B}$. In case of the first order processes, they are the molecular transition dipole operators, and in case of the second order processes such as elastic and Raman scattering, they become the molecular polarizability tensor operators. A general positive time molecular TCF for operators $\hat{A}$ and $\hat{B}$ is written as

$$f_{\hat{A}\hat{B}}(t) = \left\langle \left\langle \hat{A}(t)^{\dagger} \hat{B}(0) \right\rangle \right\rangle_M \qquad (3.1)$$

where $\langle\!\langle ... \rangle\!\rangle_M$ is the quantal average over the probability distribution of the initial state of the molecular system, and the time-dependence in the operator $\hat{A}$ is given by

$$\hat{A}(t) = e^{-\frac{i}{\hbar}\hat{H}_M t}\hat{A}(0) \; e^{+\frac{i}{\hbar}\hat{H}_M t} \qquad (3.2)$$

Here $\hat{H}_M$ the total Hamiltonian for the extended molecular system involves the nuclear as well as the electronic motions in the system, and is written as

$$\hat{H}_M = -\sum_{n=1}^{3N-6} \frac{\hbar^2}{2M_n} \frac{\partial^2}{\partial R_n^2} - \sum_{i=1}^{s} \frac{\hbar^2}{2m} \frac{\partial^2}{\partial r_i^2} + V(\mathbf{r}, \mathbf{R}) \qquad (3.3)$$

with $\mathbf{r} = (r_1, r_2, r_3, ...)$ is a set of s generalized coordinates for the motion of electrons, and $\mathbf{R} = (R_1, R_2, R_3, ...)$ is a set of $3N-6$ generalized coordinates for the vibrational motions of the nuclei. We use the Born-Oppenheimer approximation to separate the electronic and nuclear motions in the target. The description is suitable for the ground and first few electronically excited states of the target, where such a separation in the electronic and nuclear motion generally yields reasonably good results. In the Born-Oppenheimer approximation [Balint-Kurti, 75] the electronic

wave functions are the solutions of the following equations

$$[-\sum_{i=1}^{s} \frac{\hbar^2}{2m} \frac{\partial^2}{\partial r_i^2} + V(\mathbf{r}, \mathbf{R})] \, \phi_j(\mathbf{r}, \mathbf{R}) = E_j(\mathbf{R}) \, \phi_j(\mathbf{r}, \mathbf{R}) \tag{3.4}$$

This equation is parametric in the nuclear variables $\mathbf{R}$, and $\{E_j(\mathbf{R})\}$ is a set of electronic potential energy surfaces for the motion of the nuclei. The total initial wave function of the target is then written as

$$|\Psi_{Ii}(\mathbf{R})\rangle = \psi_I(\mathbf{R}) \, |\phi_i(\mathbf{R})\rangle \tag{3.5}$$

where $|\phi_i(\mathbf{R})\rangle$, the initial electronic state, depends parametrically on the nuclear variables $\mathbf{R}$, $|\psi_I\rangle$ is the nuclear vibrational wave function on the ith electronic potential energy surface, and the explicit dependence of the electronic wave functions $|\phi_i(\mathbf{R})\rangle$ over the electronic coordinates $\mathbf{r}$ is suppressed, because they are integrated out in the next step. Then, if W_I is the probability of finding the nuclear vibrational wave function in the vibrational state $|\psi_I\rangle$ of the ith electronic potential energy surface, the TCF $f_{\hat{A},\hat{B}}(t)$ as defined in Eq.(3.1) can be written as

$$f_{\hat{A},\hat{B}}(t) = \sum_{iI} W_I \, \langle \phi_i(\mathbf{R}) \mid \langle \psi_I \mid e^{+\frac{i}{\hbar}\hat{H}_M t}(\hat{A}) \\ e^{-\frac{i}{\hbar}\hat{H}_M t}(\hat{B}) \, |\psi_I\rangle |\phi_i(\mathbf{R})\rangle \tag{3.6}$$

Introducing a complete basis set in the coordinate representation

$$\sum_{jJ} |\mathbf{R}\rangle \langle \mathbf{R}|\psi_J\rangle |\phi_j(\mathbf{R})\rangle \langle \phi_j(\mathbf{R})|\langle \psi_J|\mathbf{R}\rangle \langle \mathbf{R}| = 1 \ , \tag{3.7}$$

and using the adiabatic approximation for electronic potential energy surfaces [Olson and Micha, 82] expressed as

$$\hat{H}_M|\phi_i(\mathbf{R})\rangle \approx |\phi_i(\mathbf{R})\rangle \, \mathcal{H}_i(\hat{\mathbf{R}}, \hat{\mathbf{P}}_\mathbf{R}) \tag{3.8}$$

we write Eq.(3.6) as

$$f_{\hat{A},\hat{B}}(t) = \sum_{ij} \sum_{I} W_I \int d\mathbf{R} \, \psi_I^\dagger(\mathbf{R}) \, e^{+\frac{i}{\hbar}\mathcal{H}_i(\hat{\mathbf{R}}, \hat{\mathbf{P}}_\mathbf{R})t} \, (\hat{A}(\mathbf{R}))_{ij} \\ e^{-\frac{i}{\hbar}\mathcal{H}_i(\hat{\mathbf{R}}, \hat{\mathbf{P}}_\mathbf{R})t} \, (\hat{B}(\mathbf{R}))_{ji} \, \psi_I(\mathbf{R}) \tag{3.9}$$

where $\mathcal{H}_i(\hat{\mathbf{R}}, \hat{\mathbf{P}}_{\mathbf{R}})$ is the Hamiltonian for the nuclear motion on the ith potential energy surface, and $\hat{\mathbf{P}}_{\mathbf{R}}$ is the set of the momentum operators conjugate to the operators in the set $\hat{\mathbf{R}}$. In the time-dependent formulation, we interpret the TCF $f_{\hat{A},\hat{B}}(t)$ in Eq.(3.9) as follows: at an initial time, $t' = 0$, the amplitude of the nuclear motion on the jth electronic surface is given by $(\hat{B})_{ji} \mid \psi_I \rangle$. At a later time, $t' > 0$, this amplitude propagates on the excited electronic surface with the nuclear Hamiltonian $\hat{\mathcal{H}}_j = \mathcal{H}_j(\hat{\mathbf{R}}, \hat{\mathbf{P}}_{\mathbf{R}})$. Finally, at the required time $t' = t$, the time evolved amplitude on the jth electronic surface is overlapped with the complex conjugate of $(\hat{A})_{ji} e^{(-i/\hbar \hat{\mathcal{H}}_i t)} \mid \psi_I \rangle$. In case the system has initially been prepared in a pure vibrational state $\mid \psi_I \rangle$ of the ith potential energy surface, the initial probability distribution function W_I becomes unity, and the TCF in Eq.(3.9) describes a general light-molecule interaction process involving two different electronic states i and j. If the system, however, is not initially in a pure state $\mid \psi_I \rangle$, then the finite temperature formalism, in which the initial state of the system has been prepared in a thermal equilibrium, can be introduced simply by selecting a suitable probability distribution function W_I. Such a probability distribution function is usually described by the Boltzmann distribution expressed as $W_I = \frac{e^{(-k_B \beta \mathcal{E}_I)}}{Z_\beta}$, where β is the inverse temperature, $k_B T$, at which the initial state of the system has been prepared, and $\mathcal{E}_I$, the stationary eigen state on the ith potential energy surface, is given by

$$\hat{\mathcal{H}}_i |\psi_I\rangle = \mathcal{E}_I |\psi_I\rangle \tag{3.10}$$

For a two surface problem using Eq.(3.10) in Eq.(3.9), the TCF $f_{\hat{A},\hat{B}}(t)$ is expressed in the following equivalent forms:

$$f_{\hat{A}\hat{B}}(t) = \frac{1}{Z_\beta} Tr[e^{+\frac{i}{\hbar}\widehat{\mathcal{H}}_i(t+i\beta\hbar)} \, (\hat{A})_{ij} \, e^{-\frac{i}{\hbar}\widehat{\mathcal{H}}_j t} \, (\hat{B})_{ij}] \qquad (3.11a)$$

$$= \frac{1}{Z_\beta} \int d\mathbf{R} \int d\mathbf{R}' \, \langle\mathbf{R}| \, e^{+\frac{i}{\hbar}\widehat{\mathcal{H}}_i(t+i\beta\hbar)} \, |\mathbf{R}'\rangle \, A(\mathbf{R}')$$

$$\langle\mathbf{R}'| \, e^{-\frac{i}{\hbar}\widehat{\mathcal{H}}_j t} \, |\mathbf{R}\rangle \, B(\mathbf{R}) \qquad (3.11b)$$

$$= \sum_I W_I \, e^{+\frac{i}{\hbar}\mathcal{E}_I t} \, \langle\psi_I| \, (\hat{A})_{ij} \, e^{-\frac{i}{\hbar}\widehat{\mathcal{H}}_j t} \, (\hat{B})_{ji} \, |\psi_I\rangle \qquad (3.11c)$$

where $\widehat{\mathcal{H}}_j = \mathcal{H}_j(\hat{\mathbf{R}}, \hat{\mathbf{P}}_\mathbf{R})$ is the nuclear Hamiltonian operator on the jth potential energy surface, and the $Tr[...]$ in Eq.(3.11a) is to be evaluated over the initial nuclear vibrational state $|\psi_I\rangle$ of the system. Equation (3.11b) rewrites this trace and all the operators in the coordinate representation, which is useful especially if the initial nuclear vibrational state of the system is not known, and the propagators on the ith and the jth electronic surfaces are not difficult to obtain. The form in Eq.(3.11c) is used when the initial nuclear vibrational state $|\psi_I\rangle$ and the corresponding stationary state eigenenergy $\mathcal{E}_I$ are not difficult to obtain by time-independent techniques, while the important effects, such as dissociation and rearrangement, are occuring due to the time-dependent dynamics on the excited surface.

Equations (3.11a), (3.11b), and (3.11c) present a general two-operator TCF in the adiabatic representation, where $(\hat{A})_{ij}$ and $(\hat{B})_{ji}$ are the transition moment operators between two different electronic states i and j. If the frequency range of the light source is in the infrared region, then it excites nuclear vibrations and rotations only on the ground electronic surface of the system. In our work, this corresponds to the case $j = i$, with i refering to the ground electronic state of the system. Transition moments $(\hat{A})_{ii}$ and $(\hat{B})_{ii}$ in this case become the net dipole, or the net polarization of the system in its ground electronic state, and the TCF as

expressed in Eq.(3.11a) acquires a symmetric form which can also be evaluated in our time-dependent formulation.

3.2. Complex Time TCFs and their Fourier Transforms

The usual route for computing the transition rates for various different light-molecule interaction processes that emerges from the discussion till now, is to first compute the time dependence in the TCF as defined in Eq.(3.11), and then take its Fourier transform to get the required transition rate. The route as suggested, however, is not very easy to follow for any physically interesting problem involving realistic potential energy surfaces. This is primarily due to the presence of a real time excited potential propagator in the expression for the TCF in Eqs.(3.11a, b, c). The form of this propagator is more apparent in Eq.(3.11b), where it is expressed in the coordinate representation. Computations of the matrix elements of a pure real time propagator, involving realistic potentials, is a very difficult problem in itself, so that to our knowledge, till now, there is no known numerical or analytical method that even tries to address this problem for a completely general potential. This is also the main reason that path-integral methods [Feynmann and Hibbs, 65; Schulman, 81] for evaluating a propagator in real time dynamics, though very simple to understand and physically appealing to the intuition, have remained basically a formal device, and have not been used in problems involving realistic potentials. Recently, there has been a resurgence of interests in these methods [Miller, Schwartz and Tromp, 83; Behrman, Jongeward and Wolynes, 83; Thirumalai and Berne, 83; Doll, 84], and significant advances are made towards developing numerical techniques for the evaluations of rapidly oscillating integrals in many dimensions [Chang and Miller, 87; Doll, Coalson and Freeman, 87].

Alternatively, there have been developments such as time-independent quantum mechanical coupled channel methods [Shapiro and Bersohn, 80; Heather and Light, 83], the time-dependent quantum mechanical wave-packet methods [Heller, 81; Mowrey and Kouri, 85; Sawada and Metiu, 86], and a host of other semi-classical methods [Marcus, 72; Miller, 74; Mukamel and Jortner; 76, Micha 83; Billing and Jolicard, 84; Gray and Child, 84; Henriksen, 85] which are generally based on running classical trajectories for the nuclear motions, while the electronic transitions are treated quantum mechanically. Each of these methods have their own advantages and disadvantages, and have been applied to the electronic absorption and photodissociation problems with varying degrees of success. Finite element grid methods which are based on the path-integral approach to computing a propagator in the coordinate or the phase spaces [Thirumalai, Bruskin and Berne, 83; Coalson, 85; Jackson and Metiu, 85], and are not restricted to any specific form for the potential, have not been applied to any of these light-molecule interaction processes involving realistic potential energy surfaces in more than one dimension. This can be explained very briefly by considering the coordinate space matrix elements of a real time propagator after a time interval 2ϵ as

$$K\left(X, X', 2\epsilon\right) = \int\limits_{-\infty}^{+\infty} dX'' \, \langle X|e^{-\frac{i}{\hbar}\hat{H}\epsilon}|X''\rangle \qquad (3.12)$$
$$\langle X''|e^{-\frac{i}{\hbar}\hat{H}\epsilon}|X\rangle$$

where $\hat{H}$ is a general one dimensional time-independent Hamiltonian along the variable X. For $\epsilon \to 0$, a typical expression for a short time approximation for the matrix elements appearing in the integrand of Eq.(3.12) [Schulman, 81], is written as

$$\langle X | e^{-\frac{i}{\hbar}\hat{H}\epsilon} | X' \rangle = \left(\frac{m}{2\pi i \hbar \epsilon} \right)^{\frac{1}{2}} exp\{ -\frac{m}{2i\hbar\epsilon} \left(X - X' \right)^2 \tag{3.13}$$
$$\epsilon \to \infty \qquad\qquad - i\frac{\epsilon}{2} \left(V(X) + V(X') \right) \}$$

The first term in the exponent, which corresponds to the short time approximation for the kinetic energy term in the propagator, increases as the square of the difference $(X - X')$. The oscillating nature of the exponentials therefore increases rapidly as one considers larger and larger values of $(X - X')$, whereas the magnitude of these rapidly increasing oscillations remain constant over the entire coordinate space. All of the numerical techniques for computing the integrals in Eq.(3.12), which are based on approximating the limits of the infinite integrals in Eq.(3.12) to be within some large finite region of the coordinate space, therefore do not converge to any physically meaningful result. One approach to avoid this problem is to use a transformation which shifts the problem of computing the real time TCF to another problem, in which instead one computes the same TCF for complex times, and in the end, after computing the Fourier transform of this complex time TCF, one uses some suitably defined inverse transformation to extract the required physical quantity of interest. The real to the complex time transformation of the computations in Eq. (3.12), the real short time $\epsilon \to \infty$ is replaced by an equivalent complex short time $\kappa \to \infty$, where κ has a fixed non-zero negative imaginary part. As a result, the rapidly oscillating exponentials in Eq.(3.12), which have a uniform maginutde in the entire coordinate space, are replaced by the rapidly oscillating exponentials the magnitude of which also decay rapidly, as one considers larger and larger values $(X - X')$. Therefore, the numerical evaluation of the infinite integrals, within sufficiently large finite limits in the coordinate space in Eq.(3.12), does not cause any problem.

Next, we describe the transformation from real to the complex time for a molecular TCF $f_{\hat{A},\hat{B}}(t)$ as written in Eq.(3.11), and derive the required inverse transformation that gives us the required Fourier transform of the original TCF. If initially the molecular system is in a pure nuclear vibrational state $|\psi_I\rangle$ of the ith potential energy surface, $f_{\hat{A},\hat{B}}(t)$ of Eq.(3.11c) can then be written as

$$f_{\hat{A}\hat{B}}(t) = \sum_{I,J} e^{-i\omega_{JI}t} \langle \psi_I|(\hat{A})_{ij}|\psi_J\rangle \langle \psi_J|(\hat{B})_{ji}|\psi_I\rangle \tag{3.14}$$

where $|\psi_J\rangle$ is the final nuclear vibrational state on the jth potential energy surface, and $\omega_{JI} = (\mathcal{E}_J - \mathcal{E}_I)/h$. The Fourier transform of Eq.(3.14), defined as

$$f_{\hat{A}\hat{B}}(\omega) = \frac{1}{2\pi} \int\limits_{-\infty}^{+\infty} dt \; e^{i\omega t} f_{\hat{A}\hat{B}}(t) \tag{3.15}$$

gives the familiar Golden rule result

$$f_{\hat{A}\hat{B}}(\omega) = \frac{1}{2\pi} \sum_{I,J} \langle \psi_I|(\hat{A})_{ij}|\psi_J\rangle \langle \psi_J|(\hat{B})_{ji}|\psi_I\rangle \; \delta(\omega - \omega_{JI}) \tag{3.16}$$

where the Dirac δ function conserves the energy, by requiring that the energy $\hbar\omega_{JI}$ of the electronic transition between the initial and the final nuclear vibrational states $|\psi_I\rangle$ and $|\psi_J\rangle$ is equal to the energy $\hbar\omega$ given by the light source. The Fourier transform $f_{\hat{A}\hat{B}}(\omega)$, as defined in equations (3.15), requires that the computations are done along the real time axis in the complex time plane. The transform to an axis in the complex time plane, which is parallel to the real time axis, but with a non-zero constant imaginary part, is achieved simply by replacing in Eq.(3.14) the real time t by a complex time $\tau = t - i\hbar u$, i.e we use $\widetilde{f}_{\hat{A}\hat{B}}(t) = f_{\hat{A}\hat{B}}(\tau)$ with

$$\widetilde{f}_{\hat{A}\hat{B}}(t) = \sum_{I,J} e^{-i\omega_{JI}u\hbar} e^{-i\omega_{JI}t} \langle \psi_I | (\hat{A})_{ij} | \psi_J \rangle \qquad (3.17)$$

$$\langle \psi_J | (\hat{B})_{ji} | \psi_I \rangle$$

where u is a parameter which always remains real. Using the definition in Eq.(3.15) for the Fourier transform, we can see that the Fourier transform of the complex time TCF $\tilde{f}_{\hat{A},\hat{B}}(t)$ is given by

$$\widetilde{f}_{\hat{A}\hat{B}}(\omega) = \frac{1}{2\pi} \sum_{I,J} e^{-\omega_{JI}u\hbar} \langle \psi_I | (\hat{A})_{ij} | \psi_J \rangle \qquad (3.18)$$

$$\langle \psi_J | (\hat{B})_{ji} | \psi_I \rangle \; \delta\,(\omega - \omega_{JI})$$

From equations (3.16), (3.18), and using the property of the Dirac δ function requiring $\omega_{JI} = \omega$, it follows that $f_{\hat{A}\hat{B}}(\omega)$, which defines the transition rates for different light-molecule interaction processes in the previous chapter, is given by

$$f_{\hat{A}\hat{B}}(\omega) = e^{\omega u\hbar} \widetilde{f}_{\hat{A}\hat{B}}(\omega) \qquad (3.19)$$

where $\tilde{f}_{\hat{A}\hat{B}}(\omega)$ is the Fourier transform of the complex time TCF $\tilde{f}_{\hat{A}\hat{B}}(t)$ as defined in Eq.(3.17). For a constant u this transform is taken along an axis, which is parallel to the real time axis but has a non-zero constant imaginary part. In case the initial state of the molecular system is not a pure vibrational state, but is at thermal equilibrium at the inverse temperature $k_B\beta$, we use Eq.(3.11b) of the previous section and steps similar to Eqs.(3.14–3.19), to show that if the complex time TCF for a finite temperature two-surface photoexcitation problem is given by

$$\widetilde{f}_{\hat{A}\hat{B}}(t) = \frac{1}{Z_{\bar{\beta}}} Tr \left[e^{+\frac{i}{\hbar}(t+i\bar{\beta}\hbar)\widehat{\mathcal{H}}_u} \left(\hat{A} \right)_{ij} e^{-\frac{i}{\hbar}(t-i\bar{u}\hbar)\widehat{\mathcal{H}}_l} \left(\hat{B} \right)_{ji} \right]$$

(3.20)

with $\bar{\beta} = \beta - u$, and u as the artificially introduced parameter, then $f_{\hat{A},\hat{B}}(\omega) = e^{uh\omega} \tilde{f}_{\hat{A},\hat{B}}(\omega)$, where $\tilde{f}_{\hat{A},\hat{B}}(\omega)$ is the Fourier transform of Eq.(3.20) as defined in Eq.(3.15). Some of the other works along these lines treat the artificially introduced parameter u as temperature; the computations of a complex time propagators are then suitably referred to as real time finite temperature computations. In case of an actual finite temperature computation, due to a thermal distribution for the initial state of the system, the requirement of a positive $\bar{\beta}$ in the argument of the lower surface propagator in Eq.(3.20) imposes therefore an upper limit on the choice of the parameter u. In our work, however, we do not use time-dependent computations for the propagator on the lower potential surface; therefore, we have not needed any constraint on the size of the parameter u imposed by the size of the natural β for the problem. We continue to call u simply an artificially introduced parameter, the size of which depends only upon the following competing factors. Increasing the value of u increases the damping of the upper surface oscillations and therefore increases the numerical stability of the dynamical computations. Increasing the value of u, on the other hand, also decreases the size of the numbers we are dealing with in the computations; therefore, beyond a certain value, they start to affect the overall accuracy of the computations. For each individual problem, one has to choose a compromise between these two competing factors and select a suitable range, such that u is sufficiently large for an effective damping for the upper surface oscillations, and at the same time sufficiently small so that the numbers in the computations are not too small to affect the overall accuracy. In the end, the accuracy of a particular

computation is measured by checking the stability of a computation with respect to the variations in the value of u.

The transformation of a computation along the real time axis to another computation along a parallel axis, but with a non-zero imaginary component u, is not unique. There are other transformations, such as rotating the computational axis in the complex time plane, that can achieve similar results. In fact, some of them may later prove to be more efficient than the transformation used in this work. We discuss this further in the later chapters.

Lastly, the property of the δ function for the conservation of energy in Eqs.(3.16) and (3.18), which has been used in Eqs.(3.17) and (3.20) to get the inverse transformation between $f_{\hat{A},\hat{B}}(\omega)$ and $\tilde{f}_{\hat{A},\hat{B}}(\omega)$, holds true only for a sharp spectra. Other cases, where one has to incorporate also a phenomenological line shape in the problem, such as molecular line-broadening effects, we can use modifications of the similar transformation [Coalson, 85] to achieve similar results.

3.3. Properties of the Complex Time TCFs and their Fourier transforms.

Some properties of the complex time TCF $\tilde{f}_{\hat{A},\hat{B}}(t)$, which we use later in this work, follow from its explicit expression which we write once again as

$$\tilde{f}_{\hat{A}\hat{B}}(t) = \sum_I W_I \left\langle \psi_I \left| e^{+\frac{i}{\hbar}\widehat{\mathcal{H}}_i \tau} \left(\hat{A} \right)_{ij} e^{-\frac{i}{\hbar}\widehat{\mathcal{H}}_j \tau} \left(\hat{B} \right)_{ij} \right| \psi_I \right\rangle \qquad (3.21)$$

The initial and the excited surface Hamiltonians $\widehat{\mathcal{H}}_i$ and $\widehat{\mathcal{H}}_j$, respectively, are the operators over the nuclear variables $\{\hat{\mathbf{R}}, \hat{\mathbf{P}}_{\mathbf{R}}\}$ of an extended molecular system. Sometimes these Hamiltonians may contain constant terms like $\hbar\Delta_i$ and $\hbar\Delta_j$ respectively, such that the difference $\hbar\Delta_{ij} = \hbar(\Delta_j - \Delta_i)$ may correspond simply to

a vertical displacement of the upper surface with respect to the lower one. These constant terms affect only the position of the line shape function in the frequency space. Therefore, they can be taken care of, very easily, in the definition of the Fourier transform $\tilde{f}_{\hat{A},\hat{B}}(\omega)$. If the upper and the lower surface Hamiltonians are written as $\widehat{\mathcal{H}}_j = \hat{H}_j - \hbar\Delta_j$ and $\widehat{\mathcal{H}}_i = \hat{H}_i - \hbar\Delta_i$, respectively, $\tilde{f}_{\hat{A},\hat{B}}$ in Eq.(3.22) can then be written as

$$\widetilde{f}_{\hat{A}\hat{B}}(t) = e^{-\Delta_{ji}\tau}\widetilde{F}_{\hat{A}\hat{B}}(t) \tag{3.22}$$

with its Fourier transform given by

$$\widetilde{f}_{\hat{A}\hat{B}}(\omega) = e^{-\Delta_{ji}\hbar u}\widetilde{F}_{\hat{A}\hat{B}}(\omega - \Delta_{ji}) \qquad . \tag{3.23}$$

The shifted Fourier transform $\widetilde{F}_{\hat{A},\hat{B}}(\omega - \Delta_{ji})$ is given by

$$\widetilde{F}_{\hat{A}\hat{B}}(\omega') = \frac{1}{2\pi}\int_{-\infty}^{+\infty} dt \ e^{i\omega' t}\widetilde{F}_{\hat{A}\hat{B}}(t) \tag{3.24}$$

with $\omega' = \omega - \Delta_{ji}$, and the shifted TCF $\widetilde{F}_{\hat{A},\hat{B}}(t)$ is written in a compact form as

$$\widetilde{F}_{\hat{A}\hat{B}}(t) = \sum_I W_I \left\langle \psi_I \left| \left(\hat{A}\right)_{ij} e^{-i\hat{\Omega}_j(E_I)\tau} \left(\hat{B}\right)_{ji} \right| \psi_I \right\rangle \tag{3.25}$$

Here we have used $\hat{H}_i|\psi_I\rangle = E_I|\psi_I\rangle$, and the frequency operator $\hat{\Omega}_j(E_I)$ which describes the time-evolution is given by

$$\hat{\Omega}_j(E_I) = \frac{\left(\hat{H}_j - E_I\right)}{\hbar} \tag{3.26}$$

where $\hat{H}_j$ is an operator over only the nuclear variables $\{\mathbf{R}, \mathbf{P_R}\}$ for the jth electronic surface. For two different operators $\hat{A}$ and $\hat{B}$, we define a symmetric form for the TCF as

$$\widetilde{F}^s_{\hat{A}\hat{B}}(t) = \frac{1}{2}\left(\widetilde{F}_{\hat{A}\hat{B}}(t) + \widetilde{F}_{\hat{B}\hat{A}}(t)\right) \tag{3.26}$$

which is invariant under the interchange of operators $\hat{A}$ and $\hat{B}$. Replacing t by $-t$ in Eq.(3.25)

$$\widetilde{F}_{\hat{A}\hat{B}}(-t) = \sum_I W_I \left\langle \psi_I \left| \left(\hat{A}\right)_{ij} e^{+i\hat{\Omega}_j(E_I)\tau^*} \left(\hat{B}\right)_{ji} \right| \psi_I \right\rangle \tag{3.28}$$

we see that $\widetilde{F}_{\hat{A},\hat{B}}(-t) = \widetilde{F}_{\hat{B},\hat{A}}(t)^*$. Now considering the Fourier transform $\widetilde{F}_{\hat{A},\hat{B}}(\omega)$ of Eq.(3.25) as

$$\widetilde{F}_{\hat{A}\hat{B}}(\omega) = \frac{1}{2\pi}\left\{ \int\limits_{-\infty}^{0} dt' e^{i\omega t'} \widetilde{F}_{\hat{A}\hat{B}}(t) + \int\limits_{0}^{+\infty} dt' e^{i\omega t'} \widetilde{F}_{\hat{A}\hat{B}}(t) \right\} \tag{3.29}$$

replacing in the first term t' by $-t'$, and using the property $\widetilde{F}_{\hat{A},\hat{B}}(-t') = \widetilde{F}_{\hat{B},\hat{A}}(t')^*$ we get

$$\widetilde{F}_{\hat{A}\hat{B}}(\omega) = \frac{1}{2\pi} \int\limits_{0}^{+\infty} dt' \left\{ e^{-i\omega t'} \widetilde{F}_{\hat{A}\hat{B}}(t)^* + e^{+i\omega t'} \widetilde{F}_{\hat{A}\hat{B}}(t) \right\} \tag{3.30}$$

For $\hat{B} = \hat{A}$ this gives

$$\widetilde{F}_{\hat{A}\hat{A}}(\omega) = \frac{1}{\pi} \int\limits_{0}^{+\infty} dt' Re \left\{ e^{+i\omega t'} \widetilde{F}_{\hat{A}\hat{A}}(t) \right\} \tag{3.31}$$

and for $\hat{B} \neq \hat{A}$, we use the symmetrized form, which is invariant to the interchange of the operators $\hat{A}$ and $\hat{B}$, to write

$$\widetilde{F}^s_{\hat{A}\hat{B}}(\omega) = \frac{1}{\pi} \int\limits_0^{+\infty} dt' Re \left\{ e^{+i\omega t'} \widetilde{F}^s_{\hat{A}\hat{B}}(t) \right\} \tag{3.31}$$

Equations (3.31) and (3.32) for the Fourier transforms $\widetilde{F}_{\hat{A},\hat{B}}(\omega)$ and $\widetilde{F}^s_{\hat{A},\hat{B}}(\omega)$, respectively, ensure that the physical properties represented by these Fourier transforms remain real. Furthermore, for $\hat{B} \neq \hat{A}$, we can show that the symmetrized TCF $\widetilde{F}^s_{\hat{A},\hat{B}}(t)$ can also be written as

$$\widetilde{F}^s_{\hat{A}\hat{B}}(t) = \frac{1}{2} \left\{ \widetilde{F}_{\hat{C}\hat{C}}(t) - \widetilde{F}_{\hat{A}\hat{A}}(t) - \widetilde{F}_{\hat{B}\hat{B}}(t) \right\} \tag{3.33}$$

where $\widetilde{F}_{\hat{C},\hat{C}}(t)$, $\widetilde{F}_{\hat{A},\hat{A}}(t)$ and $\widetilde{F}_{\hat{B},\hat{B}}(t)$ are the autocorrelation functions corresponding to the operators $\hat{C}$, $\hat{A}$ and $\hat{B}$, respectively, and $\hat{C} = \hat{A} + \hat{B}$. Therefore, for all physically interesting light-molecule interaction processes, from now on, we consider the evaluation and uses of the complex time autocorrelation function $\widetilde{F}_{\hat{A},\hat{A}}(t)$, which we again write in a compact form as

$$\widetilde{F}_{\hat{A}\hat{A}}(t) = \sum_I W_I \left\langle \Upsilon^I_{ji}(0) \,|\, \Upsilon^I_{ji}(\tau) \right\rangle \tag{3.34}$$

where the time-dependent amplitude $|\,\Upsilon^I_{ji}(t)\rangle$, which is evolving according to the frequency operator $\hat{\Omega}_j(E_I)$ is given by $|\Upsilon^I_{ji}(t)\rangle = \exp(-i\hat{\Omega}_j t)|\Upsilon^I_{ji}(0)\rangle$ with $|\Upsilon^I_{ji}(0) = (\hat{A})_{ji}|\psi_I\rangle$. The overlap $\langle \Upsilon^I_{ji}(0) \,|\, \Upsilon^I_{ji}(\tau)\rangle$, completely describe the time-dependence in the TCF $\widetilde{F}_{\hat{A},\hat{A}}(t)$ for a complex time $\tau = t - iu\hbar$. To compute a vibrational infrared or a rotational microwave spectra, we merely need to replace the frequency operator $\hat{\Omega}_j$ by a different frequency operator $\hat{\Omega}_i = (\hat{H}_i - E_i)/\hbar$,

and redefine the transition dipole moment operator $(\widehat{A})_{ji}$ as $(\widehat{A})_{ii}$; the total dipole operator of the system in its ith electronic state.

The physical interpretation of Eq.(3.34) is as follows: at an initial real time $t = 0$ and the complex time $\tau = -iu\hbar$, the amplitude $|\; \Upsilon_{ji}^{I}(-iu\hbar)\rangle$ is almost identical in shape, but of smaller magnitude in comparison to $|\; \Upsilon_{ji}^{I}(0)\rangle$. For later times $t > 0$, the propagation of the amplitude occurs according to the frequency operator $\hat{\Omega}_j$, and a fall off in the value of the overlap $\langle\Upsilon_{ji}^{I}(0) \; | \; \Upsilon_{ji}^{I}(\tau)\rangle$ is observed, as the amplitude $|\; \Upsilon_{ji}^{I}(\tau)\rangle$ moves away from its initial position and begins to change its shape. The short time behavior of the overlap primarily decides the position and the shape of the overall line shape in the high frequency region, whereas the long time behavior of the overlap decides its shape in the low frequency region. If the overlap decays to zero at intermediate times and shows some recurrences in the long time behavior, one finds fine structures overlaying the otherwise smooth spectra.

CHAPTER 4
FACTORIZATION OF TCFs INTO
PRIMARY AND SECONDARY REGION TCFs

We consider the evaluation of a general complex time dipole-dipole TCF $\widetilde{F}_{\hat{D},\hat{D}}(t)$ for light-molecule interaction processes, involving electronic transitions between two potential energy surfaces. In particular, we are interested in application to the photoexcitation and dissociation dynamics of extended molecular systems. The usual problem one encounters in dealing with extended molecular systems is the large number of degrees of freedom involved. If we were to apply any quantum molecular dynamics method for computing a molecular dipole TCF of an extended system with realistic potential energy surfaces, the first and the foremost consideration we would have to think of is the computational efficacy of the method for a multivariable problem. It has been observed that the computational efforts for most of the methods, where there is more than one degree of freedom in the problem, increase as the square of the number of degrees of freedom involved. Therefore, all the methods that try to compute the dynamics, simultaneously along all the coupled degrees of freedom, become more and more impractical as the number of degrees of freedom start to increase from more than one or two. To avoid this problem, we treat the dynamics of an extended molecular system in the spirit of the well-known mean field approximation, which factorizes the full dynamics of an extended molecular system into many single variable problems, with time-dependent self-consistent couplings between the motions along these uncoupled variables. As a result of such factorization the computational efforts

in a multivariable dynamical problem do not scale as the square of the number of the variables involved.

In section 4.1, we describe the sufficient conditions for, a) defining fast and localized photoexcitation processes in a large molecular system, interacting with visible or UV light, and b) factorizing the molecular dipole TCF for these cases into self-consistent primary and secondary region TCFs. Section 4.2 describes a time-dependent variational principle (TDVP) for the amplitudes $\mid \Upsilon^I(t) \rangle$, introduced in the previous chapter. Section 4.3 derives a norm conserving time-dependent self-consistent field (TDSCF) approximation for factoring these amplitudes into self-consistent primary and secondary region factors, and finally in section 4.4, we use the results of sections 4.1, 4.2, and 4.3 to factor a dipole-dipole TCF $\widetilde{F}_{\hat{D},\hat{D}}(t)$ into self-consistent primary and secondary region TCFs.

4.1. Sufficient Conditions for the Factorization of the Amplitudes

In general, light-molecule interaction processes in extended molecular systems are classified into two broad groups. First, the intramolecular process, in which a single molecule involving several vibrational and rotational degrees of freedom absorbs light in a given frequency range, depending upon which it dynamically evolves on the ground, or excited electronic surface. Second, the intermolecular process, in which an extended molecular system absorbs light in a given frequency range, followed by a dynamical evolution of the system in a given electronic state. For both cases, if the absorption of light in the extended molecular system is a fast process, we can define a sufficient condition to describe a localized region in the large molecular system, such that this region plays a more dominant role in the light-molecule interaction as compared to the rest of the system. If the frequency

of the light source is in the visible or UV region, the sufficient condition that defines such a localized region, is that the transition dipole operator $(\hat{D}(\mathbf{R}))_{ij}$ of the system, is an operator over the nuclear variables of the localized region only. In other words, the transition dipole operator, for a localized electronic excitation process in a large molecular system, is written as

$$(\hat{D}(\mathbf{R}))_{ij} = (\hat{D}(\mathbf{X}))_{ij} \tag{4.1}$$

where $\mathbf{R} = \{\mathbf{X}, \mathbf{Q}\}$ is a set of generalized nuclear variables for the entire molecular system, with $\mathbf{X} = \{X_1, X_2, X_3, ...\}$ a subset that defines the variables of the the localized region within which the important dynamics takes place, and $\mathbf{Q} = \{Q_1, Q_2, Q_3, ...\}$ the subset that contains all the remaining variables of the system. We use "primary" region for the region covered by the elements of the subset $\mathbf{X}$, and "secondary" region for the region covered by the elements of the subset $\mathbf{Q}$. With the definitions of the primary and the secondary regions of an extended molecular system at an initial time $t = 0$, in place, the sufficient condition for the factorization of the amplitude $\mid \Upsilon^I(0)\rangle$ into factors corresponding to the primary and secondary region dynamics for a later time $t > 0$, is described by writing the initial nuclear vibrational state $\mid \psi_I\rangle$ on the ith potential surface as

$$\mid \psi_I\rangle = \mid \psi_I^p\rangle \mid \psi_I^s\rangle \tag{4.2}$$

where p corresponds to the primary region dynamics and s to the secondary region dynamics. The stationary state eigenvalue E_I, corresponding to the sufficient condition in Eq.(4.2), is then written as $E_I = E_I^p + E_I^s + E_I^{ps}$, where the last term is due to the coupling between the primary and the secondary regions on the ith potential energy surface. Furthermore, it is not difficult to see that the sufficient condition in Eq.(4.2), for the factorization of the amplitude into self-consistent

primary and secondary region factors, is the validity of the time-independent Hartree (TH) approximation for the stationary state vibrational wavefunction on the ith potential surface [Bowman, 86]. Given the sufficient condition in Eq.(4.1) for the definition of a localized region in an extended molecular system is satisfied, it is not difficult to find a time-independent Hartree approximation to the stationary state eigenfunction $| \psi_I \rangle$ on the ith potential energy surface, such that

$$|\Upsilon^I(0)\rangle = |\xi^I(0)\rangle \, |\eta^I(0)\rangle \qquad (4.3)$$

where $| \xi^I(0) \rangle = (\hat{D}(\mathbf{X}))_{ij} \, | \psi_I^p \rangle$ is the initial value of the amplitude for the primary region dynamics, and $| \eta_I(0) \rangle = | \psi_I^s \rangle$ is the initial value of the amplitude for the secondary region dynamics. As we shall see later, equations (4.1) and (4.2) completely define the sufficient conditions for the factorization of the time-dependent amplitude into self-consistent motions corresponding to the primary and secondary region dynamics. Therefore, these are also the sufficient conditions for factoring the molecular dipole TCF for an extended system into primary and secondary region TCF factors.

If the frequency of the light source is in the infrared region, the sufficient condition for describing a localized process in an extended system in Eq.(4.1) can be generalized by using a series expansion for the total dipole moment of the system in a single electronic state to write it as

$$(\hat{D}(\mathbf{R}))_{ii} = \sum_{l}(\hat{D}^l(\mathbf{X}))_{ii} \, P_l(\mathbf{Q}) \qquad (4.4)$$

where $(\hat{D}^l(\mathbf{X}))_{ii}$ is the net dipole moment of the primary region when the molecular system in the ith electronic state, and $P_l(\mathbf{Q})$ is a polynomial in the variables of the secondary region. The description in the later chapters of this work, with slight

modification, can also incorporate this generalization of the sufficient conditions in Eqs.(4.1) and Eq.(4.2), to include the interaction of infrared light with extended molecular systems.

4.2. Norm Conserving Time-dependent Variational Principle (TDVP)

The time-dependent amplitude $|\Upsilon(t)\rangle$ which defines the time-dependence of the total TCF in Eq.(3.34) is a solution of the following equation of motion

$$\left(i\partial_t - \hat{\Omega}\right)|\Upsilon(t)\rangle = 0 \tag{4.5}$$

where the initial condition $|\Upsilon_0\rangle = |\Upsilon(0)\rangle$, defines the normalization N at an initial time $t = 0$, as $N = \langle \Upsilon_0 \mid \Upsilon_0 \rangle$. For a two surface problem, we have dropped in Eq.(4.5) specific references to the subscript j in the frequency operator $\hat{\Omega}_j$ and to the subscript I in the amplitude $\mid \Upsilon^I \rangle$. When the exact solution $|\Upsilon\rangle = |\Upsilon(t)\rangle$ of equation (4.5) is complicated, it is sometime desirable to replace it by an approximate solution $|\widetilde{\Upsilon}\rangle = |\widetilde{\Upsilon}(t)\rangle$ with the initial conditions $|\widetilde{\Upsilon}_0\rangle = |\widetilde{\Upsilon}(0)\rangle$ at $t = 0$. We construct an approximate solution to Eq.(4.5) by using a time-dependent variational principle (TDVP), the general form of which is similar to those given by Dirac [Dirac, 26, 30] and Frenkel [Frenkel, 34] in the earlier days, and by Mclachlan [McLachlan, 64] in later modifications, see for example [Langhhoff, Epstein and Karplus, 72] for a review. In our work, however, we also impose the conservation of the total norm N by using the well known Lagrange undetermined multiplier technique.

The variational functional is constructed in steps, by first introducing the Lagrangian

$$L\left[\Upsilon,\Upsilon^*\right] = \frac{1}{2}\left(\left\langle\Upsilon|\widehat{\mathcal{D}}\Upsilon\right\rangle + \left\langle\widehat{\mathcal{D}}\Upsilon|\Upsilon\right\rangle\right) \tag{4.6}$$

where $\widehat{\mathcal{D}} = i\partial_t - \mathcal{H}$, and the form of the Lagrangian in Eq.(4.6) is invariant under time reversal. From this, the action between the initial and the final times follows as

$$S\left[\Upsilon,\Upsilon^*\right] = \int\limits_{t_1}^{t} dt'\, L\left[\Upsilon,\Upsilon^*\right] \tag{4.7}$$

and finally the norm conserving functional for Eq.(4.5) is written as

$$S'\left[\Upsilon_\lambda,\Upsilon_\lambda^*\right] = S\left[\Upsilon_\lambda,\Upsilon_\lambda^*\right] + \int\limits_{t_1}^{t} dt'\, \lambda\left(t'\right)\,\langle\Upsilon_\lambda|\Upsilon_\lambda\rangle \tag{4.8}$$

where in our notation the subscript λ in the approximate solution $|\Upsilon_\lambda\rangle$ refers to the undetermined Lagrange multiplier λ, which is solved by using the constraint that the norm N defined as $N = \langle\Upsilon_\lambda(t)\mid\Upsilon_\lambda(t)\rangle$ is a conserved quantity. We solve equation $\delta S'[\Upsilon_\lambda^*,\Upsilon_\lambda] = 0$ with fixed boundary conditions, and treat the variations $\delta\Upsilon_\lambda^*$ and $\delta\Upsilon_\lambda$ independently of each other. We choose the variation $\delta\Upsilon_\lambda = 0$ and allow for a $\delta\Upsilon_\lambda^*$, to get

$$\langle\delta\Upsilon_\lambda|\widehat{\mathcal{D}}\Upsilon_\lambda + \lambda\Upsilon_\lambda\rangle = 0 \tag{4.9}$$

which is equivalent to

$$\widehat{\mathcal{D}}\Upsilon_\lambda + \lambda\Upsilon_\lambda = 0 \qquad, \tag{4.10}$$

The subscript λ in the approximate solution Υ_λ refers to the additional constraint, which needs to be satisfied solving for λ. Using a transformation to remove λ from Eq.(4.10), we write the trial solution Υ_λ as

$$\Upsilon_\lambda = \Phi_\lambda \, exp[i \int\limits_{t_1}^{t} dt' \, \lambda \left(t'\right)] \qquad , \qquad (4.11)$$

where Φ_λ satisfies

$$\widehat{\mathcal{D}}\Phi_\lambda = 0 \qquad (4.12)$$

and the normalization condition $N = \langle \Upsilon_\lambda | \, \Upsilon_\lambda \rangle$ gives

$$exp[-2 \int\limits_{t_1}^{t} dt' \, \{Im(\, \lambda \left(t'\right))\}] = \left(\frac{N}{\langle \Phi_\lambda | \Phi_\lambda \rangle} \right)^{\frac{1}{2}} \qquad (4.13)$$

Since $Re(\lambda)$ does not appear in the normalization constraint in Eq.(4.13), we are free to choose it equal to zero. Then the norm conserving solution to Eq.(4.5) is given by

$$\Upsilon_\lambda = N^{\frac{1}{2}} \frac{\Phi_\lambda}{\langle \Phi_\lambda | \Phi_\lambda \rangle^{\frac{1}{2}}} \qquad (4.14)$$

where $\Phi_\lambda(t)$ satisfy Eq.(4.12), and the normalization constant N is constructed from the initial conditions.

4.3. Time-dependent Self-consistent Field (TDSCF) Approximation

Expressing the norm conserving time-dependent variational principle (TDVP), of the previous section, in a compact form as

$$\langle \delta \Upsilon_\lambda | \widehat{\mathcal{D}} \Upsilon_\lambda + \lambda \Upsilon_\lambda \rangle = 0 \qquad (4.9)$$

The frequency operator $\widehat{\Omega}$, which governs the time evolution of the exact amplitude $|\Upsilon(t)\rangle$, is of the form

$$\tilde{U} = \tilde{U}_p + \tilde{U}_s + \tilde{U}_{ps} \qquad (4.16)$$

where the superscript p refers to the variables of the primary region, s to the variables of the secondary region, and ps to the coupling between the primary and the secondary regions. We write the time-dependent self-consistent field (TDSCF) approximation to Eq.(4.15) as

$$|\Upsilon(t)\rangle = |\tilde{\xi}(t)\rangle\,|\tilde{\eta}(t)\rangle \qquad (4.17)$$

where the factors $\tilde{\xi}(t)$ and $\tilde{\eta}(t)$ correspond to the self-consistent dynamics of the primary and the secondary regions, respectively. Treating the variations $\delta\tilde{\xi}(t)^*$ and $\delta\tilde{\eta}(t)^*$ independently, and choosing either $\delta\tilde{\xi}(t)^* = 0$, or $\delta\tilde{\eta}(t)^* = 0$, we get the following coupled equations

$$i\langle\tilde{\eta}|\tilde{\eta}\rangle\dot{\tilde{\xi}} + i\langle\tilde{\eta}|\dot{\tilde{\eta}}\rangle\tilde{\xi} - \langle\tilde{\eta}|\tilde{U}|\tilde{\eta}\rangle\tilde{\xi} + \lambda\langle\tilde{\eta}|\tilde{\eta}\rangle\tilde{\xi} = 0 \qquad (4.18a)$$

$$i\langle\tilde{\xi}|\tilde{\xi}\rangle\dot{\tilde{\eta}} + i\langle\tilde{\xi}|\dot{\tilde{\xi}}\rangle\tilde{\eta} - \langle\tilde{\xi}|\tilde{U}|\tilde{\xi}\rangle\tilde{\eta} + \lambda\langle\tilde{\xi}|\tilde{\xi}\rangle\tilde{\eta} = 0 \qquad (4.18b)$$

Using the transformations

$$\tilde{\xi} = \xi'\,\exp\left[\,i\int_{t_i}^{t} dx\,\frac{\langle\tilde{\eta}|\tilde{U}|\tilde{\eta}\rangle - i\langle\tilde{\eta}|\dot{\tilde{\eta}}\rangle}{\langle\tilde{\eta}|\tilde{\eta}\rangle}\,\right] \qquad (4.19a)$$

$$\underline{\eta} = \eta'\,\exp\left[\,i\int_{t_i}^{t} dx\,\frac{\langle\tilde{\xi}|\tilde{U}|\tilde{\xi}\rangle - i\langle\tilde{\xi}|\dot{\tilde{\xi}}\rangle}{\langle\tilde{\xi}|\tilde{\xi}\rangle}\,\right] \qquad (4.19b)$$

in equations (4.18a) and (4.18b), respectively, we write them for ξ' and η' in a form which is more easy to implement. Further using other transformations,

46

$$\xi' = \xi \; exp \left[i \int\limits_{t_1}^{t} dt' \lambda \left(t' \right) \right] \qquad (4.20a)$$

$$\eta' = \eta \; exp \left[i \int\limits_{t_1}^{t} dt' \lambda \left(t' \right) \right] \qquad (4.20b)$$

we remove the normalization constraint λ from the differential equations corresponding to $\xi'(t)$ and $\eta'(t)$, respectively. We find the differential equations corresponding to the self-consistent primary and secondary region amplitudes $\xi(t)$ and $\eta(t)$, respectively, in their final form as

$$i\dot{\xi} - \hat{\Omega}^p \xi - \frac{\langle \eta | \hat{\Omega}^{ps} | \eta \rangle}{\langle \eta | \eta \rangle} \xi = 0 \qquad (4.21a)$$

$$i\dot{\eta} - \hat{\Omega}^s \eta - \frac{\langle \xi | \hat{\Omega}^{ps} | \xi \rangle}{\langle \xi | \xi \rangle} \eta = 0 \qquad (4.21b)$$

Imposing the normalization constraint $N = \langle \Upsilon_\lambda(t) \mid \Upsilon_\lambda(t) \rangle$, and using the transformation equations (4.19a,b) and (4.20a,b), we write

$$N = \langle \xi\eta | \xi\eta \rangle \; exp[- \int\limits_{t_1}^{t} \{ \frac{\langle \tilde{\eta} | \dot{\tilde{\eta}} \rangle + \langle \dot{\tilde{\eta}} | \tilde{\eta} \rangle}{\langle \tilde{\eta} | \tilde{\eta} \rangle} \qquad (4.22)$$
$$+ \frac{\langle \tilde{\xi} | \dot{\tilde{\xi}} \rangle + \langle \dot{\tilde{\xi}} | \tilde{\xi} \rangle}{\langle \tilde{\xi} | \tilde{\xi} \rangle} \} dt' - 4 \int\limits_{t_1}^{t} dt' Im \left\{ \lambda \left(t' \right) \right\}]$$

Subtracting complex conjugate of Eq.(4.18a) from Eq.(4.18a), and using the result in Eq.(4.22), we express the normalization constraint as

$$exp\left[-\int\limits_{t_1}^{t} dt' Im\left\{\lambda\left(t'\right)\right\}\right] = \left(\frac{N}{\langle\xi\eta|\xi\eta\rangle}\right)^{\frac{1}{2}} \tag{4.23}$$

where again as in the previous case we are free to choose $Re(\lambda) = 0$, since the normalization constraint does not involve $Re(\lambda)$. Finally, using the transformations in equations (4.19a,b) and (4.20a,b) in the TDSCF approximation in Eq.(4.17), we get

$$N = \xi\eta\, exp[+i\int\limits_{t_1}^{t}\{\frac{i\langle\widetilde{\eta}|\dot{\widetilde{\eta}}\rangle - \langle\widetilde{\eta}|\hat{\Omega}^s|\widetilde{\eta}\rangle}{\langle\widetilde{\eta}|\widetilde{\eta}\rangle} \tag{4.24}$$

$$+\frac{i\langle\widetilde{\xi}|\dot{\widetilde{\xi}}\rangle + \langle\widetilde{\xi}|\hat{\Omega}^p|\widetilde{\xi}\rangle}{\langle\widetilde{\xi}|\widetilde{\xi}\rangle} - 2Im\left(\lambda\left(t'\right)\right)\}\ dt'\ ]$$

where again we use Eq.(4.18a) to write

$$\frac{i\langle\widetilde{\eta}|\dot{\widetilde{\eta}}\rangle - \langle\widetilde{\eta}|\hat{\Omega}^s|\widetilde{\eta}\rangle}{\langle\widetilde{\eta}|\widetilde{\eta}\rangle} + \tag{4.24}$$

$$\frac{i\langle\widetilde{\xi}|\dot{\widetilde{\xi}}\rangle + \langle\widetilde{\xi}|\hat{\Omega}^p|\widetilde{\xi}\rangle}{\langle\widetilde{\xi}|\widetilde{\xi}\rangle} = \frac{\langle\widetilde{\xi}\widetilde{\eta}|\hat{\Omega}^{ps}|\widetilde{\xi}\widetilde{\eta}\rangle}{\langle\widetilde{\xi}\widetilde{\eta}|\widetilde{\xi}\widetilde{\eta}\rangle} - \lambda$$

which together with the normalization constraint in Eq.(4.23), and the choice $Re(\lambda)$ = 0, gives the norm conserving TDSCF approximation in its final form as

$$\Upsilon_\lambda = N^{\frac{1}{2}}\frac{\xi}{\langle\xi|\xi\rangle^{\frac{1}{2}}}\frac{\eta}{\langle\eta|\eta\rangle^{\frac{1}{2}}}exp\left[i\int\limits_{t_1}^{t} dt'\frac{\left\langle\xi\eta|\hat{\Omega}^{ps}|\xi\eta\right\rangle}{\langle\xi\eta|\xi\eta\rangle}\right] \tag{4.26}$$

The amplitudes $\xi(t)$ and $\eta(t)$, corresponding to the self-consistent primary and secondary region dynamics, respectively, satisfy the following coupled equations:

$$i\dot{\xi} - \hat{\Omega}^p_{eff}(t)\,\xi = 0 \qquad (4.27a)$$

$$i\dot{\eta} - \hat{\Omega}^s_{eff}(t)\,\eta = 0 \qquad (4.27b)$$

where the time dependence in the effective frequency operators $\hat{\Omega}^p_{eff}(t)$ and $\hat{\Omega}^s_{eff}(t)$ are given by

$$\hat{\Omega}^p_{eff} = \hat{\Omega}^p + \frac{\langle\eta|\hat{\Omega}^{ps}|\eta\rangle}{\langle\eta|\eta\rangle} \qquad (4.28a)$$

$$\hat{\Omega}^s_{eff} = \hat{\Omega}^s + \frac{\langle\xi|\hat{\Omega}^{ps}|\xi\rangle}{\langle\xi|\xi\rangle} \qquad (4.28b)$$

Similar to the time-dependent Hartree (TDH) factorization of the total wave function [Schatz, 77; Gerber, Buch and Ratner, 82; Kugar, Meyer and Cederbaum, 87; Makri and Miller, 87] for a coupled many-mode problem, we also achieve a formal separation of the total amplitude, $\Upsilon(t)$, into self-consistent primary and secondary region factors $\xi(t)$ and $\eta(t)$, respectively. The time-dependence in each of these factors is governed by an effective frequency operator, which includes an average of the interaction frequency operator, over the other factor. The essential feature of the TDSCF approximation is that, while it provides the formal factorization of the dynamics of a multivariable system into primary and secondary region dynamics, it still permits the self-consistent energy exchange between these two regions through the effective couplings in the frequency operators. An essential requirement in our work is, that we must have a norm conserving form for the amplitude $\Upsilon(\tau)$ for a complex time $\tau > 0$, and a correct phase factor in Eq.(4.26). This is because we are interested in computing the overlap of the complex time amplitude with its initial

value at $\tau = 0$; therefore the phase factor an integral of the effective coupling from 0 to τ, does not get canceled by its own value at $\tau = 0$. The norm conserving form for the amplitude in Eq.(4.26) is essential because the effective frequency operators $\hat{\Omega}_{eff}^p(\tau)$ and $\hat{\Omega}_{eff}^s(\tau)$ are non-hermitian for any complex time $\tau > 0$.

4.4. Primary and Secondary Region Factorization of TCFs

Using the TDSCF factorization of the amplitude $\Upsilon(\tau)$ as shown in Eqs.(4.26–28), in Eq.(3.34) of the previous chapter, we write the complex time molecular TCF as

$$\widetilde{F}_{\hat{D}\hat{D}}(t) = \sum_I W_I N_I f_I(\tau) g_I(\tau) \; e^{i\alpha_I(\tau)} \qquad (4.29a)$$

where we have replaced the operator $\hat{A}$ by a molecular dipole operator $\hat{D}$, restored the subscript I corresponding to the sum over the initial nuclear vibrational state $|\psi_I\rangle$, and the complex time τ is given by $\tau = t - i\hbar u$. We define the "primary region TCF" $f_I(\tau)$, as a dimensionless overlap

$$f_I(\tau) = \frac{\left\langle \xi^I(0) | \xi^I(\tau) \right\rangle}{\langle \xi^I | \xi^I \rangle} \qquad (4.29b)$$

and the "secondary region TCF" $g_I(\tau)$, also as a dimensionless overlap

$$g_I(\tau) = \frac{\left\langle \eta^I(0) | \eta^I(\tau) \right\rangle}{\langle \eta^I | \eta^I \rangle} \qquad (4.29c)$$

The dimensionless primary region TCF $f_I(\tau)$ and the secondary region TCF $g_I(\tau)$, together with an overall phase factor $\alpha_I(\tau)$, which is an integral of the self-consistent coupling from 0 to τ given by

$$\alpha_I(\tau) = \int\limits_0^\tau \frac{\left\langle \xi^I \eta^I | \hat{\Omega}^{ps} | \xi^I \eta^I \right\rangle}{\langle \xi^I \eta^I | \xi^I \eta^I \rangle} \, dt' \qquad (4.29)$$

completely describe the time-dependence in the total TCF $\widetilde{F}_{\hat{D},\hat{D}}(t)$. The normalization constant N_I in Eq.(4.29a), which is computed from the given initial conditions $\xi_I(0)$ and $\eta_I(0)$ as according to

$$N_I = \left\langle \xi^I(0)\,\eta^I(0) \,|\, \xi^I(0)\,\eta^I(0) \right\rangle \qquad , \qquad (4.29d)$$

provides correct dimensions to the overall TCF.

CHAPTER 5
TIME-DEPENDENT EFFECTIVE FREQUENCY OPERATORS

In the present chapter, we consider a general nuclear vibrational Hamiltonian in a given electronic state, and solve the equations of motion for the secondary region dynamics. In section 5.1, we describe the time-dependent effective frequency operators by considering many degrees of freedoms in the secondary region interacting strongly with a single degree of freedom in the primary region. We model the strongly coupled primary and secondary regions couplings which are of arbitrary analytic form in the variables of the primary region, and have a linear and bilinear dependence in the variables of the secondary region. Section 5.2 describes the effective frequency operators for a weak coupling limit, and ignores the terms in the coupling which are bilinear in the variables of the secondary region. The solutions to the equations of motion for the secondary region operators, in both of these cases, are reduced to analytic forms, which are then used to construct the propagators for the secondary region dynamics. The primary region dynamics will be described in the next chapter by using a numerical path-integral method. In section 5.3 we derive an operator equation of motion for the primary region dynamics, show its relationship to the well known phenomenological Generalized Langevin equation (GLE) [Mori, 65], by constructing the fluctuation force term and the dissipative memory kernel, and prove the Fluctuation-Dissipation Relationship (FDR) [Van Hove, 54] explicitly for a general intermolecular process. Section 5.4 considers many degrees of freedom in the primary region dynamics interacting with a set of coupled harmonic oscillators in the secondary region dynamics.

52

5.1. Intramolecular Processes: Strongly Coupled Primary and Secondary Regions

In a general intramolecular photointeraction process, following the absorption of light in the visible and UV region, we consider electronic transitions between fixed electronic states i and j. Therefore, for notational brevity throughout this chapter, we avoid writing i and j as the specific references to the initial and the final electronic states, respectively. Consider a general nuclear vibrational Hamiltonian $\hat{H}$ in the given electronically excited state as consisting of the following terms:

$$\hat{H}^p = \frac{\hat{P}_X^2}{2m_X} + V^0\left(\hat{X}\right) \qquad (5.1a)$$

is the Hamiltonian for the primary region dynamics with an arbitrary potential $V^0(\hat{X})$ given either in a parametrized analytic form based on experimental information, or on a grid in coordinate space from ab initio or semi-empirical electronic structure calculations;

$$\hat{H}^s = \sum_k \frac{\hat{P}_k^2}{2m_k} + \frac{1}{2}m_k\omega_k^2\hat{Q}_k^2 \qquad (5.1b)$$

is the Hamiltonian for the secondary region expressed as a sum of $k(k = 1, 3...N)$ harmonic oscillators, such that the mass m_k and the frequency ω_k of the kth harmonic oscillator correspond to the mass and the frequency of the kth normal mode vibration in the molecule. The coupling between the primary and the secondary regions is expressed as

$$\hat{H}^{ps} = \sum_k \left\{ \hat{P}_k \lambda_{kX} \hat{P}_X + V^k\left(\hat{X}\right)\hat{Q}_k + \sum_{k'} \hat{Q}_{k'} V^{k'k}\left(\hat{X}\right)\hat{Q}_k \right\} \qquad (5.1c)$$

where the arbitrary functions $V^k(\hat{X})$ and $V^{kk'}(\hat{X})$ are operator dependent forces and potential curvatures, respectively, and the bilinear momentum coupling parameter λ_{kX} has dimensions of inverse mass. The arbitrary functions $V^k(\hat{X})$ and $V^{kk'}(\hat{X})$ are also given either in an experimentally parametrized analytic form, or on a grid in coordinate space as computed in an electronic structure calculation. Following the absorption of light in the visible or UV region, one finds that the primary region dynamics, describing for example rearrangement in the system due to the formation or breaking of a bond, is strongly coupled to the rest of the molecule. Therefore, we have added to the coupling the terms linear and bilinear in the operators of the secondary region. We also note that the formulation does not depend upon the strength of the various terms in the coupling, and in the next section we consider the weak coupling limit by ignoring the first and the last terms in Eq.(5.1c).

For a single degree of freedom in the primary region dynamics coupled to many degrees of freedom in the secondary region, we write the norm conserving TDSCF approximation for the amplitude $\Upsilon^I(t)$ as

$$\Upsilon^I(t) = N_I^{\frac{1}{2}}\, e^{+i\alpha_I(t)}\, \frac{\xi^I(t)}{\langle \xi^I | \xi^I \rangle^{\frac{1}{2}}} \prod_{k=1}^{N} \frac{\eta^{kI}(t)}{\langle \eta^{kI} | \eta^{kI} \rangle^{\frac{1}{2}}} \tag{5.2}$$

Here the secondary region amplitude $\eta^I(t)$ in Eq.(4.26) of the previous chapter is written as a product over k, and the amplitude $\eta^{kI}(t)$ corresponds to the kth normal mode motion in the secondary region dynamics. The time-dependent effective frequency operator $\hat{\Omega}^p_{eff}(t)$ for the primary region dynamics is given by

$$\hat{\Omega}_{eff}^p(t) = \frac{1}{\hbar}[\hat{H}^p - E_I^p + \sum_k \{p_k(t,[\eta])\,\lambda_{kX}\hat{P}_X$$
$$+ V^k(\hat{X})\,q_k(t,[\eta]) + \frac{1}{2}V^{kk}(\hat{X})\,q_k^2(t,[\eta]) \qquad (5.3)$$
$$\frac{1}{2}\sum_{k\neq k'}q_{k'}(t,[\bar\eta])\,V^{k'k}(\hat{X})q_k(t,[\eta]) - E_I^{pk}\}]$$

where we have omitted specific indices within the functional dependence for notational brevity, and on the ith potential energy surface we have written the stationary state eigenvalue E_I as $E_I = E_I^p + E_I^s + E_I^{ps}$, with $E_I^s = \sum_k E_I^k$, and $E_I^{ps} = \sum_k E_I^{pk}$. The time-dependent coefficients, which couple the primary region dynamics to the normal mode motions in the secondary region, are the normalized expectation values of the corresponding operators within the amplitudes coresponding to the secondary region dynamics. For example, the coefficient $q_k^2(t,[\eta])$ is of the form

$$q_k^2(t,[\eta]) = \frac{\langle \eta^{kI}|\hat{Q}_k^2|\eta^{kI}\rangle}{\langle \eta^{kI}|\eta^{kI}\rangle} \qquad (5.4)$$

The time-dependent effective frequency operator $\hat{\Omega}_{eff}^s(t)$ for the motion in the secondary region dynamics is given by

$$\hat{\Omega}_{eff}^s(t) = \sum_k \hat{\Omega}_{eff}^k(t) \qquad (5.5)$$

where the effective frequency operator for the kth normal mode motion in the secondary region is written as

$$\hat{\Omega}^k_{eff}(t) = \frac{1}{\hbar}[\frac{\hat{P}^2_k}{2m_k} + \frac{1}{2}m_k\bar{\omega}^2_k(t,[\xi])\,\hat{Q}^2_k + \hat{P}_k\lambda_{kX}p_X(t,[\xi])$$
$$+ \bar{v}^k(t,[\xi,\bar{\eta}])\,\hat{Q}_k + \bar{\mathcal{E}}^k(t,[\xi,\bar{\eta}]) - E^k_I - E^{pk}_I] \quad (5.6a)$$

where $\bar{\eta}$ means any $\eta_{k'}$ with $k' \neq k$. The time-dependent effective frequency $\bar{\omega}_k(t,[\xi])$, the effective force $\bar{v}^k(t,[\xi,\bar{\eta}])$, and the effective energy $\bar{\mathcal{E}}^k(\mathrm{t},[\xi,\bar{\eta}])$ between the kth normal mode in the harmonic bath, the primary region, and the rest of secondary region, are written as

$$\bar{\omega}_k(t,[\xi]) = \left\{\omega^2_k + \frac{v^{kk}(t,[\xi])}{m_k}\right\}^{\frac{1}{2}} \quad (5.6b)$$

$$\bar{v}^k(t,[\xi]) = v^k(t,[\xi]) + \frac{1}{2}\sum_{k'\neq k}\left\{v^{k'k}(t,[\xi]) + v^{kk'}(t,[\xi])\right\}q_{k'}(t,[\bar{\eta}]) \quad (5.6c)$$

$$\bar{\mathcal{E}}^k(t,[\xi,\bar{\eta}]) = \sum_{k'\neq k}\{p_{k'}(t,[\eta])\,\lambda_{k'X}p_X(t,[\xi])$$
$$+ v^{k'}(t,[\xi])\,q_{k'}(t,[\bar{\eta}]) + \frac{1}{2}v^{k'k'}(t,[\xi])\,q^2_{k'}(t,[\bar{\eta}]) \quad (5.6d)$$
$$+ \frac{1}{2}\sum_{k''\neq k'\neq k}q_{k''}(t,[\bar{\eta}])\,v^{k''k'}(t,[\xi])\,q_{k'}(t,[\bar{\eta}])\}$$

The time-dependent coefficients that couple the kth mode of the secondary region to the primary region dynamics are defined, for example, by

$$v^{k'k}(t, [\xi]) = \frac{\langle \xi^I | V^{k'k}\left(\hat{X}\right) | \xi^I \rangle}{\langle \xi^I | \xi^I \rangle} \tag{5.6e}$$

The time-dependent effective phase $\alpha(t, [\eta, \xi])$, defined in Eq.(4.29d) and needed to compute the total TCF $\widetilde{F}_{\hat{D}, \hat{D}}(t)$ in Eq.(4.29a), is given by

$$\begin{aligned}
\alpha\left(t, [\xi, \eta]\right) = \frac{1}{\hbar} \int\limits_0^t dt' \sum_k \{ & p_k\left(t', [\eta]\right) \lambda_{kX} p_X\left(t', [\xi]\right) \\
& + v^k\left(t', [\xi]\right) q_k\left(t', [\eta]\right) + \frac{1}{2} v^{kk}\left(t', [\xi]\right) q_k^2\left(t, [\eta]\right) \\
& + \frac{1}{2} \sum_{k' \neq k} q_{k'}\left(t', [\eta]\right) v^{k'k}\left(t', [\xi]\right) q_k\left(t, [\eta]\right) \}
\end{aligned} \tag{5.7}$$

The form of the effective frequency operator $\hat{\Omega}^k_{eff}(t)$ in Eq.(5.6) for the kth mode of the secondary region dynamics, is that of a linearly forced parametric oscillator. Operators $\hat{Q}_k(t)$ and $\hat{P}_k(t)$, corresponding to the kth mode motion in the secondary region dynamics, evolve according to the following equations of motion

$$\dot{\hat{Q}}_k = i \left[\hat{\Omega}^k_{eff}(t), \hat{Q}_k \right]_c \tag{5.8a}$$

$$\dot{\hat{P}}_k = i \left[\hat{\Omega}^k_{eff}(t), \hat{P}_k \right]_c \tag{5.8b}$$

where $[...]_c$ are quantum commutators. Using $\hat{\Omega}^k_{eff}(t)$ from Eq.(5.6a), it is easy to show that $\hat{Q}_k(t)$ satisfies

$$\ddot{\hat{Q}}_k + \bar{\omega}_k^2(t)\,\hat{Q}_k = \frac{\lambda_k X \dot{p}_X(t) - \bar{v}^k(t)}{m_k} \tag{5.9}$$

where we have dropped the functional dependence on ξ and $\bar{\eta}$ for notational convenience. Equation (5.9) is the equation of motion of a linearly forced parametric oscillator, therefore we solve it by separating it into a homogeneous equation and a nonlinear forcing term. We are using this approach, because it is suitable for application to computations in the complex time plane, and also because it is useful in deriving a parallel between the TDSCF dynamics and the GLE approach to stochastic dynamics.

We introduce $u_k(t)$ and $v_k(t)$, two linearly independent solutions of the homogeneous equation

$$\left[\frac{d^2}{dt^2} + \bar{\omega}_k^2(t)\right]\left\{\begin{matrix} u_k(t) \\ v_k(t) \end{matrix}\right\} = 0 \tag{5.10}$$

with the initial conditions $u_k(0) = 0$, and $v_k(0) = 1$. The full solution to the operator Eq.(5.9) is written as

$$\hat{Q}_k(t) = \hat{Q}_k(0)\,v_k(t) + \frac{\hat{P}_k(0)}{m_k\omega_k}u_k(t) + y_k(t) \tag{5.11a}$$

where $\hat{Q}_k(0)$ and $\hat{P}_k(0)$ are, respectively, the initial values of the operators $\hat{Q}_k(t)$ and $\hat{P}_k(t)$ at the initial time $t = 0$, and the the last term $y_k(t)$ is an integral of the form

$$y_k(t) = \frac{1}{m_k\omega_k}\int_0^t dt'\left\{\lambda_k X \dot{p}_X(t') - \bar{v}^k(t')\right\}u_k(t - t') \tag{5.11b}$$

Using equations (5.11a) and (5.11b) with the definitions in Eq.(5.4) for the time-dependent coffecients of the coupling between the primary and the secondary region dynamics, we express the coefficients needed to compute the effective frequency operator $\hat{\Omega}^p_{eff}(t)$ for the primary region dynamics as

$$q_k(t) = q_k(0) v_k(t) + \frac{p_k(0)}{m_k \omega_k} u_k(t) + y_k(t) \tag{5.12a}$$

$$p_k(t) = \frac{p_k(0)}{\omega_k} \dot{u}_k(t) + m_k q_k(0) \dot{v}_k(t) + m_k \dot{y}_k(t) - \lambda_{kX} m_k p_X(t) \tag{5.12b}$$

$$q_k^2(t) = q_k^2(0) v_k^2(t) + \frac{p_k^2(t)}{m_k^2 \omega_k^2} u_k^2(t) + y_k^2(t) \\ + 2 \left\{ q_k(0) v_k(t) + \frac{p_k(0)}{m_k \omega_k} u_k(t) \right\} y_k(t) \tag{5.12c}$$

where the initial values $q_k(0)$, $p_k(0)$, and $q_k^2(0)$ are defined as according to

$$q_k^2(0) = \frac{\langle \eta^{kI}(0) | \hat{Q}_k^2 | \eta^{kI}(0) \rangle}{\langle \eta^{kI}(0) | \eta^{kI}(0) \rangle} \tag{5.12d}$$

At any time t the time-dependent effective frequency operator $\hat{\Omega}^p_{eff}(t)$ depends upon the previous history of the primary and the secondary region dynamics through the term $y_k(t)$, which involves integral of the nonlinear forcing term from 0 to t, therefore, in our TDSCF approach we refer to $y_k(t)$ as a "memory" term. Furthermore, in a later section of this chapter, we show a direct relationship between the TDSCF approach and the GLE approach to stochastic dynamics, by deriving a

fluctuation-dissipation relationship between the memory kernel and the fluctuation force.

It appears from Eq.(5.11b), that the computation of the memory term $y_k(t)$ at any time t, involves knowing the integrand at all previous times $t' < t$, as well as at the present time $t' = t$. It is, however, not difficult to see that the choice of the initial conditions, $u_k(0) = 0$ and $v_k(0) = 1$, for the solutions of the homogeneous Eq.(5.10), make the integrand in the memory term $y_k(t)$ equal to zero at $t' = t$. Therefore, this choice of the initial conditions is significant in the sense that it enables us to perform the TDSCF computation, for a nonlinearly coupled primary and the secondary regions dynamics, without going through iterations at each time. In other words, these initial conditions have made it possible to perform our computations in a step by step progression along a desired axis in the complex time plane, while at the same time maintaining the self-consistency in the dynamics.

We also note that the linearly independent solutions $u_k(t)$ and $v_k(t)$ which satisfy the homogeneous Eq.(5.10) for the kth normal mode motions in the secondary region, are completely independent of the simultaneous solutions $u_{k'}(t)$ and $v_{k'}(t)$ for all $k' \neq k$. Therefore, for any secondary region made up of N coupled harmonic oscillators, we have to simultaneously solve only $2N$ uncoupled homogeneous equations of motion to achieve the self-consistent solution of the full dynamics.

The initial values $q_k(0)$, and $p_k(0)$ defined as according to Eq.(5.12d), are the normalized expectation values of the corresponding operators within the amplitude $\eta^{kI}(0)$. They can also be thought of as the mean position and momentum corresponding to the kth normal mode motion in the secondary region dynamics. If the secondary region is initially prepared at thermal equilibrium in the presence of the primary region, then we can use a suitable thermal distribution for these ini-

tial values to introduce a temperature dependence in the dynamics of the primary region operators.

We end this section by using equations (5.5–5.6) for the definition of the effective frequency operator $\hat{\Omega}^k_{eff}(t)$ for the kth mode motions in the secondary region dynamics, and equations (5.11–5.12) as the solutions for the operator Eq.(5.9), to construct the propagator for the kth mode motion in the secondary region dynamics [Yamashita and Miller, 85] as

$$
K^k\left(\hat{Q}_k, \hat{Q}'_k, t\right) = \left(\frac{m_k\omega_k}{2\pi i\hbar u_k(t)}\right)^{\frac{1}{2}} exp[\ \frac{im_k}{2\hbar u_k(t)}\times
$$

$$
\{(\hat{Q}_k^2 + \hat{Q}_k'^2)v_k(t) - 2\hat{Q}_k\hat{Q}'_k - \frac{2\hat{Q}_k}{m_k\omega_k}\int\limits_0^t f_k(t')\,u_k(t')\,dt'
$$

$$
- \frac{2\hat{Q}'_k}{m_k\omega_k}\int\limits_0^t f_k(t')\,u_k(t-t')\,dt' \tag{5.13a}
$$

$$
- \frac{2}{m_k^2\omega_k^2}\int\limits_0^t f_k(t')\,u_k(t-t')\,dt'\int\limits_0^{t'} f_k(t'')\,u_k(t'')\,dt''\ \}
$$

$$
+ \frac{i}{\hbar}\left(E^k_J + E^{pk}_J\right)t\ ]
$$

where the effective force $f_k(t)$, in the integrand, is given by

$$
f_k(t) = m_k\lambda_{kX}\dot{p}_X(t) - \bar{v}^k(t) \tag{5.13b}
$$

and the time evolution of the amplitude corresponding to the kth normal mode motion in the secondary region dynamics is described by

$$
\eta^{kI}(Q_k, t) = \int\limits_{-\infty}^{+\infty} dQ'_k\ \langle Q_k|K^k\left(\hat{Q}_k, \hat{Q}'_k, t\right)|Q'_k\rangle\ \eta^{kI}(Q'_k, 0) \tag{5.14}
$$

This is about as far as one can proceed in general, i.e. without numerically solving the homogeneous Eq.(5.10) for a given process.

5.2. Intermolecular Processes: Weak Coupling Limit

Intermolecular photointeraction processes such as overtone line broadening, dephasing, and energy transfer in an extended molecular system, following a localized absorption of light in the visible and UV region, are often described by the time evolution of a localized primary region, interacting weakly with a collection of coupled harmonic normal mode motions in the secondary region. In the formulation of the previous section, we drop the bilinear coupling terms, and keep the term which is linear in the operator dependence of the secondary region dynamics and has an arbitrary analytic form in the operator dependence of the primary region. In other words, the effective frequency operator $\hat{\Omega}^p_{eff}(t)$ for the primary region dynamics simplifies to

$$\hat{\Omega}^p_{eff}(t) = \frac{1}{\hbar} \left[\hat{H}^p - E^p_I + \sum_k \left\{ V^k\left(\hat{X}\right) q_k\left(t,[\eta]\right) - E^{pk}_I \right\} \right] \quad (5.15)$$

where the effective coupling of the primary to the secondary region is also defined by the example in Eq.(5.4). The time-dependent effective frequency operator for the kth mode of the secondary region simplifies to

$$\hat{\Omega}^k_{eff}(t) = \frac{1}{\hbar} \left[\frac{\hat{P}^2_k}{2m_k} + \frac{1}{2} m_k \omega^2_k \hat{Q}^2_k + v^k\left(t,[\xi]\right) \hat{Q}_k - \left(E^k_I - E^{pk}_I\right) \right] \quad (5.16)$$

and the time-dependent effective phase needed to compute the total TCF is written as

$$\alpha\left(t,[\xi,\eta]\right) = \sum_k \int_0^t dt' \left\{ v^k\left(t,[\xi]\right) q_k\left(t,[\eta]\right) - E_I^{pk} \right\} \qquad (5.17)$$

The form of the operator in Eq.(5.16) is that of a linearly forced harmonic oscillator. It is not very difficult to see that the homogeneous Eq.(5.10) for the functions $u_k(t)$, and $v_k(t)$ reduces to the equation of motion for a harmonic oscillator with frequency ω_k and mass m_k. Therefore, the functions $u_k(t)$ and $v_k(t)$ with the initial conditions, $u_k(0) = 0$ and $v_k(0) = 1$, simply reduce to $u_k(t) = \sin(\omega_k t)$ and $v_k(t) = \cos(\omega_k t)$, respectively. The time-dependent effective coupling $q_k(t,[\eta])$, which couples the primary region dynamics to the kth mode motions in the secondary region dynamics is given by

$$q_k\left(t\right) = q_k\left(0\right)\cos\omega_k t + \frac{p_k\left(0\right)}{m_k\omega_k}\sin\omega_k t + y_k\left(t\right) \qquad (5.18)$$

where the "memory" term $y_k(t)$ for the weak coupling case simplifies to

$$y_k\left(t\right) = -\frac{1}{m_k\omega_k}\int_0^t dt'\, v^k\left(t'\right)\sin\omega_k\left(t-t'\right) \qquad (5.19)$$

Here again, we notice that the computations for the memory term in Eq.(5.19) involve the time dependence in the effective potential $\bar{v}_j^k(t)$ only for the previous times $t' < t$. Therefore, the TDSCF computations for the primary region dynamics can be performed in a step by step progression along any chosen time axis.

Finally, the propagator for the secondary region dynamics, in the weak coupling case, is expressed in an analytic form as [Schulman, 81]

$$K^k \left(\hat{Q}_k, \hat{Q}'_k, t \right) = \left(\frac{m_k \omega_k}{2\pi i \hbar \sin \omega_k t} \right)^{\frac{1}{2}} exp[\frac{i m_k}{2 \hbar \sin \omega_k t} \{ \left(\hat{Q}_k^2 + \hat{Q}_k'^2 \right) \cos \omega_k t$$

$$- 2 \hat{Q}_k \hat{Q}'_k - \frac{2 \hat{Q}_k}{m_k \omega_k} \int_0^t dt' v^k \left(t' \right) \sin \omega_k t' - \frac{2 \hat{Q}'_k}{m_k \omega_k}$$

$$\times \int_0^t dt' v^k \left(t' \right) \sin \omega_k \left(t - t' \right) - \frac{2}{m_k^2 \omega_k^2} \qquad (5.20)$$

$$\times \int_0^t dt' v^k \left(t' \right) \sin \omega_k \left(t - t' \right) \int_0^{t'} dt'' v^k \left(t'' \right) \sin \omega_k t'' \}$$

$$+ \frac{i}{\hbar} \left(E_I^k + E_I^{pk} \right) t \ ]$$

5.2. Relationship to the Generalized Langevin Equation Approach

The method of factoring the dynamics of a large molecular system into a "primary region" consisting of a few important degrees of freedom, interacting with the rest of the system labeled as the "secondary region", is well known in statistical mechanics, where one often needs to deal with the dynamics of a "system" in thermal equilibrium with a large heat reservoir called "bath". Among many different approaches to deal with the factorization of a large system into coupled primary and secondary region dynamics, the approach based on the Generalised Langevin Equation (GLE) [Mori, 1965], solving it under different approximations for the primary region dynamics, is well covered in the literature. The terms which affect the dynamics of primary region variable, due to the coupling with a large heat reservoir, are the "fluctuation force" term and the "memory" term. The form of the fluctuation force term is decided by the dynamical and the statistical properties of the secondary region, and depends largely upon the way the secondary region is brought to a thermal equilibrium in the presence of the primary region.

If the primary region is coupled to an infinite heat reservoir for a sufficiently long time, the primary region also attains a steady state due to a relationship between the memory kernel and the fluctuation force, this relationship is often referred to as the Fluctuation-Dissipation Theorem [Van Hove, 54; Berne, 71]. The GLE is a stochastic differential equation with additive fluctuation force and dissipative memory terms.

Starting with the time-dependent effective frequency operator $\hat{\Omega}^p_{eff}(t)$ in Eq.(5.15), we derive an operator equation for the primary region dynamics, show its relationship with the GLE by constructing the fluctuation force and the memory kernel terms, and finally derive the Fluctuation-Dissipation Relationship(FDR) for our TDSCF dynamics.

The time evolution of the operators $\hat{X}$ and $\hat{P}_X$ for the primary region dynamics is described by the following operator equations

$$\dot{\hat{X}} = i \left[\hat{\Omega}^p_{eff}(t), \hat{X} \right]_c \qquad (5.21a)$$

$$\dot{\hat{P}}_X = i \left[\hat{\Omega}^p_{eff}(t), \hat{P}_X \right]_c \qquad (5.21b)$$

Using Eq.(5.15) for the effective frequency operator, Eq.(5.21b) is written as

$$\dot{\hat{P}}_X = \frac{i}{\hbar} \left[V^0\left(\hat{X}\right), \hat{P}_X \right]_c + \sum_k \frac{i}{\hbar} \left[V^k\left(\hat{X}\right), \hat{P}_X \right]_c q_k(t) \qquad (5.22)$$

where we avoid the functional dependence in $q_k(t)$ for notational simplicity. From Eq.(5.18) the effective coupling $q_k(t)$ is written as

$$q_k(t) = \left(q_k(0) + \frac{1}{m_k\omega_k}v^k(0)\right)\cos\omega_k t + \frac{p_k(0)}{m_k\omega_k}\sin\omega_k t$$

$$-\frac{v^k(t)}{m_k\omega_k} - \frac{1}{m_k\omega_k^2}\int\limits_0^t dt'\dot{v}^k(t')\cos\omega_k(t-t') \quad (5.23)$$

where we have used integration by parts in the memory term in Eq.(5.19), and substituted the result in Eq.(5.18). Using Eq.(5.23) in Eq.(5.22) and rearranging the result we get

$$\dot{P}_X - i\left[\hat{\Omega}^{Mod}\left(\hat{X},\hat{P}_X,t\right),\hat{P}_X\right]_c = \sum_k \{ \frac{1}{\hbar^2}\left[V^k\left(\hat{X}\right),\hat{P}_X\right]_c$$

$$\times \int\limits_0^t dt'\frac{\left\langle\left[V^k\left(\hat{X}\right),\hat{P}_X^2\right]_c\right\rangle}{2m_k m_X\omega_k^2}\cos\omega_k(t-t')$$

$$+ R_k(t) \} \quad (5.24)$$

where the commutator involving the modified frequency operator $\hat{\Omega}_j^{Mod}(t)$ given by

$$\hat{\Omega}^{Mod}\left(\hat{X},\hat{P}_X,t\right) = \frac{1}{\hbar}\left[\frac{\hat{P}_X^2}{2m_X} + V^k\left(\hat{X}\right) - \sum_k\frac{v^k(t)}{m_k\omega_k^2}V^k\left(\hat{X}\right) - E_I^p\right],$$

$$(5.25a)$$

describes the time-dependence in the uncoupled primary region dynamics in the presence of a stationary secondary region, and the fluctuation force $R_k(t)$ is given by

$$R_k(t) = \frac{i}{\hbar}\left[V^k\left(\hat{X}\right),\hat{P}_X\right]_c\left\{\left(q_k(0) + \frac{v^k(0)}{m_k\omega_k}\right)\cos\omega_k t + \frac{p_k(0)}{m_k\omega_k}\sin\omega_k t\right\}.$$

$$(5.25b)$$

The integrand in Eq.(5.23) has been simplified to the form in Eq.(5.24) by using the equation of motion of the operator $V^k(\hat{X})$ to write

$$\dot{v}^k = \frac{i}{\hbar} \left\langle \left[V^k\left(\hat{X}\right), \frac{\hat{P}_X^2}{2m_X} \right]_c \right\rangle \qquad (5.25c)$$

with

$$\langle [...]_c \rangle = \frac{\langle \xi(0) | [...]_c | \xi(0) \rangle}{\langle \xi(0) | \xi(0) \rangle} \qquad . \qquad (5.25d)$$

The form of Eq.(5.24), a general operator equation for the primary region dynamics in the presence of a weakly coupled secondary region, is an analogue of the GLE in our TDSCF approach. We have considered a coupling which is linear in the variables of the secondary region, and has a general analytic form $V^k(\hat{X})$ in the variables of the primary region. Therefore, Eq.(5.24) for the primary region dynamics in our TDSCF approach is more general than the usual GLE given in the literature. As an example, we consider a simple case of $V^k(\hat{X}) = \Gamma_k \hat{X}$, with Γ_k a free force constant, and use this in Eq.(5.24) to write it as

$$\dot{\hat{P}}_X - i \left[\hat{\Omega}^{Mod}\left(\hat{X}, \hat{P}_X, t\right), \hat{P}_X \right]_c - \int_0^t dt' M\left(t - t'\right) \left\langle \frac{\hat{P}_X}{m_X} \right\rangle = R(t) \qquad (5.26)$$

where

$$M\left(t - t'\right) = \sum_k M_k\left(t - t'\right) \qquad (5.27a)$$

and

$$R\left(t - t'\right) = \sum_k R_k\left(t - t'\right) \tag{5.27b}$$

with

$$M_k\left(t - t'\right) = \frac{\Gamma_k^2}{m_k\omega_k}\cos\omega_k\left(t - t'\right) \tag{5.28a}$$

and

$$R_k\left(t\right) = \Gamma_k\left\{\left(q_k\left(0\right) + \frac{\Gamma_k}{m_k\omega_k^2}x\left(0\right)\right)\cos\left(\omega_k t\right) + \frac{p_k\left(0\right)}{m_k\omega_k}\sin\left(\omega_k t\right)\right\} \tag{5.28b}$$

respectively. Equation (5.26) is the analogue of the usual GLE for a bilinearly coupled system-bath problem, where the fluctuation force term $R(t)$ and the memory kernel $M(t-t')$ are given in Eqs(5.27a) and (5.27b), respectively. It is not difficult to see that the primary region dynamics depends upon the initial values of the secondary region operators $\hat{Q}_k(0)$ and $\hat{P}_k(0)$ only through the fluctuation force term $R(t)$, which contains the normalized expectation values $q_k(0)$ and $p_k(0)$, given for example by

$$q_k\left(0\right) = \frac{\left\langle\eta^k\left(0\right)\left|\hat{Q}_k\left(0\right)\right|\eta^k\left(0\right)\right\rangle}{\left\langle\eta^k\left(0\right)\left|\eta^k\left(0\right)\right\rangle\right.} \tag{5.29}$$

Therefore, the fluctuation force term $R(t)$ can be given a stochastic interpretation by observing that these expectation values are described by a distribution function which depends upon the initial temperature of the system. If the initial state of the secondary region is an equilibrium state, then the distribution of all the bath operators is the same and consequently $R(t)$ is Gaussian (Central Limit Theorem). The mean value of the resulting Gaussian depends upon the form of the distribution function. If initially the secondary region has been brought to the equilibrium in the

presence of the primary region, a suitable choice of the distribution function, which give the mean value of the fluctuation force equal to zero, is a displaced Boltzman distribution function [Zwanzig, 73; Lindenberg and Seshadri, 82] expressed as

$$W(\mathbf{q}(0), \mathbf{p}(o)), \beta) = \frac{1}{Z^s} \exp(-\beta \sum_k [\frac{p_k^2(0)}{2m_k} + \frac{1}{2} m_k \omega_k^2 \{q_k(o) + \frac{\Gamma_k}{m_k \omega_k^2} x(o)\}^2])$$
(5.30)

The thermal averaged correlation function of the force term $R(t)$ then is written as

$$\langle R(t) R(t') \rangle_{en} = \sum_k \sum_{k'} \int d\mathbf{q}(0) \int d\mathbf{p}(0) \; W(\mathbf{q}(0), \mathbf{p}(0)), \beta)$$
$$\times R_k(q_k(0), p_k(0), t) \, R_{k'}(q_{k'}(0), p_{k'}(0), t)$$
(5.31)

where $R_k(q_k(0), p_k(0), t)$ and $R_{k'}(q_{k'}(0), p_{k'}(0), t')$ are as defined in Eq.(5.28b). Using the distribution function $W(\mathbf{q}(0), \mathbf{p}(0))$ in Eq.(5.31), we obtain the correlation function of the fluctuation force

$$\left\langle R(t) \, R(t') \right\rangle_{en} = k_B T \sum_k \frac{\Gamma_k^2}{m_k \omega_k^2} \cos \omega_k \left(t - t'\right)$$
(5.32)

which is the same as

$$\left\langle R(t) \, R(t') \right\rangle_{en} = k_B T \, M \left(t - t'\right) \quad .$$
(5.33)

This shows a FDR between the memory kernel $M(t - t')$ and the fluctuation force $R(t)$. For the more general operator equation in (5.24) for the primary region dynamics, we get a similar relationship between the memory kernel and the fluctuations in the force.

5.4. Treatment of Many Degrees of Freedom in the Primary Region Dynamics

To treat many degrees of freedom $l = 1 \, to \, L$ in the primary region dynamics, we generalize the Hamiltonian operators of section 5.1, and write

$$\hat{H}^p = \sum_{l=1}^{L} \frac{\hat{P}_l^2}{2m_l} + V^0(\hat{\mathbf{X}}) \, , \tag{5.34a}$$

$$\hat{H}^s = \sum_{k=1}^{N} \frac{\hat{P}_k^2}{2m_k} + \frac{1}{2}m_k\omega_k^2\hat{Q}_k^2 \quad , \tag{5.33b}$$

$$\hat{H}^{ps} = \sum_k \{ \sum_l \hat{P}_k\lambda_{kl}\hat{P}_l + V^k(\hat{\mathbf{X}})\hat{Q}_k - \frac{1}{2}\sum_{k'\neq k}\hat{Q}_k V^{k'k}(\hat{\mathbf{X}})\hat{Q}_k \} \tag{5.33c}$$

where $\hat{\mathbf{X}} = \{\hat{X}_1, \hat{X}_2, ...\hat{X}_L\}$ are the operators of position variables of the primary region, and k runs over all the harmonic modes in the secondary region dynamics. Using the TDSCF approximation

$$\Upsilon^I = N_I^{\frac{1}{2}} \frac{\xi^I(\mathbf{X})}{\langle \xi^I \mid \xi^I \rangle^{\frac{1}{2}}} \prod_k \frac{\eta^{kI}(Q_k)}{\langle \eta^{kI} \mid \eta^{kI} \rangle^{\frac{1}{2}}} \exp(i\alpha(t)) \tag{5.34}$$

the time-dependent frequency operator for the primary region dynamics is given by

$$\hat{\Omega}^p_{eff}(t) = \frac{1}{\hbar}[\hat{H}^p - E_I^p + \sum_k \{ \sum_l p_k(t)\lambda_{kl}\hat{P}_l \\ + q_k(t)V^k(\hat{\mathbf{X}}) + \frac{1}{2}q_k^2(t)V^{kk}(\hat{\mathbf{X}}) \\ \frac{1}{2}\sum_{k'\neq k} q_{k'}(t)V^{k'k}(\hat{\mathbf{X}})q_k(t) - E_I^{kp} \}] \tag{5.35}$$

and the time-dependent effective frequency operator for the kth mode of the secondary region dynamics is given by

$$\hat{\Omega}^k_{eff}(t) = \frac{1}{\hbar}[\frac{\hat{P}_k^2}{2m_k} + \frac{1}{2}m_k\bar{\omega}_k^2(t)\hat{Q}_k^2 + \sum_l \left\{ \hat{P}_k\lambda_{kl}p_l(t) \right\} \\ + \bar{v}^k(t)\hat{Q}_k + \bar{\mathcal{E}}^k(t) - E_I^k - E_I^{kp}] \tag{5.36a}$$

with

$$\bar{\omega}_k = \left[\omega_k^2 + \frac{v^{kk}(t)}{m_k}\right]^{\frac{1}{2}} \tag{5.36b}$$

$$\bar{v}^k(t) = v^k(t) + \frac{1}{2}\sum_{k'\neq k}\left\{v^{k'k}(t) + v^{kk'}(t)\right\}q_{k'}(t) \tag{5.36c}$$

$$\bar{\mathcal{E}}^k(t) = \sum_{k'\neq k}\{\sum_l p_{k'}(t)\,\lambda_{k'l}p_l(t) + v^{k'}(t)\,q_{k'}(t)$$
$$\frac{1}{2}\sum_{k''\neq k'\neq k}q_{k''}(t)\,v^{k''k'}(t)\,q_{k'}(t)\ \} \tag{5.36d}$$

where the time-dependent coefficients of the coupling between the primary and the secondary region dynamics are defined as in sections 5.1 and 5.2. The effective frequency operator for the kth mode of the secondary region dynamics is still similar to that of an operator for a linearly forced parametric oscillator. Therefore, the solution to the equations of motions for the secondary region dynamics, obtained as described in section 5.1 and substituted in Eq.(5.36), give the multi-variable time-dependent frequency operator $\hat{\Omega}_{eff}^p(t)$. One can use Eq. (5.35) to deal with the dynamics of a multi-variable primary region coupled to a harmonic secondary region. If, however, the computations of a complex time propagator in two or three dimensions are prohibitive, a further simplification is achieved by using an SCF assumption for the primary region, so that

$$\frac{\xi^I(\mathbf{X})}{\langle\xi^I\mid\xi^I\rangle^{\frac{1}{2}}} = \prod_l\frac{\xi^{II}(X_l)}{\langle\xi^{II}\mid\xi^{II}\rangle^{\frac{1}{2}}} \tag{5.37}$$

in Eq.(5.34) to write the TDSCF approximation as

$$\Upsilon^I = N_I^{\frac{1}{2}} \prod_l \frac{\xi^{lI}(X_l)}{\langle \xi^{lI} \mid \xi^{lI} \rangle^{\frac{1}{2}}} \prod_k \frac{\eta^{kI}(Q_k)}{\langle \eta^{kI} \mid \eta^{kI} \rangle^{\frac{1}{2}}} \exp(i\alpha(t)) \qquad (5.38)$$

The time-dependent effective frequency operator for the primary region dynamics is then written as

$$\hat{\Omega}_{eff}^p(t) = \sum_l \hat{\Omega}_{eff}^l(t) \qquad (5.39a)$$

with

$$\begin{aligned}
\hat{\Omega}_{eff}^l(t) = \frac{1}{\hbar} \Big[\; & \frac{\hat{P}_l^2}{2m_l} + v^0\left(\hat{X}_l, t\right) + \sum_k \{ \; p_k(t) \lambda_{kl} \hat{P}_l \\
& + v^k\left(\hat{X}_l, t\right) q_k(t) + \frac{1}{2} v^{kk}\left(\hat{X}_l, t\right) q_k^2(t) \\
& + \frac{1}{2} \sum_{k' \neq k} q_{k'}(t) v^{k'k}\left(\hat{X}_l, t\right) q_k(t) \\
& + \sum_{l' \neq l} p_k(t) \lambda_{kl'} p_{l'}(t) - E_I^{lk} \} - E_I^l \; \Big] \qquad (5.39b)
\end{aligned}$$

where $v^0(\hat{X}_l, t), v^k(\hat{X}_l, t)$ and $v^{k'k}(\hat{X}_l, t)$ are defined for example by

$$v^{k'k}(\hat{X}_l, t) = \frac{\langle \ldots \xi^{(l-1)I} \xi^{(l+1)I} \ldots \mid V^{k'k}(\hat{\mathbf{X}}) \mid \ldots \xi^{(l-1)I} \xi^{(l+1)I} \ldots \rangle}{\langle \ldots \xi^{(l-1)I} \xi^{(l+1)I} \ldots \mid \ldots \xi^{(l-1)I} \xi^{(l+1)I} \ldots \rangle} \qquad (5.39c)$$

The effective frequency operator for the motion along the lth degree of freedom of the primary region can be used to compute its complex time propagator, and the computational efforts for the full primary region propagator scales linearly with the number of degrees of freedom in the primary region dynamics, instead of quadratically, as would happen if no SCF assumption was made for the primary region dynamics.

CHAPTER 6
PATH-INTEGRAL APPROACH TO THE PRIMARY REGION DYNAMICS

The path-integral approach to the primary region dynamics is described mainly by considering the time-evolution of the primary region amplitude $|\xi(t)\rangle$ according to

$$i\frac{\partial}{\partial t}|\xi(t)\rangle = \hat{\Omega}^p(t)\,|\xi(t)\rangle \qquad , \qquad (6.1)$$

where the time-dependent effective frequency operator $\hat{\Omega}^p(t)$ has been described in the previous chapter. We write the integral solution of Eq.(6.1) in coordinate space as

$$\langle X|\xi(t)\rangle = \int\limits_{-\infty}^{+\infty} dX_0\ K^p(X,X_0,t)\ \langle X_0|\xi(0)\rangle \qquad (6.2)$$

where $K^p(X,X_0,t)$, the real time propagator for the primary region dynamics, is written as

$$K^p(X,X_0,t) = \int\limits_{-\infty}^{+\infty} dX_{N-1}...\int\limits_{-\infty}^{+\infty} dX_1 \left\langle X \left| e^{-\hat{\Omega}^p_{N-1}\Delta t}\right| X_{N-1}\right\rangle$$
$$...\left\langle X_1 \left| e^{-\hat{\Omega}^p_0\Delta t}\right| X_0\right\rangle \qquad (6.3)$$

In Eq.(6.3), we have divided the total time t into N short time steps of length $\Delta t = \frac{t}{N}$ where $N \to \infty$. The time-dependence in the frequency operator $\hat{\Omega}^p_i$ during the ith step in time for i going from 0 to $N-1$, is described in Eqs(5.3) and (5.15) of the previous chapter. In the Lagrangian formulation of the propagator the

73

multidimensional integral in Eq.(6.3) is also written as a functional integral, which is equivalent to a summation over all possible paths between the initial and the final positions in coordinate space. The number of all such possible paths is infinite; therefore, since their inception in the early sixties, the path-integral (PI) methods [Feynmann and Hibbs, 65], though very appealing to the physical intuition, have mostly been used as formal devices. In recent years, these methods have also been shown to be a convenient numerical tool in the studies of many-body quantum mechanical systems, and have been used in the computations of imaginary as well as complex time propagators. All of the recently developed numerical approaches to the multidimensional integral in Eq.(6.3), or equivalently to a functional integral in the Lagrangian formalism, are in general separated into two broad groups. Firstly, there are the discretized PI formulations, in the cartesian coordinate space [Thirumalai, Bruskin and Berne, 83], and in the discretized phase space by using the Fast Fourier Transform (FFT) alogorithms [Kosloff and Kosloff, 83; Hellsing, Nitzan and Metiu, 86]. Secondly, there are the Monte Carlo based approaches to the multidimensional integrals; by Fourier Coefficient path-integration (FPI) methods [Coalson, Freeman and Doll, 86], by random walk methods [Miller, Schwartz and Tromp; 83], and by using Metropolis Monte Carlo schemes [Behrman, Jongeward and Wolynes, 83].

In section 6.1, we briefly review a discretized PI formulation in the cartesian coordinate space known as the Numerical Matrix Multiplication (NMM) method [Thirumalai, Bruskin and Berne, 83], and discuss its shortcomings due to which it becomes impractical for use in physical problems involving more than one degree of freedom. Section 6.2 describes the evaluation of the complex time memory term $y(\tau)$ introduced in the previous chapter, and introduces a restricted matrix

multiplication (RMM) method to efficiently compute a complex time propagator for the primary region dynamics. By deforming the integration contour in the complex time plane, we describe in section 6.3 an efficient transformation from real to complex time, and show that the efficiency of the RMM method can further be increased by using this new transformation.

6.1. Numerical Matrix Multiplication (NMM) Method and its Shortcomings

For simplicity, we consider only a Cartesian Hamiltonians in one dimension, i.e, the form of the general Hamiltonian is expressed as

$$\hat{H} = \frac{\hat{P}_X^2}{2m_X} + V\left(\hat{X}\right) \tag{6.4}$$

where m_X is the reduced mass for the degree of freedom along which $\hat{X}$ and $\hat{P}_X$ are the associated position and momentum operators. The solution to the time-dependent Schrodinger equation for the time-independent Hamiltonian of Eq.(6.4) is obtained by writing the coordinate space propagator as

$$K\left(X, X', \beta\right) = \left\langle X \left| e^{-\beta \hat{H}} \right| X' \right\rangle \tag{6.5}$$

where [according to Thirumalai, Bruskin and Berne; 83, and also for simplicity] we are considering the propagator along the imaginary time axis such that $t = -i\beta\hbar$. For a time-independent Hamiltonian, using $\exp(-2\kappa\hat{H}) = \exp(-\kappa\hat{H}).exp(-\kappa\hat{H})$, it is easy to show that

$$K\left(X, X'; 2\kappa\right) = \int\limits_{-\infty}^{+\infty} dX'' \, K\left(X, X''; \kappa\right) \, K\left(X'', X'; \kappa\right) \tag{6.6}$$

Starting with $K(X, X'; \kappa)$, one can iterate Eq.(6.6) N times to get $K(X, X'; 2^N \kappa)$ in terms of $K(X, X'; \kappa)$. If κ is chosen such that $\kappa = \frac{\beta}{2^N}$, then N iterations yield the desired propagator in Eq.(6.5). If N is sufficiently large then κ is small enough to write the short time approximation for $K(X, X'; \kappa)$ as

$$K\left(X, X'; \kappa\right) = \left(\frac{m_X}{2\pi\hbar\kappa}\right)^{\frac{1}{2}} exp\left[-\frac{m_X}{2\hbar^2\kappa}\left(X - X'\right) - \frac{\kappa}{2}\left\{V\left(X\right) + V\left(X'\right)\right\}\right]$$

(6.7)

The infinite integral in Eq.(6.6) is first replaced by a finite integral; this can be done firstly, because the diagonal terms in Eq.(6.7), for which $X' = X$, are exponentially damped by the contributions from the potential energy factor $\exp\{-\kappa V(X)\}$ for large values of X under the presumption that one is dealing with binding potentials, and secondly, because the far off-diagonal terms are damped by the kinetic energy factor $\exp\{-(m_X/2\hbar^2\kappa)(X - X')^2\}$. A grid is constructed of $M+1$ equally spaced points over this finite range. If Δ is the spacing between these equally spaced grid points, and using the trapezoidal rule for the finite integral in the coordinate space, each integration in Eq.(6.6) then becomes a simple numerical matrix multiplication expressed as

$$K\left(i\Delta, j\Delta; 2\kappa\right) = \Delta \sum_{l=1}^{M+1} K\left(i\Delta, l\Delta; \kappa\right) K\left(l\Delta, j\Delta; \kappa\right)$$

(6.8)

where the real positive nature of κ ensures the numerical stability of the procedure.

The advantages of using the NMM for the integral in Eq.(6.6) are its ability to deal with any binding potentials, and the fast convergence towards the final imaginary time $\beta\hbar$ because during each iteration the initial imaginary time κ increases by a factor of 2.

The main disadvantage of the NMM method is that the number of grid points needed to span the appropriate region of a one dimensional potential is typically of the order of 10^2. In one dimension, each NMM step for a 100×100 matrix requiring about 10^6 mathematical operations, is very well within the limits of present day computers. However, if one were simply to extend this procedure to a two dimensional problem, the matrix size of $10^4 \times 10^4$, with each NMM step requiring roughly 10^{12} operations, starts to reach the limits of present day computing capabilities. Therefore, a straightforward extension of the NMM method to physical problems, involving more than one or two degrees of freedom, is impractical. One suggested way of improving upon this is to use some higher order quadrature instead of the simple trapezoidal rule. Given the appropriate weight factors for the selected grid points in the coordinate space, one uses a far smaller number of the total grid points in each NMM step. This improvement, however, has never been implemented in any numerical computations till now, and its usefulness is more in doubt if one is using the NMM method for computing the propagator for a time-dependent Hamiltonian.

Thirumalai and Berne recommend the use of the NMM method only for attractive or binding potentials, because otherwise the number of grid points to effectively sample a repulsive potential in the coordinate space becomes too large. So that even in one dimension this increase in the number of grid points in the NMM procedure is reflected in a quadratic decrease in the computational efficacy of the overall method.

Lastly, the fast convergence to the final imaginary time β for the problem is achieved only for time-independent Hamiltonians; the method as described above does not work for a time-dependent Hamiltonian.

6.2. The Complex Time Propagator for the Primary Region Dynamics

The NMM method for a one dimensional time-independent Hamiltonian, can be easily extended to computations in the complex time plane by replacing in the above description the imaginary time $-i\beta\hbar$ by a complex time $\tau = t - iu\hbar$ with u as a constant real parameter. Therefore, the short imaginary time $\kappa = \frac{-i\beta\hbar}{2^N}$ is replaced by the short complex time $\epsilon = \frac{\tau}{2^N}$. The complex time propagator matrix for one dimensional time-independent Hamiltonian is then written as

$$\mathbf{K}(\tau) = \Delta^{N-1}.\mathbf{K}(\epsilon)^{N-1} \tag{6.9}$$

where if N is sufficiently large and ϵ sufficiently small, the short time approximation for the propagator; $K_{ij}(\epsilon) = K(i\Delta, j\Delta, \epsilon)$, is written as

$$K_{ij}(\epsilon) = \left(\frac{m_X}{2\pi i\hbar\epsilon}\right)^{\frac{1}{2}} D(i-j) \, exp\left[i\frac{2^N m_X}{2\hbar t}\Delta^2 (i-j)^2 + \frac{i\epsilon}{2}(V_i + V_j)\right] \tag{6.10}$$

where Δ is the spacing between any two successive grid points in a $(M+1) \times (M+1)$ matrix over a range R given by $R = M\Delta$, and V_i and V_j are the potentials at the ith and the jth grid points respectively. The contributions from the decay factor $D(i-j)$, given by

$$D(i-j) = exp\left[-\frac{2^{N-1}m_X\Delta^2}{u}(i-j)^2\right] \quad , \tag{6.11}$$

are equal to one for the on-diagonal terms for which $i = j$, and decay rapidly as $exp(-C(i-j)^2)$ for $i \neq j$, where the decay constant C depends upon the choice of the parameters M and N. The contributions from the off-diagonal terms in the

short time complex matrix $\mathbf{K}(\epsilon)$ can be increased or decreased by decreasing or increasing the value of the decay constant C.

In the TDSCF approach the effective frequency operators, which govern the time-evolution in the primary region dynamics, are time-dependent. Therefore, the NMM method in which the initial complex time ϵ increases by a factor of 2 during each iteration, does not work. However, the complex time-evolution in the primary region amplitude $\xi(X, \tau)$ can still be written in a discretized path-integral formulation by discretizing a finite region in the coordinate space within which the primary region amplitude $\xi(X, \tau)$ evolves on the upper potential energy surface. For a primary region dynamics, evolving with a time-dependent effective frequency operator, the discretized PI formulation is then written as a time-ordered matrix product

$$\mathbf{K}(\tau) = \Delta^{(N-1)} . \mathbf{K}^{(N-1)}(\epsilon) . \mathbf{K}^{(N-2)}(\epsilon) ... \mathbf{K}^{(0)}(\epsilon) \tag{6.12}$$

where $\epsilon = \frac{\tau}{N}$, and $\mathbf{K}^{(l)}(\epsilon)$ is a complex time matrix at the lth step in time with l going from 0 to $N - 1$. The progression from the lth step to the $(l + 1)^{th}$ step is simply a finite complex element matrix multiplication.

We note that the complex time TCF $\widetilde{F}_{\hat{D}, \hat{D}}(\tau)$ and its Fourier transforms $\widetilde{F}_{\hat{D}, \hat{D}}(\omega)$ are computed on a contour along which the the parameter u, which defines the imaginary component of the complex time $\tau = t - iu\hbar$, remains a constant. As shown in Fig.1, the complex time TCF and its Fourier transform are computed along a path $\mathcal{C}$ along which the parameter u remains a constant and the real time t' varies from 0 to $t \to \infty$. To effectively compute the Fourier transform along the path $\mathcal{C}$, one needs complex time TCF for many values of t' between 0 and t. The complex time $\tau' = t' - iu\hbar$ corresponding to each of these values of t' is therefore divided by an integer N and the time-ordered matrix multiplication for

the primary region dynamics is performed at each instant τ_l along the path $\mathcal{C}'$. To complete the discussion about the computations of a complex time propagator for the primary region dynamics, it is natural that we now consider the evaluations of the complex time effective frequency operators along the path $\mathcal{C}'$.

The time-dependence in the effective frequency operator $\hat{\Omega}^p(\tau')$ along a path $\mathcal{C}'$ in the complex time plane, as described in equations (5.3) and (5.15) of the previous chapter, is through the coupling between the primary and secondary region dynamics. For simplicity, we consider intermolecular processes in which the effective coupling at the lth step along $\mathcal{C}'$, is written as

$$q(\tau_l) = q(0)\cos(\omega\tau_l) + \frac{p(0)}{m\omega}\sin(\omega\tau_l) + y(\tau_l) \qquad (6.13a)$$

where the memory term $y(\tau_l)$ is an integral in the complex time plane

$$y(\tau_l) = -\frac{1}{m\omega}\int_0^{\tau_l} dt_c \, v(t_c)\sin\omega(\tau_l - t_c) \qquad (6.13b)$$

and at the lth step $\tau_l = l\epsilon'$ with $\epsilon' = \frac{\tau'}{N}$. Provided the time-dependent effective force $v(t_c)$ is an analytic function in the complex time plane, the value of the complex integral in the memory term is independent of the path $\mathcal{C}'$. Among many possible approaches to the evaluation of the integral in the complex time plane we have successfully used two alternate ways to compute the memory term in Eq.(6.13b).
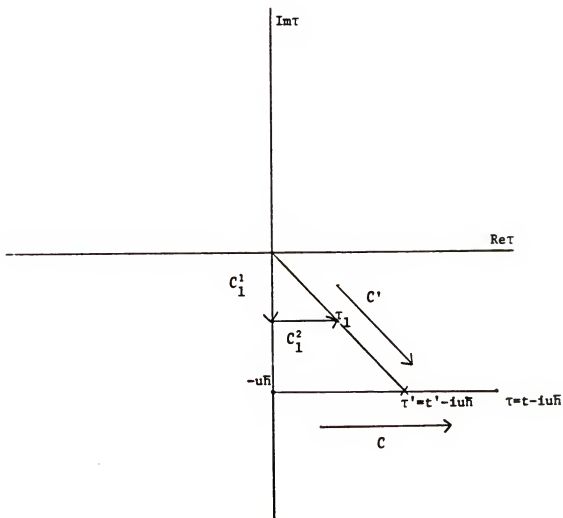
Figure 1. Computations of the primary region propagator in the complex time plane.

The first approach uses the analytic property of the memory term in the complex time plane; according to which, the memory term is first computed along the negative imaginary time $t_c = -iu'\hbar$ for many different values of $0 < u' < u$, and then uses these values at $u' = u_l$ to analytically continuing the memory term to the complex time plane at $\tau_l = t_l - iu_l\hbar$ by using a numerical Pa·de' approximant (Schlessinger's Point Method [Appendix B]) scheme. Numerical analytic continuation for the complex time computations has also been used for computing the Flux-Flux TCFs [Miller et al., 83] for reaction rates , and the dipole-dipole TCFs [Thirumalai and Berne; 83] for spectroscopic properties. However, the numerical analytic continuation methods though accurate for short real time processes, with $t \leq u\hbar$, are not very accurate for physical processes involving long real times $t >> u\hbar$. Therefore, in our second approach to the computations of the integral in Eq.(6.13b), we avoid the numerical analytic continuation and write the integration of the memory term in the complex time plane as a sum of the integrals along the paths $\mathcal{C}_l^1$ and the path $\mathcal{C}_l^2$, i.e

$$\int\limits_0^{\tau_l} (...) \, dt_c = \int\limits_{\mathcal{C}_l^1} (...) \, dt_c + \int\limits_{\mathcal{C}_l^2} (...) \, dt_c \qquad (6.14)$$

where as shown in Fig.1, the path $\mathcal{C}_1^1$ at the real time $t = 0$, along the negative imaginary axis involves a real integral from $0 \rightarrow -iu_l\hbar$, and is followed by the path $\mathcal{C}_1^2$ along which the imaginary time $-iu_l\hbar$ remains constant while the real time varies from $0 \rightarrow t_l$. Substituting in the first term $t_c = -iu'\hbar$, and in the second term $t_c = t' - iu_l\hbar$, the memory term $y(\tau_l)$ in Eq.(6.13b) at the complex time $\tau_l = t_l - iu_l\hbar$ is written as

$$y\left(\tau_l\right) = \frac{1}{m\omega} \int\limits_0^{u_l} du'\, v\left(-iu'\hbar\right) \sinh\omega\left(u_l - u'\right)\hbar$$

$$- \frac{1}{m\omega} \int\limits_0^{t_l} dt'\, v\left(t' - iu_l\hbar\right) \sin\omega\left(t_l - t'\right) \qquad (6.15)$$

and the integrals in the above equation are evaluated numerically. Using the same procedure in the complex integrals in Eq.(5.20), we can also simplify the propagator for the secondary region dynamics as

$$K^s\left(Q, Q', \tau'\right) = \left(\frac{m\omega}{2\pi i\hbar \sin\omega\tau'}\right)^{\frac{1}{2}} exp[\ \frac{im\omega}{2\hbar \sin\omega\tau'}$$
$$\times\ \{\ \left(Q^2 + Q'^2\right)\cos\omega\tau' - 2QQ' - \frac{2Q}{m\omega}I_1\left(\tau'\right)$$
$$- \frac{2Q'}{m\omega}I_2\left(\tau'\right) - \frac{2}{m^2\omega^2}I_3\left(\tau'\right)\ \}$$
$$+ \frac{i}{\hbar}\left(E_I^s - E_I^{ps}\right)\tau'\ ] \qquad (6.16a)$$

where

$$I_1\left(\tau'\right) = -\int\limits_0^{u} du'\, v\left(-iu'\hbar\right) \sinh\left(\omega u'\hbar\right)$$
$$+ \int\limits_0^{t'} dt''\, v\left(t'' - iu\hbar\right) \sin\left(t'' - \omega u\hbar\right) \qquad (6.16b)$$

$$I_2\left(\tau'\right) = -\int\limits_0^{u} du'\, v\left(-iu'\hbar\right) \sinh\omega\left(u - u'\right)\hbar$$
$$+ \int\limits_0^{t'} dt''\, v\left(t'' - iu\hbar\right) \sin\omega\left(t - t''\right) \qquad (6.16c)$$

and

$$I_3\left(\tau'\right) = \int\limits_0^u du' v\left(-iu'\hbar\right) \sinh\omega\left(u - u'\right)\hbar \int\limits_0^{u'} du'' v\left(-iu''\hbar\right) \sinh\omega u''\hbar$$

$$- \int\limits_0^{t'} dt'' v\left(t'' - iu\hbar\right) \sin\omega\left(t' - t''\right) \int\limits_0^u du' v\left(-iu'\hbar\right) \sinh\omega u'\hbar$$

$$+ \int\limits_0^{t'} dt'' v\left(t'' - iu\hbar\right) \sin\omega\left(t' - t''\right)$$

$$\times \int\limits_0^{t''} dt''' v\left(t''' - iu'\hbar\right) \sin\omega\left(t''' - iu'\hbar\right) \quad (6.16d)$$

The complex time computations of the primary region dynamics for a dipole-dipole TCF and its Fourier transform are illustrated in Fig. 2. The dipole-dipole TCF $\widetilde{F}_{\hat{D},\hat{D}}(\tau')$ is computed along $\mathcal{C}$ for many points $\tau' = t' - iu\hbar$. The path-integral method, through an efficient restricted matrix multiplication (RMM) method (to be described in the next paragraph) for the primary region dynamics, is used along the path $\mathcal{C}'$ joining 0 and τ'. The memory terms needed to perform the RMM procedure along $\mathcal{C}'$ are computed numerically according to Eq.(6.15) by using the force term $v(\tau)$ at the grid points shown in Fig.2. The grid points needed to compute the memory term at any complex time τ_l are the points for which the corresponding complex times are less than τ_l; therefore, the force terms at these grid points are already known from the previous computations.
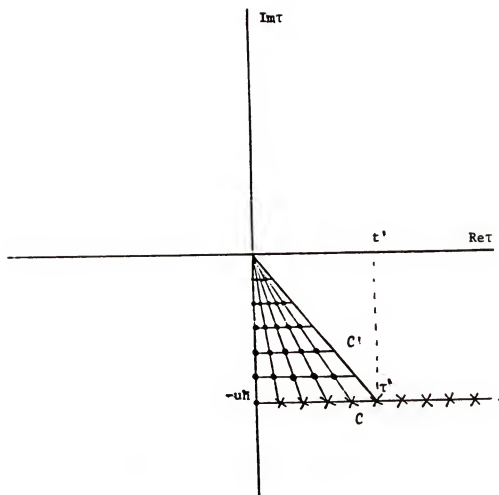
Figure 2. Complex time computations for the TCF and its Fourier transform; discretization of the complex time plane.

Lastly, we explain the efficient Restricted Matrix Multiplication (RMM) method mentioned in the preceding paragraph. As mentioned before, even in a one dimensional problem, the straightforward numerical matrix multiplication (NMM) [Thirumalai and Berne, 83] is suitable mostly for binding or attractive potentials where the range of the matrix sampling the potential is fixed by the range of the potential. Therefore, for the nonbinding and repulsive potentials, the method becomes unsuitable even in one dimensional problems. We use two properties of the short time approximation to the complex matrix $\mathbf{K}(\epsilon)$ in Eq.(6.10) to efficiently incorporate a linear increase with the range of the potential.

Firstly, the short time approximation for the complex time matrix element $K_{ij}(\epsilon)$ as written in Eq.(6.10) is invariant to the interchange of i and j, i.e $K_{ij}(\epsilon) = K_{ji}(\epsilon)$. Therefore, by using the property that the product of two symmetric matrices is a symmetric matrix, we reduce the comptational efforts in any NMM iteration by a factor of two.

More importantly, the second property comes from separating, in the short time approximation for the complex time matrix element $K_{ij}(\epsilon)$, a completely real decay factor $D(i - j)$. For diagonal elements, i.e for $j = i$, the decay factor $D(0)$ is one. For $j \neq i$ the decay factor, $D(i - j) \propto \exp(-C(i - j)^2)$, starts to cause a rapid decay in the magnitudes of the off-diagonal matrix elements as one goes away from the diagonal. Since suitable grid spacings, are generally achieved by keeping the decay constant C within a range $0.1 \leq C \leq 1.0$ [Thirumalai, Bruskin and Berne, 83; Coalson, 85], the corresponding decay factor for far off-diagonal matrix elements, i.e $(i - j) \geq 15$ is typically of the order of $\sim 10^{-40}$. This means that the contributions from the far off-diagonal matrix elements rapidly approach zero as one goes further away from the diagonal. Instead of using the

full matrix in an NMM step, we use the rapidly decaying property of the decay factor $D(j - i)$, and suggest a natural cut-off in the contributions from the far off-diagonal matrix elements. The name Restricted Matrix Multiplication (RMM) hence refer to the NMM procedure where the contributions from the far off-diagonal elements beyond a suitable cut-off are chosen as zero. If M_c is the suitable cut off beyond which we are ignoring the contributions from the off-diagonal elements in a $(M + 1) \times (M + 1)$ matrix, the number of mathematical operations needed to perform a restricted matrix multiplication (RMM) step are typically of the order of $\sim (M + 1) \times M_c^2$ as opposed to the operations $\sim (M + 1)^3$ needed in an equivalent NMM step. Therefore, as the size of the matrix starts to increase from $(M+1) \times (M+1)$ to $(M+L+1) \times (M+L+1)$, the RMM step for the computations of the same accuracy needs only $\sim L \times M_c^2$ extra operations, whereas for the similar increase in the matrix size the NMM step will need L^3 extra operations. In typical applications both M and L are generally of the order of ~ 100 whereas the cut-off parameter M_c is generally of the order of ~ 10. Therefore, specially for unbound potentials, the efficacy of the RMM procedure is manyfold as compared to that of the NMM procedure.

6.3. A More Efficient Transformation from Real to Complex Time

As mentioned before the transformation from real to complex time along a contour for which the imaginary part $-iu\hbar$ remains a constant, is not unique. We also note that having separate computation paths, for the complex time Fourier transform along $\mathcal{C}$ and for the RMM steps along $\mathcal{C}'$, is not very efficient. This is because the computations being done along two separate contours require information on many more points on the complex time grid, as compared to a situation where $\mathcal{C}$

and $\mathcal{C}'$ coincide, i.e where the Fourier transform computation is done along the RMM computation path. By deforming the path C for the complex time Fourier transform, we show that there exists another transformation, for which the Fourier transform contour overlaps with the RMM contour, making the computations for this new transformation more efficient.

The line shape function for a general two surface photointeraction process is related to the complex time Fourier transform

$$F_{\hat{D}\hat{D}}(\omega) = \frac{e^{uh\omega}}{2\pi} \int\limits_{-\infty}^{+\infty} dt' \ e^{i\omega t'} \widetilde{F}_{\hat{D}\hat{D}}\left(t' - iu\hbar\right) \qquad (6.17)$$

of the complex time dipole-dipole TCF $\widetilde{F}(\tau')$ with $\tau' = t' - iu\hbar$. We can rewrite Eq.(6.17) as

$$F_{\hat{D}\hat{D}}(\omega) = \lim_{t \to \infty} \frac{Re}{\pi} \int\limits_{-\infty}^{t} dt' \ e^{i\omega(t' - iu\hbar)} \widetilde{F}_{\hat{D}\hat{D}}\left(t' - iu\hbar\right) \qquad (6.18)$$

where we have used $\widetilde{F}(-t' - iu\hbar) = \widetilde{F}(t' - iu\hbar)^*$, and for constant u we have taken the exponential factor containing u inside the integral. As shown in Fig.(3), deforming the integration path $\mathcal{C}$ we rewrite the integral as

$$\int\limits_{\mathcal{C}} dz' e^{i\omega z'} \widetilde{F}_{\hat{D}\hat{D}}\left(z'\right) = \int\limits_{\mathcal{C}_i} dz' e^{i\omega z'} \widetilde{F}_{\hat{D}\hat{D}}\left(z'\right) + \int\limits_{\mathcal{C}_c} dz' e^{i\omega z'} \widetilde{F}_{\hat{D}\hat{D}}\left(z'\right) \qquad (6.19)$$

where the complex integration variable $z' = t' - iu\hbar$.
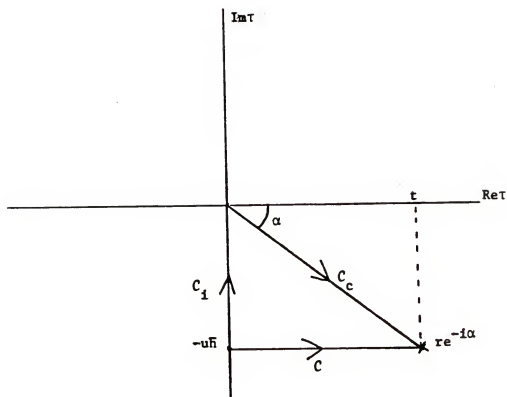
Figure 3. Deformation of the Fourier transform contour.

In the first term we use $z' = -iu'\hbar$ to show that

$$\int_{\mathcal{C}_i} dz' e^{i\omega z'} \widetilde{F}_{\hat{D}\hat{D}}(z') = i\hbar \int_0^u du' \, e^{\omega u'} \widetilde{F}_{\hat{D}\hat{D}}(-iu'\hbar) \qquad (6.20)$$

where $\widetilde{F}_{\hat{D},\hat{D}}(-iu'\hbar)$ is real; therefore, the contribution to the line shape function from the first term in the deformed path, $\mathcal{C}_i$, is equal to zero. In the second term, we use $r = \sqrt{t^2 + u^2}$ and $\alpha = \arcsin\frac{u}{\sqrt{t^2+u^2}}$ with $r \to \infty$ for constant small angle α, corresponding to $t \to \infty$ for constant u, and we rewrite the second term as

$$\int_{\mathcal{C}_c} dz' e^{i\omega z'} \widetilde{F}_{\hat{D}\hat{D}}(z') = \int_0^{re^{-i\alpha}} dz' \, e^{i\omega z'} \widetilde{F}_{\hat{D}\hat{D}}(z') \qquad (6.21)$$

Replacing the integration variable $z' = r' \exp(-i\alpha)$ for constant α, and rearranging the integrand we get

$$F_{\hat{D}\hat{D}}(\omega) = \lim_{r \to \infty} \frac{Re}{\pi} e^{-i\alpha} \int_0^r dr' \, e^{+i\omega r' e^{-i\alpha}} \, \widetilde{F}_{\hat{D}\hat{D}}(r' e^{-i\alpha}) \qquad (6.22)$$

where the Fourier transform integration and the complex time dipole-dipole TCF $\widetilde{F}(r' \exp(-i\alpha))$ for a constant positive angle α, are evaluated along the same path $\mathcal{C}_c$. We also note that, instead of first translating the integration range in the lower half of the complex time plane by a constant amount $-iu\hbar$, and then deforming the resultant path as $\mathcal{C} = \mathcal{C}_i + \mathcal{C}_c$ to achieve the new integration path in Eq.(6.22), we could have directly obtained the desired transformation of the integrals merely by rotating the real time axis by a constant negative angle $\alpha = -\arcsin\frac{u}{\sqrt{t^2+u^2}}$ where u is a real parameter.

CHAPTER 7
APPLICATIONS AND RESULTS

In this chapter we present applications of the TCF approach to the interaction of light with a polyatomic system. Section 7.1 describes application to the electronic absorption spectra for a model one-dimensional problem with two electronic potential surfaces. The upper and the lower potential energy surfaces are modeled by displaced Morse potentials [Coalson, 85] in one dimension. Computations of the complex time TCF and its Fourier transform for this model are performed to provide a check of the convergence of the numerical path-integral method. In section 7.2, we use the dipole-dipole TCF of an extended molecular system within a TDSCF approximation to study the photodissociation dynamics of methyl iodide (CH_3I) on the potential energy surface of an electronically excited state. Realistic potentials energy surfaces for this well known example are taken from a Gaussian Wave-packet Dynamics (GWD) study of the same problem [Lee and Heller, 82]. Using the TDSCF approximation in chapters 4 and 5, the photodissociation dynamics of CH_3I has been factored into a primary and a secondary region dynamics. The complex-time evolution of the primary region amplitude is performed through an efficient discretized path-integral method, whereas the complex time propagator for the secondary region amplitude is constructed analytically according to Eqs.(6.16a,b,c,d) in the previous chapter. The total cross-section for the photodissociation of CH_3I from its ground vibrational state, using our TDSCF approach, is compared to that of the GWD approach of Lee and Heller. The TDSCF approach to photointeraction processes in many dimension, coupled with a path-

integral method for the primary region dynamics, is independent of any particular functional form of the initial amplitudes for the primary and the secondary region dynamics, and of any particular functional form for the primary region potential. An additional application to the photodissociation dynamics of vibrationally excited CH_3I, for which the initial values of the primary and the secondary region amplitudes are not restricted to simple Gaussian functions, are described for many vibrationally excited states in section 7.3.

7.1. Electronic Absorption Spectra of a Model Two-Potential Problem

For a two surface electronic absorption problem the complex time dipole-dipole TCF $\widetilde{f}_{\hat{D},\hat{D}}(t)$ of Eq.(3.11b) at the temperature $(k_B\beta)^{-1}$ is written in the coordinate representation as

$$\widetilde{f}_{\hat{D}\hat{D}}(t) = \frac{1}{Z_\beta} \int dX \int dX' \left\langle X \left| e^{+\frac{i}{\hbar}\hat{H}_l(\tau+i\beta\hbar)} \right| X' \right\rangle$$
$$D\left(X'\right) \left\langle X' \left| e^{-\frac{i}{\hbar}\hat{H}_u\tau} \right| X \right\rangle D\left(X\right) \quad (7.1)$$

where $\hat{H}_l$ and $\hat{H}_u$ are the Hamiltonians for the lower and the upper potential energy surfaces, the complex time $\tau = t - iu\hbar$, and Z_β is the partition function at the initial inverse temperature $k_B\beta$. Electronic excitations in a single nuclear variable problem, such as in diatomics, are described by one dimensional potential energy curves. We model the lower and the upper potential energy curves as two displaced one dimensional Morse oscillator potentials [Reimers, Wilson, and Heller, 83; Thirumalai and Berne, 85; Coalson; 85], expressed as

$$V_l(X) = V_0 \left(1 - e^{-\alpha X}\right)^2 \quad , \quad (7.2a)$$

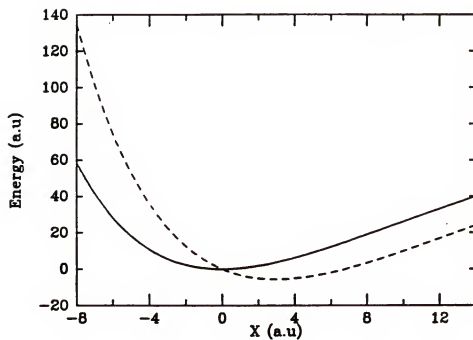**Upper and Lower Potential Energy Surfaces**

Figure 4. Model one dimensional Morse potentials for the ground ——— , and the excited — — —— electronic potentials for a two state electronic absorption problem (see text).

$$V_u(X) = V_0 \left(1 - e^{a(X-a)}\right)^2 - V_0 \left(1 - e^{aa}\right)^2 \qquad . \qquad (7.2b)$$

In what follows we choose the same parameters as Coalson's [Coalson, 85], which are listed in table 7–1.

Table 7-1
Input Parameters For Electronic Absorption Problem

$$a = 3.0au$$

$$V_0 = 100.25au$$

$$\alpha = 0.071au$$

$$m = 1.0au$$

$$\beta = 0.64au$$

$$u = 0.32au$$

The upper and the lower potential energy surfaces of Eq.(7.2a,b) when plotted in the coordinate space are given in Fig.4. Using $\beta = 0.64au$ and the parameter $u = 0.32au$ in Eq.(7.1), we rewrite it as

$$\widetilde{f}_{\hat{D}\hat{D}}(t) = \frac{1}{Z_\beta} \int dX \int dX' \left\langle X \left| e^{-\hat{H}_l \tau^*} \right| X' \right\rangle \\ D(X') \left\langle X' \left| e^{-\hat{H}_u \tau} \right| X \right\rangle D(X) \qquad (7.3)$$

where $\tau = t - i0.32$, and we have also dropped the factor $\frac{1}{Z_\beta}$ from the TCF because it can be taken care of in the normalization of the resulting cross-section. The complex matrix for the path-integral method with time-independent Hamiltonian is set up by discretizing the coordinate X within in a range $-11 \geq X \geq 14$ on a

$(M+1) \times (M+1)$ matrix, and discretizing the complex time $\tau = t - i0.32$ into short time steps of width $\epsilon = \frac{\tau}{2^N}$. The real time t is varied between $0 \geq t \geq 10$ in the increments of $\Delta t = 0.1au$. We compute the upper surface propagator for many values of $\tau = t - i0.32$ by N NMM steps for $N = 1$ with $M = 100$, and for $N = 4$ with $M = 125$. These choices of the parameters M and N keep the decay constant C, as described in chapter 6, within the suitable range $0.1 \leq C \leq 1.0$. As shown in Eq.(7.3a,b), the lower potential energy surface has the same analytic form as the upper potential energy surface, but is displaced by a constant amount a with respect to the upper potential energy suface. The lower surface propagator is computed from the upper surface propagator by complex conjugating and displacing the matrix elements of the upper surface propagator by an integer amount $J = \frac{a}{\Delta}$, where a is the displacement between the upper and the lower potential energy surfaces, and Δ is the spacing between any two successive grid points. The propagators for the upper and the lower surface dynamics are then used in Eq.(7.3) to compute the complex time dipole-dipole TCF $\widetilde{f}_{\hat{D},\hat{D}}(t)$, the real and the imaginary part of which are plotted in figures 5a and 5b, respectively, as a function of real time t.

Using the relation $\widetilde{f}_{\hat{D},\hat{D}}(-t) = \widetilde{f}_{\hat{D},\hat{D}}(t)^*$, the real and the imaginary parts of the TCF $\widetilde{f}_{\hat{D},\hat{D}}(t)$, as a function of positive real time $t > 0$, are sufficient for the computation of the Fourier transform $\widetilde{f}_{\hat{D},\hat{D}}(\omega)$ and the corresponding line shape function, $L(\omega) = exp(u\omega)\widetilde{f}_{\hat{D},\hat{D}}(\omega)$, which is shown in figures 6 and 7. The structure less dashed line in Fig.6, refers to the Fourier transform integral evaluated only for short time processes, i.e the real time limits in the Fourier transform integral such as to truncate the TCF $\widetilde{f}_{\hat{D}\hat{D}}(t)$ after its initial decay at $t = 2.0au$.
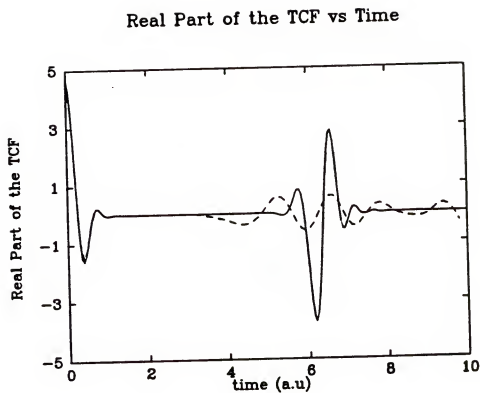
Real Part of the TCF vs Time

Figure 5a. Real part of the complex time TCF $\widetilde{f}_{\hat{D},\hat{D}}(t)$ as a function of real time t; ——— for $N = 4, M = 125$ and — — —for $N = 1, M = 100$.

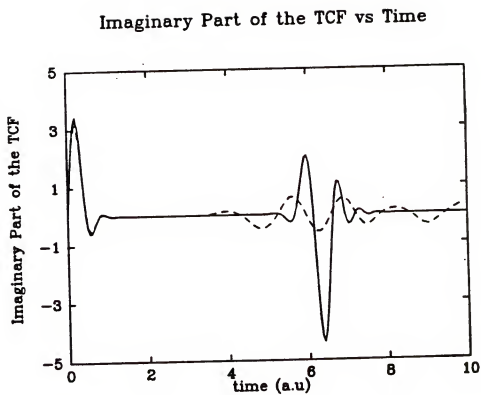Figure 5b. Imaginary part of the complex time TCF $\widetilde{f}_{\hat{D},\hat{D}}(t)$ as function of real time t; ——— for $N = 4, M = 125$, and — — — — for $N = 1, M = 100$.
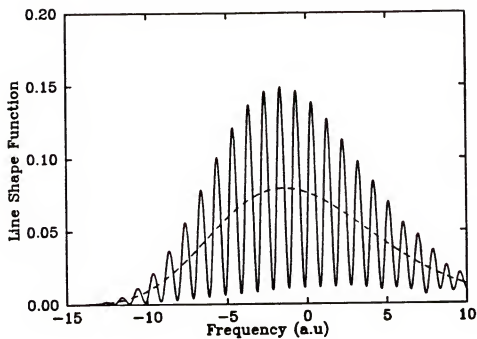
Figure 6. Line shape function for a two-potential electronic absorption problem; ___ corresponds to retaining the short time behaviour in the TCF, — — — — corresponds to intermediate time behaviour in the TCF (See text)
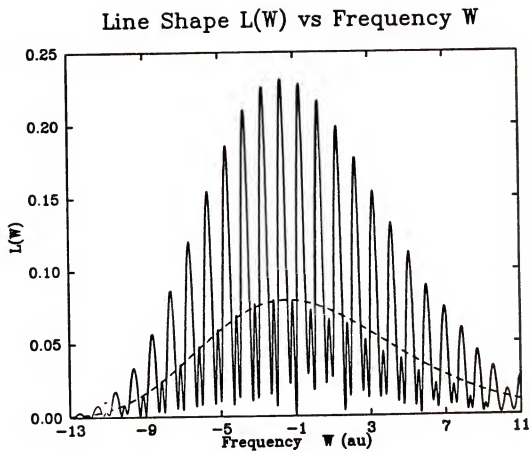
Figure 7. Higher order overtones in the lineshape functions corresponding to long time recurrences in the TCF

The highly oscillating solid line in Fig.6 corresponds to retaining the first recurrence in the intermediate time behaviour, while suppressing any further recurrences in the long time behaviour. This is achieved simply by introducing in the Fourier transform integral a Gaussian decay factor, $L_d(t) = \exp(-dt^2)$, where $d = 0.02$. If the decay factor $L_d(t)$ is removed from the Fourier transform integral, the higher order recurrences in the TCF, which are not even seen in figures 5a and 5b, are reflected in the lineshape function as the higher order overtone structures shown in Fig.7.

After checking the convergence of our results by using the full NMM procedure with $N = 5$, which agreed with the results for $N = 4$, we also found agreement with the results of Coalson, who has used the same parameters and the same method. We repeated the computations for several fixed times, $t = 1.0, 2.0, 3.5$, and 5.0, successively ignoring more and more far off-diagonal matrix elements each time, until a suitable cut off for the RMM method was achieved. We found that for $N = 4$ and $M = 125$, and $M_c \geq 25$ the values of the real and the imaginary parts of the TCF using the RMM procedure remain converged to within 10^{-6} of the full NMM results.

7.2. Photodissociation of CH₃I from its Ground Vibrational State.

We consider CH_3I as a realistic polyatomic system which undergoes rearrangement in an electronically excited state, following the absorption of light in the visible and UV region. We use a) the TDSCF approximation for factoring the TCF of the system into self-consistent primary and secondary region TCFs, b) the RMM iteration procedure for the primary region dynamics, c) analytic construction of the

secondary region dynamics, and d) compute the total TCF for the process, which is then used for computing the total cross-section.

The photodissociation of CH_3I molecule in an electronically excited state is theoretically interesting, firstly, because of the apparent validity of its treatment as a pseudotriatomic molecule [Shapiro and Bersohn, 80; Lee and Heller, 82; and Sundberg et al., 86], and secondly, because of its utilization as a test case in many of the studies of photodissociation in polyatomic systems. In the pseudotriatomic model, the dissociation of CH_3I is described by two coordinates; r_{CI} is the distance between the C atom and the I atom, and r_{CH_3} is the distance from the C atom to the plane containing the three H atoms. The nuclear vibrational motions in the molecule along the coordinates r_{CI} and r_{CH_3} will be refered to as the CI streatch, and the umbrella mode oscillations of CH_3 respectively. The kinetic energy, and the ground and the first excited potential energy surfaces in these two coordinates, are given by Shapiro and Bersohn [Shapiro and Bersohn, 80]. An alternative set of coordinates, which avoid the momentum coupling in the kinetic energy terms, are the mass weighted Jacobi coordinates [Lee and Heller, 82] R and r, given by

$$r = r_{CH_3} \qquad (7.4a)$$

$$R = r_{CI} + \frac{m_{H_3}}{m_c + m_{H_3}} r_{CH_3} \qquad (7.4b)$$

The ground and the first excited potential energy surfaces of CH_3I in the Jacobi coordinates are as shown in Fig.8. In this work, however, we use normal mode coordinates of CH_3I in its ground electronic state [Lee and Heller, 82]. The transformations from the Jacobi coordinates r and R to the mass weighted normal mode coordinates X and Y are given by

$$\begin{pmatrix} X \\ Y \end{pmatrix} = \begin{pmatrix} 7.830 & -0.176 \\ 0.618 & 4.939 \end{pmatrix} \begin{pmatrix} R - 4.1670 \\ r - 0.6197 \end{pmatrix} \qquad (7.5)$$

i.e the coordinate X is dominated by the dissociation variable R and the coordinate Y is dominated by the umbrella mode variable r. The normal mode analysis is useful in assigning two oscillator vibrational quantum numbers (n_X, n_Y) to the initial nuclear vibrational states on the ground electronic potential energy surface, and in providing harmonic oscillator basis functions for the SCF approximation to the initial nuclear vibrational states. The ground and the first excited potential energy surfaces, in the normal mode coordinates X and Y, are expressed as

$$\begin{aligned} V_{gr}(X,Y) = &-0.245 + 0.178 \left[exp\left(-0.899 B\left(X,Y\right)\right) - 1 \right]^2 \\ &+ \left[0.0362 + 0.1101 exp\left(-0.4914 B\left(X,Y\right)\right) \right] \\ &\times \left[0.2019Y - 4.5434 \times 10^{-3} X \right. \qquad (7.6a) \\ &\left. + 0.6197 \left(1 - exp\left(-0.4914 B\left(X,Y\right)\right)\right) \right]^2 \end{aligned}$$

with

$$B(X,Y) = 0.1287X - 2.4659 \times 10^{-2} Y \quad , \qquad (7.6b)$$

and

$$\begin{aligned} V_{ex}(X,Y) = &\, 4.071 \times 10^{-2} exp\left(-0.1567X + 0.4327 \times 10^{-1} Y\right) \\ &+ 5.631 \times 10^{-2} exp\left(-0.1783X - 0.6044 \times 10^{-2} Y\right) \\ &+ 3.620 \times 10^{-2}(-0.1594 \times 10^{-1} X \\ &\qquad\qquad\qquad + 0.2091Y + 0.6197)^2 \quad (7.7) \end{aligned}$$

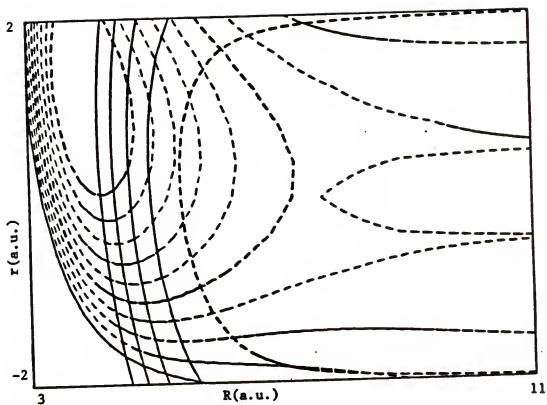respectively, where all energies are in Rydberg and the distances are in Bohr.

Figure 8. Two-dimensional contour plots of the ground and the first excited electronic potential energy surfaces of CH_3I in Jacobi coordinates r and R.

The ground state Hamiltonian, expanded to quadratic terms about the minimum in the potential [Lee and Heller, 82], is expressed in the normal mode coordinates as

$$\hat{H}_{gr} = 0.4982 \times 10^{-2} \left(-\frac{1}{2}\frac{\partial^2}{\partial X^2} + \frac{1}{2}X^2 \right)$$
$$+ 0.1103 \times 10^{-1} \left(-\frac{1}{2}\frac{\partial^2}{\partial Y^2} + \frac{1}{2}Y^2 \right) + ... \qquad , \qquad (7.8)$$

This defines effective masses, and the force constants for the harmonic oscillator basis functions $g_i(X)$ and $g_j(Y)$ along the normal mode coordinates X and Y, respectively. The general form of these basis functions [Messiah, 62] are given for example by

$$g_i(X) = \left(\frac{m_X \omega_X}{\pi \hbar 2^{2i}(i!)} \right)^{\frac{1}{4}} exp \left(-\frac{m_X \omega_X X^2}{2\hbar} \right) H_i \left[\left(\frac{m_X \omega_X}{\hbar} \right)^{\frac{1}{2}} X \right] \qquad (7.9)$$

where m_X and ω_X, the effective mass and the frequency for the X normal mode respectively, are given by Eq.(7.8). Treating the normal mode coordinate X as the primary region variable, and the normal coordinate Y as the secondary region variable, we expand the SCF solutions $\langle X \mid \psi_I^p \rangle$ and $\langle Y \mid \psi_I^s \rangle$, for the initial nuclear vibrational wavefunction on the ground potential energy surface, as

$$\langle X|\psi_I^p \rangle = \sum_i C_i^p g_i(X) \qquad (7.10a)$$

$$\langle Y|\psi_I^s \rangle = \sum_j C_j^s g_j(Y) \qquad , \qquad (7.10b)$$

where the expansion coefficients C_i^p and C_j^s are obtained by diagonalizing the full ground state Hamiltonian with the full initial nuclear vibrational wavefunction $\langle XY|\psi_I \rangle = \langle X|\psi_I^p \rangle \langle Y|\psi_I^s \rangle$. The ground and first few excited eigenvalues on the ground electronic surface, obtained by using three basis functions each in the

expansions in Eqs.(7.10a) and (7.10b), are compared with those of Lee and Heller in the Table 7–2.

Table 7-2
First Few Eigenvalues on the Ground Electronic Surface

(n_X, n_Y)	E_{SCF}	E_{exact}
$(0,0)$	$0.109437eV$	$0.108656eV$
$(1,0)$	$0.179039eV$	$0.175237eV$
$(2,0)$	$0.242616eV$	$0.240799eV$
$(0,1)$	$0.260396eV$	$0.260514eV$
		(see APPENDIX C)

the ground nuclear vibrational wave function corresponding to the eigenvalue $(0,0)$, given by

$$
\psi_{(0,0)}(X,Y) = [0.996726g_0(X) + 8.07921 \times 10^{-2}g_1(X) \\
+ 3.11935 \times 10^{-3}g_2(X)] \times [0.999921g_0(Y) \\
- 1.23387 \times 10^{-2}g_1(Y) - 2.27367 \times 10^{-3}g_2(Y)]
$$

$$(7.11)$$

is used in the self-consistent treatment of the primary and secondary region dynamics on the excited potential energy surface. Following Lee and Heller, we assume that the electronic transition dipole moment operator, between the ground and the first excited potential energy surface, is a constant. Therefore the SCF solutions $|\psi_I^p\rangle$ and $|\psi_I^s\rangle$, on the ground potential energy surface are equal to the initial amplitudes $\xi^I(0)$ and $\eta^I(0)$, respectively. The coupling terms in the excited state

potential of Eq.(7.7) are expanded in powers of the secondary region variable Y, and only the terms which are linear in Y are retained. Therefore, the excited state potential of Eq.(7.7) can be expressed in the following simplified form

$$V_{ex}(X,Y) = V^0(X) + V^1(X)Y + \frac{1}{2}AY^2 \qquad (7.12a)$$

where

$$\begin{aligned} V^0(X) = {} & 3.620 \times 10^{-2} \left(0.6197 - 0.1594 \times 10^{-1}X\right)^2 \\ & + 4.071 \times 10^{-2}e^{-0.1567X} + 5.631 \times 10^{-2}e^{-0.1783X} \end{aligned}$$
$$(7.12b)$$

$$\begin{aligned} V^1(X) = {} & 2.0 \times 0.2019 \times 3.620 \times 10^{-2} \left(0.6197 - 0.1594 \times 10^{-1}X\right) \\ & 4.071 \times 10^{-2}e^{-0.1567X} - 5.631 \times 10^{-2}e^{-0.1783X} \end{aligned}$$
$$(7.12c)$$

and

$$A = 2.0 \times 3.620 \times 10^{-2} \times 0.2019^2 \qquad (7.12d)$$

We have chosen to work with this simplified form of the excited state potential, because we are mainly interested on whether a TDSCF approximation can indeed be used for intramolecular dynamical processes involving dissociation in an electronically excited state, and secondly on, whether it reproduces the general features of the spectra of a dissociating polyatomic system. We have found that answer to

both these questions is affirmative. The analytic form of the complex time propagator, for a harmonic secondary region coupled linearly to an arbitrary general motion in the primary region dynamics, was described in chapter 6.

To determine the range of values for the parameter u in the complex time $\tau = t - iu$, in atomic units, we first ignore the coupling between the primary and the secondary regions, and at $t = 0$ use the full NMM method for the primary region dynamics along the negative imaginary time axis for different values of u in the range $0 \geq u \geq 100$. To do this, we use imaginary time steps of length $\epsilon = 3au$, and a coordinate grid spacing $\Delta = 0.106au$ on a 75×75 matrix in a range $-4 \geq X \geq +4$, within which the initial value of the amplitude is sufficiently greater than zero. These, together with the effective mass $m_X = 200.723au$ along the normal mode coordinate X, keep the decay constant, $C = 0.38$, within the range $0.1 < C \leq 1.0$ [Thirumalai and Berne, 83; Coalson, 85]. The upper bound on u is fixed, firstly, by noticing that for $u > 40au$ the value of the primary region TCF at the initial time $t = 0$ is smaller than about 10^{-8}, and secondly, by knowing that for the complex time dynamics this value will decrease even further. For the lower bound on u the complex time computations for the primary region dynamics were performed for u between $1 < u < 15$. We noticed that for $u \leq 7$ the results for the complex time primary region TCF do not remain bound, i.e the amplitude of the envelop of the oscillating TCF start growing to values which are larger than the amplitude of the first maxima. Consequently, the suitable range for the allowed values of u is chosen as $8 \leq u \leq 40$. For the set of results presented in this section, we have used $u = 15au$, and have checked that these values remain converged to within 10^{-6} for varying u in the range $10 < u < 35$.

For the complex time primary region dynamics (including the self-consistent

coupling with the secondary region dynamics), we discretize the space along the normal mode coordinate X in a range $-6 \geq X \geq 8$, within which the complex time primary region amplitude $\xi(X, \tau)$ evolves and spreads on the upper potential energy surface, on a 115×115 matrix. For fixed $u = 15au$, the complex time $\tau = t - iu$ is incremented from $\tau = 0 - i15$ by increasing real time t in steps of $\Delta t = 4au$ until the total TCF is decayed sufficiently. Each of these complex times τ is distretized into short complex time steps $\epsilon = \frac{\tau}{N}$ with $N = 5$. These choices for the parameters M and N, keep the the decay constant, $C = 0.505$, within the required range. The complex time computations, using the full NMM method for several fixed complex times τ were performed repeatedly by dropping more and more far off-diagonal elements from the computations, untill a suitable cut-off point was reached. For the set of parameters chosen above, i.e for $C = 0.505$, a cut-off point $M_c \geq 18$ keeps the results of the RMM method converged to within 10^{-6} of those of the full NMM method.

Table 7-3
Computational Parameters for the Primary Region Dynamics

$$u = 15au$$

$$X_{min} = -6au$$

$$Xmax = +8au$$

$$M = 115$$

$$M_c = 25$$

$$N = 5$$

Comparisons of the complex time evolution of the primary and secondary region amplitudes are done in figures 9a,b,c and 10a,b,c; where at different real times t, we plot the real parts of the complex primary and the secondary region amplitudes.
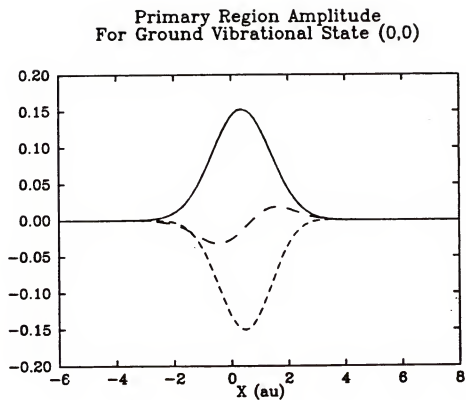
Figure 9a. Real part of the primary region amplitude along the normal mode coordinate X at the real time $t = 0$ au _____ , $t = 16$ au _ _ _ _, and $t = 32$ au .....
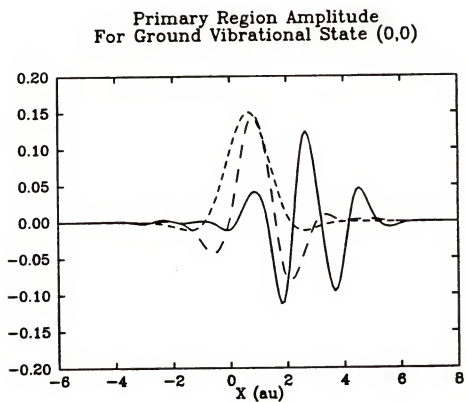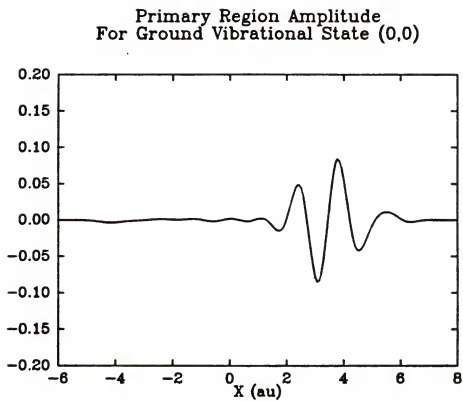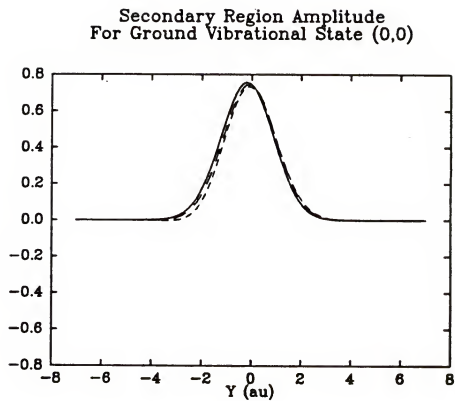
Primary Region Amplitude
For Ground Vibrational State (0,0)

Figure 9b. Real part of the primary region amplitude along the normal mode coordinate X at the real time $t = 64$ au .... , $t = 128$ au $\_\,\_\,\_\,\_$, and $t = 256$ au $\_\_\_\_$.

Figure 9c. Real part of the primary region amplitude along the normal mode coordinate X at the real time $t = 360$ au ___

Secondary Region Amplitude
For Ground Vibrational State (0,0)

Figure 10a. Real part of the secondary region amplitude along the normal mode coordinate Y at the real time $t = 0$ au _____ , $t = 16$ au _ _ _ _, and $t = 32$ au .....
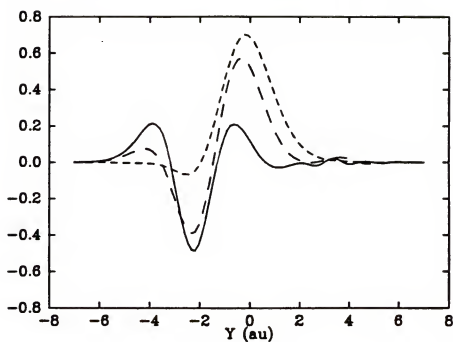
Figure 10b. Real part of the secondary region amplitude along the normal mode coordinate Y at the real time $t = 64$ au .... , $t = 128$ au $\_\ \_\ \_\ \_$, and $t = 256$ au $\_\_\_\_$.
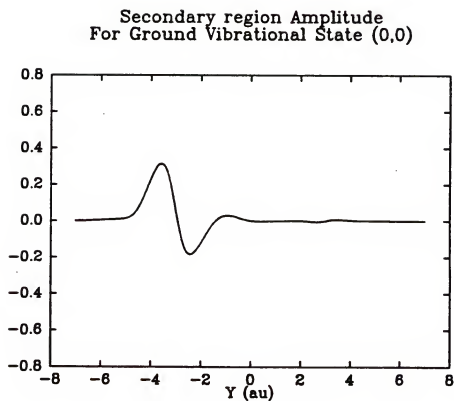
Figure 10c. Real part of the secondary region amplitude along the normal mode coordinate Y at the real time $t = 360$ au _____ .

For the ground vibrational $(0,0)$ state of CH_3I, the amplitudes for the primary and the secondary region dynamics start as simple gaussian functions at the initial real time $t = 0$ and the corresponding complex time $\tau = -iu$; as the later real time $t > 0$ increases, these amplitudes move from their initial positions, and also simultaneously change their shape. In particular, the contrast between the fast oscillating motion of the primary region amplitude and the slowly oscillating motion of the secondary region amplitude, is clearly displayed in these figures. The complex time amplitudes $\xi^{(0,0)}(X, \tau)$ and $\eta^{(0,0)}(Y, \tau)$ are then used for computing the dimensionless primary region TCF $f^{(0,0)}(\tau)$, the secondary region TCF $g^{(0,0)}(\tau)$, and the time-dependent phase factor $\alpha^{(0,0)}(\tau)$ as defined in equations (4.29b,c,d). The primary and the secondary region TCFs together with the phase factor are sufficient to describe the complex time-dependence in the the total TCF, $\widetilde{F}^{(0,0)}(\tau)$. The superscript $(0,0)$ in these expressions means that on the ground electronic surface there are no excitations along the normal mode coordinates X (dominated by the CI stretch mode), and none along the normal mode coordinate Y (dominated by the umbrella mode vibrations in the CH_3 fragment). The real parts of the complex TCFs; $f^{(0,0)}(\tau)$, $g^{(0,0)}(\tau)$, and $\widetilde{F}^{(0,0)}(\tau)$ as function of real time t are plotted in figures 11, 12 and 13, respectively. Finally, in figure 14 we compare the total cross-section for the photodissociation of CH_3I from its ground vibrational state, plotted as a function of incident photon energy, with those of the Gaussian Wavepacket Dynamics method [Lee and Heller, 82]. The discrepencies in the peak position, and in the full width at half maximum (FWHM) are very small, and may be attributed to our approximations expanding the excited state potential in the secondary region variable Y and, retaining only the terms linear in Y, and using the SCF form for the initial nuclear vibrational state $\psi_{(0,0)}(X, Y)$.

116

**Real Part of the Primary Region TCF
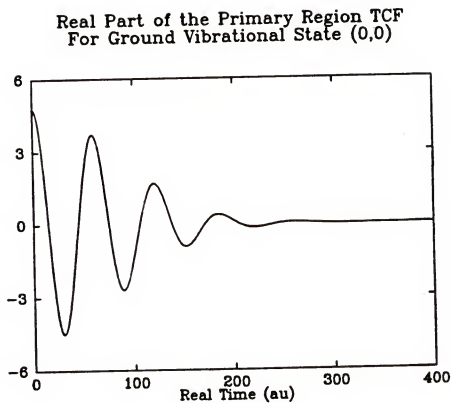For Ground Vibrational State (0,0)**

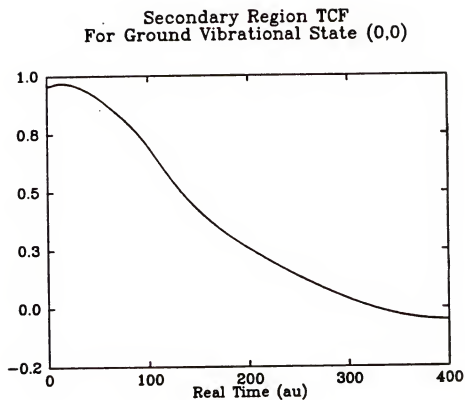Figure 11. Real part of the dimensionless primary region TCF $f^{(0,0)}(t)$ as a function of real time t.

Figure 12. Real part of the dimensionless secondary region TCF $g^{(0,0)}(t)$ as a function of real time t.
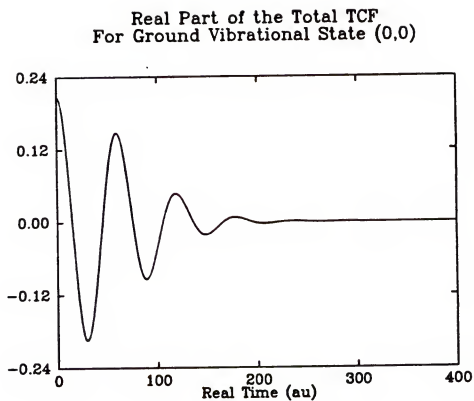
Real Part of the Total TCF
For Ground Vibrational State (0,0)

Figure 13. Real part of the total TCF $\widetilde{F}^{(0,0)}(\tau)$ as a function of real time t.

Peak Normalized Total Cross–section
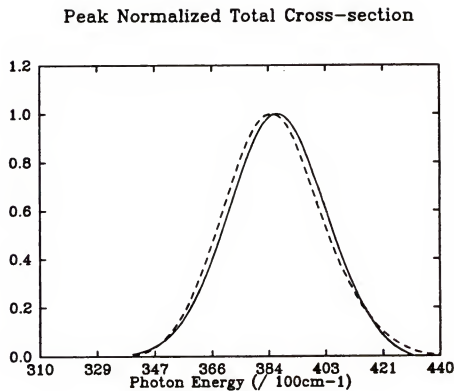
Figure 14. Peak normalized total cross section for the photodissociation of CH_3I from its ground vibrational state; ———— TDSCF approach, – – – – Gaussian Wavepacket Dynamics approach [Lee and Heller;82].

7.3. Photodissociation of CH$_3$I from initially excited vibrational states.

The main advantage of using our TDSCF approach in more than one dimension, is the absence of any constraint on the allowed functional form of the time-dependent amplitudes for the primary and secondary region dynamics, and the primary region potential. Consequently, the extension of the TDSCF approach to the photodisociation dynamics of CH$_3$I in initially excited vibrational states, where the initial form of the complex amplitudes are not restricted only to simple Gaussian shapes, is straightforward. In the above description of the self-consistent primary and secondary region dynamics, we simply replace the SCF form of the ground vibrational state $\psi_{(0,0)}(X, Y)$ by the required excited vibrational state $\psi_{(n_X, n_Y)}(X, Y)$ where n_X and n_Y are the number of vibrational quanta along the dissociation dominated normal mode coordinate X, and the umbrella mode motion dominated normal mode coordinate Y, respectively. The peak position and the shape of the total cross-section in the frequency spectrum are determined by the primary region TCF, whereas the inclusion of the secondary region TCF provide a modulation in the peak shape of the cross-section. As we consider the inclusion of excited vibrational states ($n_X = 1, 2, 3...$) in the primary region dynamics, we find that increasing number of nodes in the initial amplitude are directly reflected in the appearance of extra peaks in the total cross-section. On the other hand, a similar inclusion of excited vibrational states ($n_Y = 1, 2, 3...$) along the secondary region dynamics does not directly show in extra peaks in the cross-section. The computational parameters for the dynamics in the primary and the secondary region are same as those of in the Table 7–2. In figures (15a,b,c) and (16a,b,c) we show the time developments for the primary and the secondary region amplitudes for initially excited states (1,0) and (0,1), respectively.
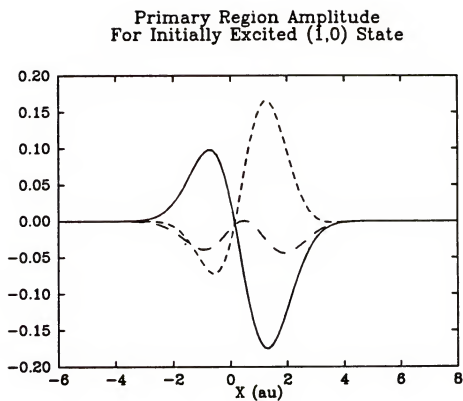
**Primary Region Amplitude
For Initially Excited (1,0) State**

Figure 15a. Real part of the primary region amplitude for initially excited $(1,0)$ state of CH_3I at different real times $t = 0$ au ———— , $t = 16$ au $-\,-\,-\,-$, and $t = 32$ au .... .
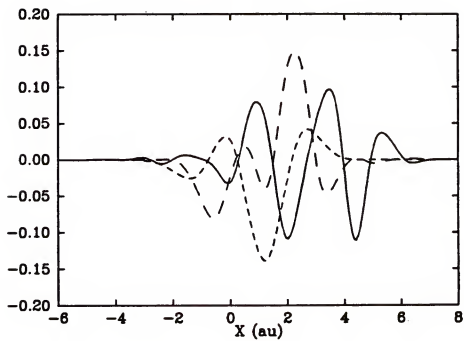
Figure 15b. Real part of the primary region amplitude for initially excited
$(1,0)$ state of CH_3I at different real times $t = 64$ au .... , $t = 128$ au $----$
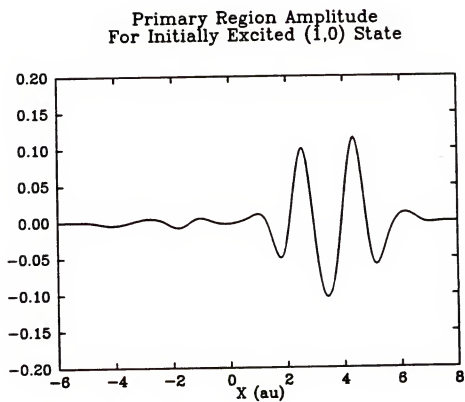, and $t = 256$ au _____ .

Figure 15c. Real part of the primary region amplitude for initially excited $(1, 0)$ state of CH$_3$I at the real time $t = 360$ au _____ .
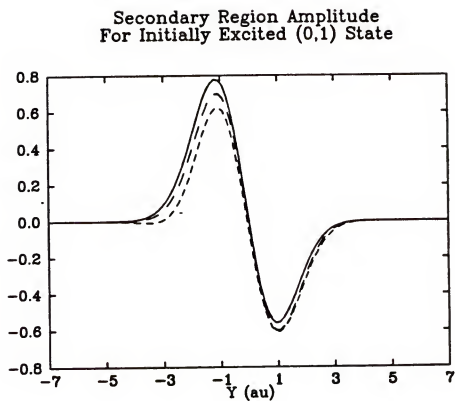
**Secondary Region Amplitude
For Initially Excited (0,1) State**

Figure 16a. Real part of the secondary region amplitude for initially excited (0,1) state of CH$_3$I at $t = 0$ au ——— , $t = 16$ au − − − − , and $t = 32$ au .... .

Secondary Region Amplitude
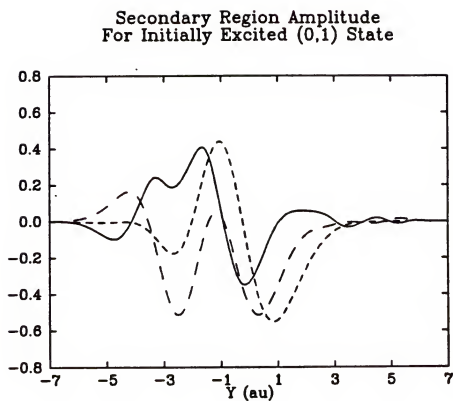For Initially Excited (0,1) State

Figure 16b. Real part of the secondary region amplitude for initially excited
(0,1) state of CH_3I at $t = 64$ au .... , $t = 128$ au $----$, and $t = 256$
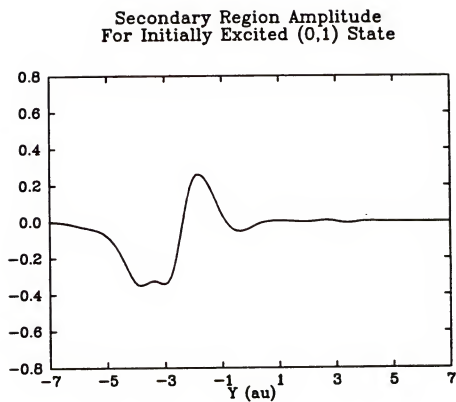au ___ .

Figure 16c. Real part of the secondary region amplitude for initially excited $(0,1)$ state of CH$_3$I at $t = 360$ au ____ .

The complex amplitudes corresponding to the initially excited $(1,0)$ and $(0,1)$ nuclear vibrational states are then used for computing the total TCFs $\widetilde{F}^{(1,0)}(\tau)$ and $\widetilde{F}^{(0,1)}(\tau)$, respectively. The real parts of these TCFs as functions of real time t and the resulting total cross-sections as functions of photon energy are shown in Figs.17a,b and Fig.18, respectively. Modulations of the fast oscillations in the TCF, corresponding to the $(1,0)$ vibrationally excited CH_3I as shown in Fig.17a, are reflected in the appearance of an additional peak in the corresponding total cross-section in Fig.18, whereas the modulations of the slow decay of the TCF in the $(0,1)$ case as shown in Fig.16b appear merely as a shoulder structure in the corresponding total cross-section. At present there are no quantum mechanical computations for the photodissociation of CH_3I from initially excited vibrational states. However, qualitatively, the general features of our total cross-sections for $(1,0)$ and $(0,1)$ vibrationally excited CH_3I agree well with two semi-classical computations, i.e the semi-classical wave-packet dynamics method [Sundberg et al., 86] for differently parametrized potential energy surfaces, and the Self-consistent Eikonal Method (SCEM) [Swaminathan, Stodden and Micha, 88] for the same potential energy surfaces. Both of these methods also show two peaks in the total cross-section of the photodissociation of the $(1,0)$ initially excited CH_3I, and a single non-symmetric peak in the $(0,1)$ case. Qualitatively, the shapes of our total cross-sections are closer to the wavepacket computations [Sundberg et al., 86], as opposed to the SCEM computations, which uses the same potential energy surfaces as in our work. This is probably because in the SCEM technique, which is based on running classical trajectories for the nuclear motions, the low energy region of the spectrum is not very accurate, because at low energies the classical trajectories do not properly sample the required non-allowed region of the potential.
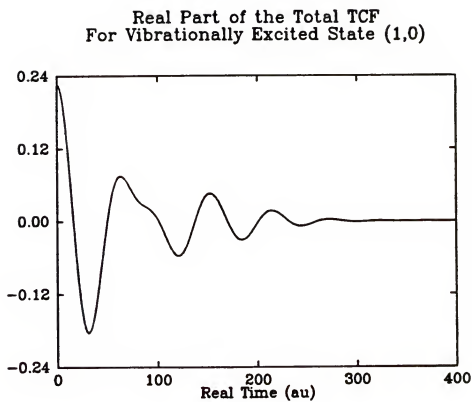
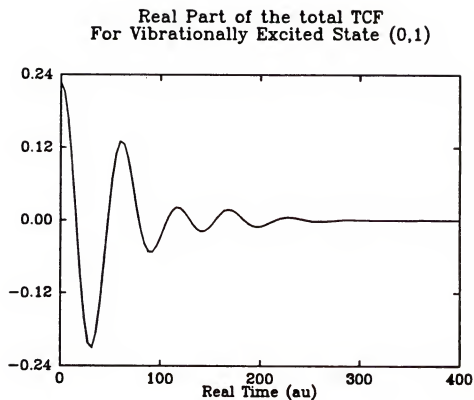Figure 17a. Real part of the complex TCF $\widetilde{F}^{(1,0)}(\tau)$ as a function of real time t.

Figure 17b. Real part of the complex TCF $\widetilde{F}^{(0,1)}(\tau)$ as a function of real time t.
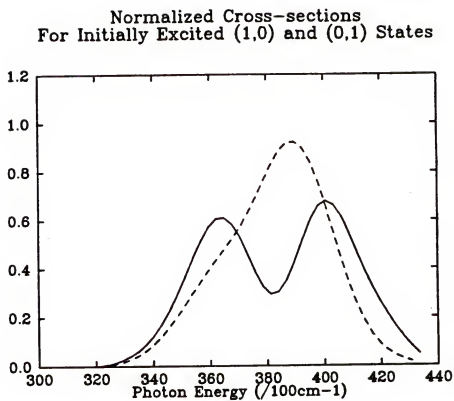
Figure 18. Total cross-section for vibrationally excited CH₃I for a single excitation in the secondary region dynamics $- - --$ $(0,1)$, and a single excitation in the primary region dynamics _____ $(1,0)$.

Using five basis functions each in the SCF expansions for $\langle X|\psi_I^p\rangle$ in Eq.(7.10a) and $\langle Y|\psi_I^s\rangle$ in Eq.(7.10b), we obtained nuclear vibrational wavefunctions and the corresponding eigenvalues for the other excited states as well [Appendix C], and have used them in further studies of the photodissociation of vibrationally excited CH_3I. In Fig.19a, we keep the vibrational quantum number n_Y fixed to $n_Y = 0$ and check the effects of increasing the number of vibrational excitations along the the normal mode coordinate X. We note that for each additional vibrational excitation in the primary region dynamics, there is an additional extra peak in the spectrum. The heights of these additional peaks are not equal, peaks in the high energy regions of the spectrum corresponding to the short time behaviour of the TCF are found to be higher than the peaks in the low energy regions of the cross-section. As we increase the number of vibrational quanta in the initial state, we note that the overall center of the spectrum, which is a maximum for even number of vibrational excitations such as in $(0,0)$ and $(2,0)$ cases, and is a minimum for odd number of vibrational excitations such as in $(1,0)$ and $(3,0)$ cases, gradually shifts towards the low energy region of the spectrum. In Fig.19b, we keep n_Y fixed to $n_Y = 1$, and check the effects of increasing the number of initial vibrational excitations in the primary region dynamics. In addition to the appearance of a shoulder structure due to the excitation in the secondary region dynamics, we also note a growth in the size of this structure as we increase the number of vibrational excitations in the primary region dynamics, so that in $(2,1)$ and $(3,1)$ vibrationally excited CH_3I this structure becomes like an additional peak. We also note that the heights of the peaks in $(1,1), (2,1)$, and $(3,1)$ vibrationally excited CHI are generally bigger than the heights of the corresponding peaks in the $(1,0), (2,0)$, and $(3,0)$ cases.

Figure 19a. Comparison of cross sections for vibrational excitations in CH_3I along the CI stretch mode: $(1,0)$...., $(2,0)$ – – – –, and $(3,0)$ ____ , with the cross-section for no excitation in the umbrella mode: $(0,0)$ ($\bullet$).

**Normalized Cross−sections
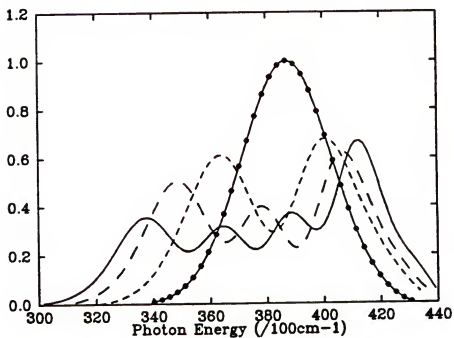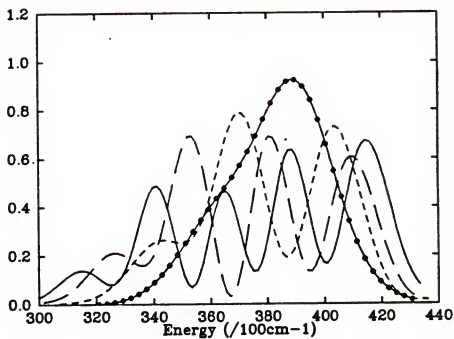For Vibrational Excitations In The CI Mode**

Figure 19b. Comparison of cross sections for vibrational excitations in CH_3I along the CI stretch mode: $(1,1)$......, $(2,1)$ − − − −, and $(3,1)$ _____ , with the cross-section for a single excitation in the umbrella mode: $(0,1)$ (•).

In Fig.20a, we keep the quantum number n_X corresponding to the initial vibrational excitations in the primary region dynamics fixed to $n_X = 0$, and see the effect of increasing the number of initial vibrational excitations in the secondary region dynamics. As before, we note the appearance of a shoulder structure in $(0,1)$ vibrationally excited CH_3I, and that this gradually grows almost to an additional peak in the $(0,3)$ case. The heights of the main peak in the $(0,1), (0,2)$ and $(0,3)$ peaks are also modulated as we put more and more initial vibrational energy in the secondary region dynamics. In Fig.20b, we fix $n_X = 1$ and gradually increase the number of vibrational excitation energy in the secondary region dynamics. Here also the two peak structure of the $(1,0)$ case is modulated by an additional shoulder structure in the $(1,1)$ case, which grows and spreads towards the low energy region of the spectrum in the $(1,2)$ and $(1,3)$ cases. We also note a modulation in the heights of the main peaks as we increase the number of initial excitations in the secondary region dynamics. Hence, in addition to being able to produce highly structured cross-sections for the photodissociation of vibrationally excited CH_3I, as shown in figures 19a,b and 20a,b; the TDSCF approach to the dynamics also shows the effect of a self-consistent energy redistribution between the primary and the secondary regions in these cases.

Figure 20a. Comparison of cross sections for vibrational excitations in CH_3I along the umbrella mode: $(0,1)$......, $(0,2)$ – – – –, and $(0,3)$ ____ ,with the cross-section for zero excitation in the CI stretch mode:$(0,0)$ (•).
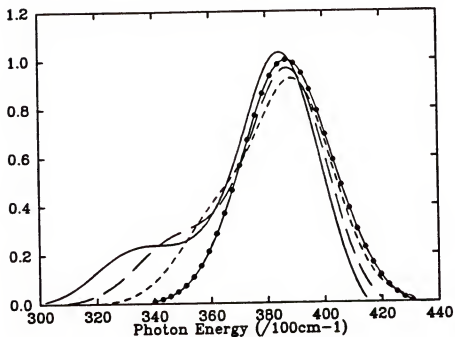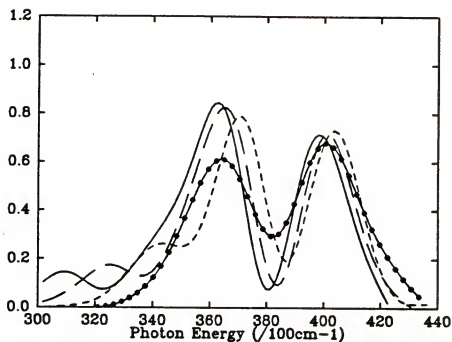
Figure 20b. Comparison of cross sections for vibrational excitations in CH_3I along the umbrella mode: $(1,1)$......, $(1,2)$ — — —, and $(1,3)$ ——— ,with the cross section for a single excitation in the CI stretch mode $(1,0)$ ($\bullet$).

CHAPTER 8
DISCUSSION AND CONCLUSIONS

In chapters 2 through 6 we have developed a general time-dependent quantum mechanical approach to the interaction of visible and UV light with extended molecular systems. Light sources in this frequency range generally excite nuclear vibrational motions, accompanied by transitions between different electronic states of the system. We have considered the interaction of visible and UV light with a large molecular system as a two step process: the interaction of light with a large molecule system, treated like a photon-molecule collision process, excites electronic transitions in the molecular target; and is followed by a dynamical evolution of the target on the excited potential energy surface. The discussion of our work in this chapter is also accordingly ordered, i.e first, we discuss treatment of light-molecule interactions as a photon collision process, and then consider the dynamical evolution of a large molecular system, from the given initial conditions to the required final conditions. At the end, we discuss application and results of this approach to study the electronic absorption spectra of a model two potential problem, and the photodissociation dynamics of a realistic molecular system (CH_3I) from its ground and excited nuclear vibrational states.

We have described transition rates for all first and second order photointeraction processes as the time integrals of the product of the molecular TCFs of the target, and the radiation field TCFs of the light source. The method of separating the light-molecule interaction into a radition field factor and a molecular target factor is completely general, and can be extended to a similar separation of the light-

137

molecule interaction to higher order. An explicit incorporation of the statistical and the dynamical properties of the light source in the formalism is achieved by the separation of the radiation field TCFs from the molecular TCFs. As examples of the inclusion of the statistical properties of the light source in the formalism, we have constructed the radiation field TCFs of thermal, chaotic and coherent light sources. We have found, that the expressions for our transition rates for thermal light, in the time domain description, are equivalent to the usual energy domain descriptions [Louisell, 73; Loudon, 83], except that a statistical distribution for the number of photons is also included in the transition rates. In the case of the chaotic light source, which is a laser operating below the threshold, the form of the transition rates are found to be the same as those in the thermal light case. The exact numbers of photons in the transition rates for the thermal light are replaced by a mean number of photons in the transition rates for chaotic light. We also note, that this mean number of photons is described by the initial statistical distribution of the electric field amplitude of the experimental laser source used. For the coherent light-molecule interaction processes, we have found additional terms in the transition rates, due to the coherent nature of the light source. The magnitudes of these additional transition rates are described by the initial statistical distribution of the electric field amplitude and phase, given by an experimental laser source.

In chapters 3 and 4 we have discussed the evolution of a large system through a molecular TCF approach. Using the Born-Oppenheimer approximation to separate electronic and nuclear motions in the target, we have written a general molecular TCF for a two-surface electronic excitation problem in the electronic adiabatic representation. A transformation from real to complex time of these molecular TCFs is also described, so that their computations by a numerical path-integral method

become feasible. The transformation to the complex time of the TCFs, in which the imaginary part of the complex time remain fixed, is not very efficient. Therefore, in a later chapter, we have derived another transformation, which achieves the same objective, and computationally is more efficient to implement. Furthermore, we also show that the complex time dependence in these TCFs is described by the dynamical evolution of an amplitude under the influence of a frequency operator. We have factored the amplitude of the total system into self-consistent primary and secondary region amplitudes and a time dependent phase factor. A TDSCF approximation for this purpose is derived such that norm conservation in the TDSCF approximation and a correct phase factor, essential requirements in our work, are also satisfied. The correct phase factor is required, because in computing the TCFs from the complex time amplitudes, the time-dependent phase factor does not get canceled. The norm conserving form for the factorization of the amplitude is essential, because the effective frequency operators, $\hat{\Omega}^p_{eff}(\tau)$ and $\hat{\Omega}^s_{eff}(\tau)$ which govern the dynamics of the self-consistent primary and secondary regions, respectively, are non-hermitian for all complex time $\tau > 0$. The main advantage of a TDSCF approximation, and the factorization of a multivariable dynamics into primary and secondary region dynamics, is the allowance of a self-consistent energy exchange between strongly coupled primary and secondary regions during the evolution.

Many intramolecular photointeraction processes in large systems are modeled by considering an arbitrary general motion in the primary region dynamics, strongly coupled to many harmonic degrees of freedom in the secondary region dynamics. The strong coupling between the primary and the secondary region dynamics is modeled by considering the terms in the coupling which are completely general in the variables of the primary region, and have a linear and bilinear dependence in

the variables of the secondary region. Weak coupling limit of this case, which is more suitable for intermolecular processes, is also considered by ignoring the terms in the coupling which are bilinear in the variables of the secondary region. For both of these cases, the solutions to the equations of motion for the secondary region dynamics are reduced to simple analytic forms. We have used these solutions for constructing the time-dependent couplings to the primary region dynamics, and also for constructing the propagators for the secondary region dynamics. The form of the time-dependent couplings are such that the self-consistent solution of the full problem is possible without going through many iterations at each step in time.

We have discussed a direct relationship between our TDSCF approach and the Generalized Langevin Equation (GLE) approach to the dynamics of large systems. An operator equation for the primary region dynamics, which contains a fluctuation force term and a memory term, is derived. We have shown that the fluctuation force term in this operator equation is dependent upon the initial conditions of the secondary region dynamics only through the expectation values of the secondary region operators. The fluctuation force term is therefore given a stochastic interpretation by observing that the initial values of these expectation values are described by a distribution function which depends upon the initial temperature of the system. If initially, at $t = 0$, the secondary region is brought to a thermal equilibrium in the presence of the primary region, then we can consider a displaced Boltzmann distribution function for the initial values of these expectation values, and explicitly derive a Fluctuation-Dissipation Relationship (FDR) between the fluctuation force and the memory kernel in our TDSCF approach. The use of the displaced Boltzman distribution function, instead of the usual Boltzman distribution function, is required to satisfy the central limit theorem for the fluctuation force at

$t = 0$, and also to facilitate a correct FDR between the ensemble averaged TCF of the fluctuation force and the memory kernel.

We have also discussed treatment of many degrees of freedom in the primary region, coupled linearly and bilinearly to many harmonic degrees of freedom in the secondary region. We have shown that for a few degrees of freedom in the primary region, it is possible to explicitly treat the primary region dynamics without further approximations.

Using a discretized coordinate space, we have developed an efficient path-integral method for the primary region dynamics that we have referred to as the Restricted Matrix Multiplication (RMM) method. The RMM method is based on the recently introduced numerical matrix multiplication (NMM) method [Thirumalai, Bruskin and Berne, 83], but avoids its problems, which include a quadratic scaling of the computational efforts with respect to any increase in the range, and the dimensionality of the potentials, and the inability to deal with time-dependent potentials. The efficient RMM method uses matrix multiplication between a complex time matrix corresponding to the propagator up to a certain time and a short complex time matrix corresponding to the short time propagator for the next step in time. Since, at each step in time, we are using the short time propagator for the previous step, it is easy to deal with the time-dependent potentials in the RMM method. The term restricted matrix multiplication refers to the fact that instead of using full matrices in the multiplication at any given step in time, we have used the property that the off-diagonal matrix elements in the complex time propagator decrease rapidly away from the diagonal, to find a suitable cut-off point. The contributions of the far off-diagonal matrix elements beyond this cut-off point, in the RMM method, are ignored without affecting the accuracies of the computations.

If M_c is the number of the off-diagonal terms to be retained in a RMM method, and $M \times M$ is the size of the full matrix, the number of the mathematical operations needed to perform a single RMM step is typically of the order of $\sim M \times M_c^2$ as opposed to the M^3 mathematical operations needed in a single NMM step. Therefore, the computational efforts for the RMM method do not scale quadratically with the increase in the range of the potential. We must mention that the RMM method for the primary region dynamics, which we have used in this work, is independent of any form of the potential in the primary region dynamics; therefore, it is capable of describing important quantum effects such as tunneling and barrier crossing in the primary region dynamics.

We have used a transformation from real to the complex time of the TCFs, so that the real part of the complex time always remains constant. We note that, for such a transformation, the contours of the complex time path-integral for the primary region dynamics, and that of the Fourier transform integral of the complex time TCFs, do not agree. Consequently, in this work, we would have needed information on many more points on the complex time grid, as compared to the situation, where these two contours would overlap. By deforming the contour of the Fourier transform path in the complex time plane, we have derived another transformation in which the contour of the Fourier transform integral and the contour of the numerical path integral method do agree.

We discuss in what follows our applications of our approach, and suggestions for further research.

a) Electronic Absorption Spectra of a Model Two-Potential Problem

The complex time computations of the TCF in a single spatial dimension were performed by using the complex time NMM method. The results of this computation on one hand provided a check of the accuracy of the numerical method for the primary region dynamics, to be attempted in the next application, and also a check of the convergence of the results of the RMM method to the results of the full NMM method. The physical and the computational parameters needed for modeling this problem were the same as those of Coalson [Coalson, 85]. It was found that the real and the imaginary parts of the TCF, and the resulting line shape function, computed from their Fourier transforms, agree very well with the results of Coalson. The real and the imaginary parts of the TCF obtained by using the RMM method, for which the overall computation time in the RMM method was reduced by a factor 12 as compared to the time used in the full NMM method, remained converged to within 10^{-6} of those of the full NMM method. The only instructive aspect of the dynamics that can be inferred from these results, is noted by observing a correlation between the recurrences in the intermediate and the long time behaviour of the TCF, and the appearance of the fine structures in the line shape functions. The structureless smooth line shape function is described primarily by the short time behaviour of the TCF, i.e the Fourier transform integral for this type of line shape function is obtained by truncating the TCF after its first decay. The highly oscillating line shape function is obtained by retaining in the Fourier transform integral the first recurrence in the TCF, while at the same time suppressing any further recurrences that may be present in the longer time behaviour. The appearance of higher order overtones in the line shape function is a confirmation of the presence of these further recurrences in the TCF.

b) Photodissociation of CH_3I from its Ground Vibrational State

Within a TDSCF approximation, we have factored the TCF for a realistic polyatomic system (CH_3I) into self-consistent primary and secondary region TCFs. We have used the efficient RMM method for the primary region dynamics, and have constructed the propagator for the secondary region dynamics analytically. The real time behaviour of the primary and secondary region amplitudes provide a useful insight into the complete dynamical evolution of the system. At $t = 0$ both of these amplitudes start out as simple gaussian function; as the positive real time, $t > 0$, increases the amplitudes start to move from their initial positions and also begin to change their shapes. The dynamics along the normal mode coordinate X, which is dominated by the dissociation variable R, is characterised by the fast oscillating motions of the primary region amplitude as it moves away from its initial position. The dynamics along the normal mode coordinate Y, which is dominated by the umbrella mode motion variable r, is characterised by very slow oscillatory motions of the secondary region amplitude as it also moves away from its initial position. The contrast between the fast oscillating motions of the primary region amplitude and the slow oscillating motions of the secondary region amplitude are reflected directly in the real time dependence of the primary and the secondary region TCFs. Comparing the real time behaviour of the total TCF with those of the primary and the secondary region TCFs, we note that the real time-dependence in the total TCF is described predominantly by the real time behaviour of the primary region TCF. The inclusion of the secondary region TCF and a time-dependent phase factor, as described in chapter 4, is required only to provide a modulation of the overall time-dependence so that the resultant Fourier transform of the total TCF produces the correct cross-section.

The theoretical results for the total cross-section of the photodissociation of CH_3I from its ground vibrational state are compared with those of Lee and Heller. The results of Lee and Heller [Lee and Heller, 82], which are obtained by using the same potential energy surfaces as are used in our work, are also verified by other quantum mechanical and semi-classical computations [Gray and Child, 84; Henrikson, 85; Stodden and Micha, 87]. Therefore, we can assume that for the given potential energy surfaces the results of Lee and Heller are reliable. We have found a close agreement of our total cross-section with those of Lee and Heller. Small discrepancies in the peak position, and in the full width at half maximum, can be attributed to our approximations: expanding the excited state potential in the secondary region variable Y to retain only the terms linear in Y, and using the SCF form for the initial nuclear vibrational state.

Comparing the time-dependence in the primary and the secondary region TCFs, we note that the vibrations in the primary region dynamics, dominated by the motions along the dissociation variable R, are much faster than the umbrella mode vibrations in the secondary region dynamics, so that there is a natural separation in the time scales of these two vibrations in the dissociating CH_3I. It is perhaps this separation in the time scales of these two vibrations that has played a significant role in a correct factorization of the full dynamics into a primary region dynamics along the dissociation variable R, and a secondary region dynamics along the umbrella mode vibration variable r.

Studying the detailed dynamics of the primary and the secondary region, we note that at $t = 0$ both the primary and the secondary region amplitudes start out as simple Gaussian functions, however, after a sufficiently long-time evolution the shapes of these amplitudes have been modulated so much that they are very

different from simple Gaussian functions. Any attempt, therefore, to represent these time evolved amplitudes with a single gaussian function is bound to give incorrect results. Some of the approximate quantum mechanical methods, which are based on the the Gaussian Wavepacket Dynamics (GWD) method and use a single gaussian wavepacket for the dynamics, have also reached the similar conclusions [Thirumalai, Bruskin and Berne, 85]. This problem is generally remedied by instead using a collection of Gaussian wavepackets, such that each of these wavepackets evolves under a different set of equations. However, for the long time dynamics of an extended molecular system, one may then need to follow the simultaneous evolution of such a large number of coupled Gaussian wavepackets that the whole computation may become impractical.

c) Photodissociation of CH_3I from Initially Excited Vibrational States

The computations of the cross-sections for the photodissociation dynamics of vibrationally excited CH_3I were attempted next. We note that the extension of the method to the complex time evolution of the primary and secondary region amplitudes, which are not simple Gaussian functions, is straightforward. Comparing the evolution of the primary and the secondary region amplitudes, for the initially excited $(1,0)$ and $(0,1)$ states of CH_3I, we again notice a contrast between the fast oscillations of the primary region amplitude and the slow oscillations of the secondary region amplitude. The nodal structure of the primary region amplitude in the $(1,0)$ case is reflected in the modulation of the fast oscillations in the corresponding total TCF, whereas the nodal structure of the secondary region amplitude in $(0,1)$ case causes a modulation only in the slow decay of the total TCF. The modulation of the fast oscillations in the total TCF of $(1,0)$ case are reflected in the appearance of an extra peak in the cross-section, whereas the modulations of

the slow decay of the total TCF in $(0,1)$ case appear merely as a shoulder structure in the cross-section. This is a further confirmation of our earlier stated conjecture that the shape and the position of the peak in the total cross-section is determined primarily by the primary region dynamics, whereas the inclusion of the secondary region dynamics causes only a modulation in the shape of the peak so as to provide an overall correct cross-section.

At present, there are no fully quantum mechanical computations of the photodissociation dynamics of CH_3I from initially excited vibrational states. The general features of our cross-sections in the vibrationally excited $(1,0)$ and $(0,1)$ cases, are reported also by two other semi-classical computations [Sundeberg et al., 86; Swaminathan, Stodden and Micha, 88]. However, we further note that, while both the semi-classical computations have correctly reported two asymmetric peaks in the cross-section for the $(1,0)$ case and a single asymmetric peak in the cross-section for $(0,1)$, we could provide further insight on the contrasting nature of the dynamics along the dissociation variable R and the umbrella mode motion variable r by following their time-evolution.

A detailed study of the photodissociation dynamics of CH_3I from the other vibrationally excited initial states was attempted next. We fixed the number of vibrational quantum in the secondary region dynamics, and studied the effect of increasing the vibrational excitation energy in the primary region dynamics. We have found that for each additional vibrational excitation in the primary region dynamics, there is an additional peak in the cross section. The heights of these additional peaks are not uniform; the heights of the peaks in the high energy region of the cross section, determined primarily by the short-time behaviour of the TCF, are generally larger than the heights of the peaks in the low energy region,

determined mainly by the intermediate and the long time behaviour of the TCF. This confirms that the total cross-section of the photodissociation of CH_3I, which is a direct process on a smoothly repulsive potential energy surface, is determined primarily by the short time dynamics in the Frank Condon region.

As we put more and more vibrational excitation energy in the primary region dynamics, we note a modulation in the height of the peak corresponding to the secondary region dynamics. This means, that some of the extra vibrational energy given to the primary region dynamics has also been transferred to the secondary region dynamics. A reverse of this vibrational energy exchange, from the primary region dynamics to the secondary region dynamics, was also observed by fixing the vibrational quantum excitations in the primary region dynamics and varying the excitation energy in the secondary region dynamics.

The cross-sections for the photodissociation of CH_3I from the other vibrationally excited initial states, have not been verified by any other theoretical computation or experimental observation. However, since the self-consistent dynamics in our TDSCF approximation method does not depend upon the shapes of the primary and the secondary region amplitudes, we expect that the cross-sections for these other vibrationally excited states of CH_3I, as reported in this work, are generally correct, and confirm the allowance of a self-consistent energy exchange between the primary and the secondary region dynamics.

d) Suggestions For Further Research

Some extensions and applications of the TDSCF approximation method, as developed and presented in this work, are straightforward. Simple examples along these lines would be applications to the photodissociation dynamics of CD_3I and

CF_3I. In the case of CD_3I one can easily study the effect of isotopic mass variations on the photodissociation, while in CF_3I one has to incorporate the C-F stretch mode vibrations besides the umbrella mode vibration [Van Veen et al., 85]. Within a TDSCF approximation, the umbrella mode vibrations and the C-F stretch mode vibrations will constitute the two-mode dynamics of the secondary region, whereas the translational motion I* along the dissociation variable will be treated as the primary region dynamics. Since the experimentally parametrized potential energy surfaces for both of these cases are already reported in the literature, the study of the photodissociation dynamics of CD_3I and CF_3I using the TDSCF approximation method should be easy.

Application to molecular systems in which there are more than one degree of freedom in the primary region dynamics could also be contemplated. The most straightforward example in this case would be the TDSCF treatment of CH_3I, without expanding the coupling in the excited state potential (as was done in this work). The arbitrary general motions along the normal mode coordinates X and Y, would constitute two degrees of freedom in the primary region.

An important aspect of our TDSCF approach is the ability of the numerical method to deal with any form of the potential in the primary region dynamics. A possibility would hence be an application in which the ability of the method to deal with explicit quantum effects, such as tunneling and barrier crossing in the primary region dynamics, is tested. A recently available example for comparison, for which the parameters for the potential energy surfaces and the results of a quantum mechanical close-coupling (CC) computation are listed in the literature, is the photofragmentation dynamics of CH_3NO_2 [Pernot et al., 87]. In this test case, the dissociation along the C-N axis in the excited electronic state is hindered by the

presence of a barrier along this coordinate, and the primary region motion along the dissociation variable is coupled to the harmonic internal motions of the NO_2 fragment, which would constitute the secondary region of the system.

The use of our approach for the long time evolution of the amplitudes could be contemplated. The results for the long time dynamics could be used to study state-to-state cross sections for the photodissociation of CH_3I from its ground and excited vibrational states.

The development of the formalism, as presented in this work, considers dynamical evolution of the system only on a single potential energy surface, i.e, we have not considered the situation in which more than one potential energy surface is responsible for the dynamics of the system [Stodden and Micha, 87; Coalson 88]. If there are more than two electronic potential energy surfaces in the formalism, so that the evolution of the amplitudes on any one of these potential energy surfaces is also coupled to the other by the presence of a non-radiative potential coupling between the two surfaces, the frequency operator for the dynamics of this coupled excited surface problem is written in a matrix form as

$$\widetilde{\Omega} = \begin{pmatrix} \hat{\Omega}_{11} & \hat{\Omega}_{12} \\ \hat{\Omega}_{21} & \hat{\Omega}_{22} \end{pmatrix} \tag{8.1}$$

where $\hat{\Omega}_{11}$ and $\hat{\Omega}_{22}$ are the uncoupled frequency operators for the uncoupled dynamics on the two potential energy surfaces, and $\hat{\Omega}_{12} = \hat{\Omega}_{21}^{\dagger}$ is the coupling operator between the two. A zeroth order evolution of the amplitudes on the two potential energy surfaces, by ignoring the coupling between the two, can still be performed through our TDSCF approximation method. A perturbative inclusion of the coupling frequency operators $\hat{\Omega}_{12}$ and $\hat{\Omega}_{21}$ in the formalism, causing a mixing

of amplitudes during the dynamics, could also be attempted in future work.

Another interesting area of extension of the formalism would be the inclusion of anharmonic degrees of freedom in the secondary region dynamics. To our knowledge, none of the mean field methods developed so far try to include anharmonicity in the normal mode vibrations of the secondary region dynamics. Our treatment could be related to previous work [Vilallonga and Micha, 87] on effects of anharmonicity on atom-polyatomic energy transfer. This would provide additional flexibility in the definition of the primary and secondary regions.

Lastly, we must note that in this work we have mainly focussed on the dynamics of polyatomic systems, therefore, we have used the TDSCF approximation for factoring the normal mode space of the system into primary and secondary regions. Since the general approach, as presented in this work, is not restricted only to the normal mode motions, a possibility would be to apply the method to the dynamics in condensed media, where the dynamics of many interacting quasi particles could be separated into primary and secondary regions, and a numerical method could be developed for the exact dynamics in the primary region.

APPENDIX A
SECOND ORDER TRANSITION RATES

The radiation field polarizability tensor TCF for all second order processes is written as

$$f_{\eta'\zeta'\eta\zeta}^{R}\left(u,u',t\right) = \left\langle\left\langle \hat{\phi}_{\eta'\zeta'}\left(u',t\right)^{\dagger} \hat{\phi}_{\eta\zeta}\left(u,0\right)\right\rangle\right\rangle_{R} \quad . \qquad (A.1)$$

The electric field polarizability tensor operator $\hat{\phi}_{\eta\zeta}(u,0)$, as given in Eq.(2.15), can be expanded as

$$\hat{\phi}_{\eta\zeta}\left(u,0\right) = \hat{\phi}_{\eta\zeta}^{++}\left(u,0\right) + \hat{\phi}_{\eta\zeta}^{+-}\left(u,0\right) + \hat{\phi}_{\eta\zeta}^{-+}\left(u,0\right) + \hat{\phi}_{\eta\zeta}^{--}\left(u,0\right) \qquad (A.2)$$

where for example

$$\hat{\phi}_{\eta\zeta}^{+-}\left(u,0\right) = \hat{E}_{\eta}^{(+)} \frac{\hat{M}_R}{\hat{M}_R^2 - \hbar^2 u^2} \hat{E}_{\eta}^{(-)} \qquad , \qquad (A.3)$$

the operator $\hat{M}_R$ is as defined in chapter 2, and we have used $\hat{E}_{\eta} = \hat{E}_{\eta}^{(+)} + \hat{E}_{\eta}^{(-)}$. Using Eq.(A.2) in Eq.(A.1) the polarizability tensor TCF, in the photon number representation, is written as

$$f_{\eta'\zeta'\eta\zeta}^{R}\left(u,u',t\right) = \left\langle\left\langle \hat{\phi}_{\eta'\zeta'}^{++}\left(u',t\right)^{\dagger} \hat{\phi}_{\eta\zeta}^{++}\left(u,0\right)\right\rangle\right\rangle_{R} + \left\langle\left\langle \hat{\phi}_{\eta'\zeta'}^{+-}\left(u',t\right)^{\dagger} \hat{\phi}_{\eta\zeta}^{+-}\left(u,0\right)\right\rangle\right\rangle_{R}$$
$$+ \left\langle\left\langle \hat{\phi}_{\eta'\zeta'}^{-+}\left(u',t\right)^{\dagger} \hat{\phi}_{\eta\zeta}^{-+}\left(u,0\right)\right\rangle\right\rangle_{R} + \left\langle\left\langle \hat{\phi}_{\eta'\zeta'}^{--}\left(u',t\right)^{\dagger} \hat{\phi}_{\eta\zeta}^{--}\left(u,0\right)\right\rangle\right\rangle_{R}$$
$$(A.4)$$

The first term in Eq.(A.4) correspond to two photon absorption, the second to the fluorescent processes, the third to elastic and Raman scatterings, and the fourth is for spontaneous and stimulated emission of two photons. Other cross-terms do not contribute because they do not conserve the number of photons.

For example, we can use the third term in Eq.(A.4) to write the polarization tensor TCF of the light source, for Raman scattering processes, as

$$f_{\eta'\zeta'\eta\zeta}^{Raman}\left(u,u',t\right) = \left\langle\left\langle \hat{\phi}_{\eta'\zeta'}^{-+}\left(u',t\right)^{\dagger}\hat{\phi}_{\eta\zeta}^{-+}\left(u,0\right)\right\rangle\right\rangle_R \qquad (A.5)$$

Using Eqs.(2.18–2.20) it is not difficult to expand the TCF in Eq.(A.5) as

$$f_{\eta'\zeta'\eta\zeta}^{Raman}\left(u,u',t\right) = \left(\frac{\hbar}{2\epsilon_0 V}\right)\delta_{\zeta'\zeta}\sum_s W_s N_s \delta_{\zeta,\zeta'}\sum_{\vec{k}_\eta}\delta_{\eta'\eta}\omega_{\vec{k}_\eta}\omega_{\vec{k}_s}\hat{\epsilon}_\eta^2\hat{\epsilon}_{\zeta_s}^2$$
$$e^{-i\left(\omega_{\vec{k}_s}-\omega_{\vec{k}_\eta}\right)t}\frac{\left(\hbar\omega_{\vec{k}_s}-i\epsilon^R\right)}{\left[\left(\hbar\omega_{\vec{k}_s}-i\epsilon^R\right)^2-\hbar^2 u'^2\right]} \qquad (A.6)$$
$$\frac{\left(\hbar\omega_{\vec{k}_s}+i\epsilon^R\right)}{\left[\left(\hbar\omega_{\vec{k}_s}+i\epsilon^R\right)^2-\hbar^2 u^2\right]}$$

where W_s is the statistical distribution of N_s photons in a mode $s=(\vec{k}_s,\hat{\epsilon}_{\zeta_s})$ with energy $\hbar\omega_{\vec{k}_s}$. The transition rate for a general Raman scattering process in the time domain description, obtained by using Eq.(A.6) in Eq.(2.27) and analytically evaluating the integrals over u and u', is written as

$$R^{Raman} = \left(\frac{\hbar}{2\epsilon_0 V}\right)\sum_s W_s N_s \sum_{\vec{k}_\eta\eta}\omega_{\vec{k}_\eta}\omega_{\vec{k}_s}\hat{\epsilon}_\eta^2\hat{\epsilon}_{\zeta_s}^2$$
$$\int_{-\infty}^{+\infty}dt\, e^{+i\left(\omega_{\vec{k}_\eta}-\omega_{\vec{k}_s}\right)t}\left\langle\left\langle \hat{X}_{\eta\zeta_s}\left(t\right)^{\dagger}\hat{X}_{\eta\zeta_s}\left(0\right)\right\rangle\right\rangle_M \qquad (A.7)$$

where

$$\hat{X}_{\eta\zeta_s}(0) = \hat{D}_\eta \frac{1}{E^M + \hbar\omega_{\vec{k}_s} + i\epsilon - \hat{H}_M} \hat{D}_{\zeta_s} \qquad (A.8)$$

is the molecular polarizability tensor operator for the target molecule, and the time dependence in this operator is solely governed by the Hamiltonian of the target, i.e

$$\hat{X}_{\eta\zeta_s}(t) = e^{-\frac{i}{\hbar}\hat{H}_M t} \hat{X}_{\eta\zeta_s}(0) \; e^{+\frac{i}{\hbar}\hat{H}_M t} \qquad . \qquad (A.9)$$

APPENDIX B
NUMERICAL ANALYTIC CONTINUATION

The problem considered here is the numerical analytic continuation of a function $f(x)$, given the values of the function at the K points $x_i (i = 1, 2...K)$. One well known technique of numerical analytic continuation by rational fractions is the Pade approximant method, the use of which, however, requires the coefficients of the Taylor series expansion of $f(x)$. The Schlessinger's point method [Schlessinger, 68], similar in spirit to the Pade approximant method, is instead based on the representation of $f(x)$ by rational fractions, and uses only the values of the function at a given set of points.

The point method is based on the representation of the function at a given set of points by

$$f(x_i) = \frac{P_N(x_i)}{Q_M(x_i)} \quad , \quad i = 1....N + M + 1 \quad (B.1)$$

where

$$P_N(x) = \sum_{k=0}^{N} p_k x^k$$
$$Q_M(x) = \sum_{k=0}^{M} q_k x^k \quad (B.2)$$

Rearranging Eq.(B.1) one obtains a set of $N + M + 1$ linear equations for $N + M + 1$ unknown p's and q's.

155

A more efficient way to effect the point type of representation is obtained by using continued fractions. To do this, consider the continued fraction

$$C_N(x) = \cfrac{f(x_1)}{1 + \cfrac{a_1(x - x_1)}{1 + \cfrac{a_2(x - x_2)}{1 + ... \cfrac{}{\cfrac{a_N(x - x_N)}{1}}}}} \qquad (B.3)$$

It is easy to see that $C_N(x_1) = f(x_1)$ and that the coefficients $a_1...a_N$ can be chosen so that $C_N(x_i) = f(x_i)$. The coefficients a_j in Eq.(B.3) are determined recursively from the formula

$$a_j = \frac{1}{(x_j - x_{j+1})}\{1 + \cfrac{a_{j-1}(x_{j+1} - x_{j-1})}{1 + \cfrac{a_{j-2}(x_{j+1} - x_{j-2})}{1 + ...}}$$

$$... + \cfrac{a_j(x_{j+1} - x_j)}{1 - \frac{f(x_1)}{f(x_{j+1})}} \; \} \qquad (B.4)$$

with

$$a_1 = \frac{\{[f(x_1)/f(x_2)] - 1\}}{(x_2 - x_1)} \qquad . \qquad (B.5)$$

APPENDIX C
SCF EIGENVALUES and EIGENFUNCTIONS

```
     SCF coefficients for (0,0)
        CP                    CS
0.9967284059640        0.99992129098795
8.0792096484369D-02   -1.23386486695677D-02
3.19934884824560-03   -2.27367045806380-03
                       ES                            EPS
5.2675109285449D-03    6.7930625343156D-03      -4.0169340561566D-03
     E(0,0)   =        8.043639406704DD-03
     SCF coefficients for (1,0)
        CP                    CS
8.2039108543589D-02    0.99975548326356
-0.97791519095421     -2.2085185913337D-02
-0.1922276358132B     -1.1037425480124D-03
        EP                    ES                            EPS
1.0195151579200D-02    9.0966254686394D-03      -6.3278156489762D-03
     E(1,0)   =        1.2963961398863D-02
     SCF coefficients for (0,1)
        CP                    CS
0.9929426572004       -1.5912198657396D-02
0.11822018162167      -0.99944224407830
9.4303067565885D-03    2.935988224795 3D-02
        EP                    ES                            EPS
1.0860245523785D-02    1.7891976191543D-02      -9.6124749139322D-03
     E(0,1)   =        1.9139746801395D-02
     SCF Coefficients for (1,1)
        CP                    CS
0.11876956673886      -2.3940237480153D-02
-0.96472325967676     -0.99887928B2731
-0.23495280857082      4.0617369098342D-02
        EP                    ES                            EPS
1.5746576488681D-02    2.0095421757910D-02      -1.1809400069577D-02
     E(1,1)   =        2.4032598177014D-02
     SCF Coefficients for (3,0)
        CP                    CS
1.5798871824954D-02   -0.99967786508303
-2.4974466984030D-02   2.5334180493168D-02
0.32261114169622       9.2643352437270D-04
-0.84782678341756      1.2176546302277D-03
-0.41980765622034     -6.6331753138563D-05
        EP                    ES                            EPS
1.999843107151 6D-02   1.2851509975508D-02      -1.0083628506251D-02
     E(3,0)   =        2.2766312540772D-02
     SCF Coefficients for (2,1)
        CP                    CS
-1.1431394075059D-02  -3.5129412140848D-02
0.25203921154663      -0.99779421024850
-0.88546300889190      5.6238813365018D-02
-0.38277108867786     -1.7967262680218D-03
-7.6075806932522D-02   2.5702224089621D-03
        EP                    ES                            EPS
2.0595041286636D-02    2.2432566310398D-02      -1.4160855518207D-02
     E(2,1)   =        2.8866752078828D-02
     SCF Coefficients for (2,0)
        CP                    CS
-5.1220220292604D-03  -0.99946258622104
0.20241294293276       3.2753284133340-02
-0.91948962493189     -3.9948251330055D-02
-0.33269077247215      1.2641843950966D-03
-5.3464427221515D-02  -8.3811681449883D-05
        EP                    ES                            EPS
1.5073114711977D-02    1.1447526160939D-02      -8.6877554924933D-03
     E(2,0)   =        1.7832885380423D-02
```

157

SCF Coefficients for (3,1)

CP	CS	
1.6390661983180D-02	-2.1545029807526D-02	
-3.9397996996330D-02	-0.99906974566358	
0.37178544438281	3.7208893384953D-02	
-0.81036971037964	2.2905899813564D-03	
-0.45083868294623	2.3888157958995D-03	
EP	ES	EPS
2.5530802219188D-02	2.3743167197191D-02	-1.5429970336933D-02
E(3,1) =	3.3843999079446D-02	

SCF coefficients for (0,2)

CP	CS	
-0.98732804812872	-1.8056661051899D-03	
-0.15586673870250	-3.4519753651433D-02	
-2.1948138441787D-02	-0.99811648229037	
-1.9366257119792D-02	5.0628486759489D-02	
-5.6667846867243D-03	2.3172320095829D-03	
EP	ES	EPS
1.6366745947212D-02	2.8999861818118D-02	-1.5151036605712D-02
E(0,2) =	3.0215571159619D-02	

SCF Coefficients for (0,3)

CP	CS	
-0.98043470108244	-1.3363921202065D-03	
-0.19275011449047	-2.8461322257134D-03	
-3.2853518085547D-02	-5.6885781988173D-02	
-2.1557264133552D-02	-0.9955246063534	
-7.1498943887409D-03	7.5397423443674D-02	
EP	ES	EPS
2.1922499352493D-02	4.0074902404277D-02	-2.0715945310681D-02
E(0,3) =	4.1281456446089D-02	

SCF coefficients for (1,2)

CP	CS	
0.15908194189023	-1.1438528709273D-03	
-0.93866044635406	-5.0603770102181D-02	
-0.29658955223327	-0.99625581324658	
-6.3944553417524D-02	7.0067409031740D-02	
-3.9436427959584D-02	-1.6919858235142D-03	
EP	ES	EPS
2.1239326215826D-02	3.1422980867415D-02	-1.7615703830078D-02
E(1,2) =	3.5046603253163D-02	

SCF coefficients for (1,3)

CP	CS	
0.19493681408523	-1.2880436744038D-03	
-0.91499001974979	-1.9539643892144D-03	
-0.34015682865364	-7.5989741313275D-02	
-8.4662836984030D-02	-0.99243908846012	
-4.3799997756808D-02	9.6357344703184D-02	
EP	ES	EPS
2.6642806097533D-02	4.2465049624273D-02	-2.3030333210761D-02
E(1,3) =	4.6077522511044D-02	

SCF Coefficients for (4,0)

CP	CS	
6.4410500860338D-03	-0.99790811482856	
-3.6266392096938D-02	-6.3779166082072D-02	
8.1150950654262D-02	1.0233873792702D-02	
-0.39563982745886	2.6226699935523D-03	
0.91407161197266	4.1981867102966D-05	
EP	ES	EPS
2.6825547377424D-02	1.9641598824394D-02	-1.6778493534479D-02
E(4,0) =	2.9688652667339D-02	

BIBILIOGRAPHY

P. M. Agrawal and L. M. Raff, J. Chem. Phys. 1982, **77**, 3946.

G. G. Balint-Kurti, Adv. Chem. Phys. 1975, **30**, 137.

G. G. Balint-Kurti and M. Shapiro, J. Chem. Phys. 1981, **61**, 137.

E. C. Behrman, G. A. Jongeward and P. G. Wolynes, J. Chem. Phys. 1983, **79**, 6277.

B. J. Berne, *Physical Chemistry, an advanced treatise.*, 1971, **8B.** ed. by D. Henderson, (Academic, New York).

P. H. Berens and K. R. Wilson, J Chem. Phys. 1981, **74**, 4872.

G. G. Billing and G. Jolicard, J. Phys. Chem. 1984, **88**, 1820.

J. M. Bowman, Acc. Chem. Res. 1986, **19**, 202.

J. Chang and W. H. Miller, J. Chem. Phys. 1987, **87**, 1684.

R. D. Coalson, Adv. Chem. Phys. 1988, submitted.

R. D. Coalson, J. Chem. Phys. 1985, **83** 688.

R. D. Coalson, J. Chem. Phys. 1987, **86**, 6823.

R. D. Coalson, D. L. Freeman and J. D. Doll, J. Chem. Phys. 1986, **85**, 4567.

P. A. M. Dirac, Proc. R. Soc. London 1926, **A 112**, 673.

P. A. M. Dirac, Proc. R. Soc. London 1927, **114**, 710.

P. A. M. Dirac, Proc. Cambridge. Phil. Soc. 1930, **26**, 376.

P. A. M. Dirac, *The Principles of Quantum Mechanics*, 3rd ed. 1947, (Clarendon Press, Oxford).

J. D. Doll, J. Chem. Phys. 1984, **81**, 3536.

J. D. Doll, R. D. Coalson and D. L. Freeman, J. Chem. Phys. 1987, **87**, 1641.

M. D. Feit, J. A. Fleck, Jr. and A. J. Steiger, J. Comput. Phys. 1982, **47**, 412.

159

R. P. Feynman and A. R. Hibbs, *Quantum Mechanics and Path Integrals*, 1965 (McGraw-Hill, New York).

D. Forster, *Hydrodynamic Fluctuations, Broken Symmetry, and Correlation Functions*, 1975 (The Benjamin/Cummings Pub. Co., Reading, Massachusetts).

J. Frenkel, *Wave Mechanics*, 1934 (Clarendon Press, Oxford).

R. B. Gerber, V. Buch and M. A. Ratner, J. Chem. Phys. 1982, **77**, 3022.

S. K. Gray and M. S. Child, Mol. Phys. 1984, **51**, 189.

R. W. Heather and J. C. Light, J. Chem. Phys. 1983, **78**, 5513.

W. Heitler, *The Quantum Theory of Radiation*, 3rd ed., 1954 (Clarendon Press, Oxford).

E. J. Heller, J. Chem. Phys. 1975, **62**, 1544.

E. J. Heller, Acc. Chem. Res. 1981, **14**, 386.

B. Hellsing, A. Nitzan and H. Metiu, Chem. Phys. Lett. 1986, **123**, 523.

N. E. Henriksen, Chem. Phys. Lett. 1985, **121**, 139.

G. Herzberg, *Molecular Spectra and Molecular Structure Vol.1*, 2nd ed. 1950 (Van Nostrand, Princeton).

B. Jackson and H. Metiu, J. Chem. Phys. 1985, **82**, 5707; ibid **83**, 1952.

J. R. Klauder and E. C. G. Sudarshan, *Fundamentals of Quantum Optics*, 1968 (Benjamin, New York).

D. Kosloff and R. J. Kosloff, J. Comput. Phys. 1983, **52**, 35.

R. J. Kosloff, J. Phys. Chem. 1988, **92**, 2087.

H. A. Kramers and W. Heisenberg, Z. Phys. 1925, **31**, 681.

J. Kugar, M. D. Meyer and l. S. Cederbaum, Chem. Phys. Lett. 1987, **140**, 525.

P. W. Langhoff, S. T. Epstein and M. Karplus, Rev. Mod. Phys. 1972, **44**, 602.

S. Y. Lee and E. J. Heller, J. Chem. Phys. 1979, **71**, 4777.

S. Y. Lee and E. J. Heller, J. Chem. Phys. 1982, **76**, 3035.

K. Lindenberg and V. Seshadri, Physica A 1982, **109**, 483.

R. Loudon, *The Quantum Theory of Light*, 2nd ed., 1983 (Clarendon Press, Oxford), Chaps. 3, 5, and 7.

W. H. Louisell, *Quantum Statistical Properties of Radiation*, 1973 (Wiley, New York), pp. 296–303.

S. W. Lovesey, *Condensed Matter Physics Dynamic Correlations*, 1980 (Benjamin/Cummings, Reading, Massachusetts).

N. Makri and W. H. Miller, J. Chem. Phys. 1987, **87**, 5781.

R. A. Marcus, J. Chem. Phys. 1972, **56**, 311; ibid, 3548.

A. D. McLachlan, Mol. Phys. 1964, **8**, 39.

D. A. McQuarrie, *Statistical Mechanics*, 1976 (Harper and Row, New York).

D. A. McQuarrie, *Quantum Chemistry*, 1983 (University Science Books, Mill Valley, California).

A. Messiah, *Quantum Mechanics*, 1962 (North-Holland, Amsterdam) Vols.1, 2.

D. A. Micha, Chem. Phys. Lett. 1977, **46**, 188.

D. A. Micha, J. Chem. Phys. 1979, **70**, 565–570, 3165–3170.

D. A. Micha, Int. J. Quantum. Chem. 1981, **S15**, 643.

D. A. Micha, Int. J. Quantum Chem. 1983, **23**, 551.

D. A. Micha, Int. J. Quantum. Chem. 1986, **S19**, 443.

D. A. Micha and Z. Parra, J. Phys. Chem. 1988, **92**, 3236.

W. H. Miller, Adv. Chem. Phys. 1974, **25**, 69.

W. H. Miller, S. D. Schwartz and J. W. Tromp, J. Chem. Phys. 1983, **79**, 4889.

H. Mori, Prog. Theor. Phys. 1965, 34, 399.

R. C. Mowrey and D. Kouri, Chem. Phys. Lett. 1985, **119**, 289.

S. Mukamel, S. Abe, Y. J. Yan and R. Islampour, J. Phys. Chem. 1985, **89**, 201.

S. Mukamel and J. Jortner, J. Chem. Phys. 1976, **65**, 3735.

J. A. Olson and D. A. Micha, Int. J. Quantum Chem. 1982, **22**, 971.

P. Pernot, O. Atabek, J. A. Beswick and Ph. Millie', J. Phys. Chem. 1987, **91**, 1397.

J. R. Reimers, K. R. Wilson and E. J. Heller, J. Chem. Phys. 1983, **79**, 4749.

M. Sargent, 3rd., M. O. Scully and W. E. Lamb, Jr., *Laser Physics*, 1974 (Addison-Wesley, Reading, Massachusetts), Chaps. 7, 9, 15, and 18.

S. Sawada and H. Metiu, J. Chem. Phys. 1986, **84**, 6293.

G. C. Schatz, Chem. Phys. 1977, **24**, 263.

L. Schlessinger, Phys. Rev. 1968, **167**, 1411.

M. Schubert and B. Wilhelmi, *Nonlinear Optics and Quantum Electronics*, 1986 (Wiley, New York).

L. S. Schulman, *Techniques and Applications of Path Integration*, 1981 (Wiley, New York).

M. Shapiro and R. Bersohn, J. Chem. Phys. 1980, **73**, 3810.

D. Srivastava and D. A. Micha, Int. J. Quantum Chem. 1987, **S21**, 229.

C. D. Stodden and D. A. Micha, Int. J. Quantum. Chem. 1987, **S21**, 2239.

R. L. Sundberg, D. Imre, M. O. Hale, J. L. Kinsey and R. D. Coalson, J. Am. Chem. Soc. 1986, **90** 5001.

P. K. Swaminathan, C. D. Stodden and D. A. Micha, J. Chem. Phys. 1988, submitted.

D. Thirumalai and B. J. Berne, J. Chem. Phys. 1983, **79**, 5029.

D. Thirumalai and B. J. Berne, J. Chem. Phys. 1984, **81**, 2512.

D. Thirumalai and B. J. Berne, Chem. Phys. Lett. 1985, **116**, 471.

D. Thirumalai, E. J. Bruskin and B. J. Berne, J. Chem. Phys. 1983, **79**, 5063.

D. Thirumalai, E. J. Bruskin and B. J. Berne, J. Chem. Phys. 1985, **83**, 230.

L. Van Hove, Phys. Rev. 1954, **95**, 249.

G. N. A. Van Veen, T. Baller, A. E. DE Vries and M. Shapiro, Chem. Phys. 1985, **93**, 277.

E. Vilallonga and D. A. Micha, J. Chem. Phys. 1987, **86**, 759.

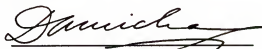K. Yamashita and W. H. Miller, J. Chem. Phys. 1985, **82**, 5475.

R. Zwanzig, J. Stat. Phys. 1973, **9**, 215.

BIOGRAPHICAL SKETCH

Deepak Srivastava was born on July 22, 1957, in Lucknow, India. All of his early education took place in Lucknow. In the Fall of 1977 he completed his undergraduate education in physics and received a B.Sc (Hons.) degree from Lucknow University. The same year he joined Delhi University at New Delhi, India, and began his graduate education. In the Fall of 1980 he graduated from Delhi University with a Master of Philosophy (M.Phil) degree in ionospheric physics.
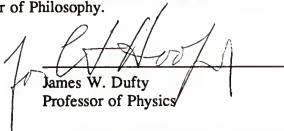
In the Fall of 1981 he came to the USA, and enrolled in the Department of Physics at the University of Florida for further studies. After a successful completion of the qualifying examination for the admission to the Ph.D program in the Fall 1983, he joined the Quantum Theory Project in the spring of 1984, and began research for his doctoral thesis.

I certify that I have read this study and in my openion it conforms to acceptable standards of scholarly presentation and is fully adequate, in scope and quality, as a dissertation for the degree of Doctor of Philosophy.
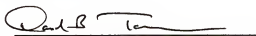
David A. Micha, Chairman
Professor of Chemistry and Physics

I certify that I have read this study and in my opinion it conforms to acceptable standards of scholarly presentation and is fully adequate, in scope and quality, as a dissertation for the degree of Doctor of Philosophy.
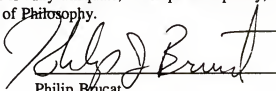
James W. Dufty
Professor of Physics

I certify that I have read this study and in my opinion it conforms to acceptable standards of scholarly presentation and is fully adequate, in scope and quality, as a dissertation for the degree of Doctor of Philosophy.
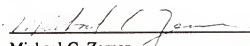
David B. Tanner
Professor of Physics

I certify that I have read this study and in my opinion it conforms to acceptable standards of scholarly presentation and is fully adequate, in scope and quality, as a dissertation for the degree of Doctor of Philosophy.

Philip Brucat
Assistant Professor of Chemistry

I certify that I have read this study and in my opinion it conforms to acceptable standards of scholarly presentation and is fully adequate, in scope and quality, as a dissertation for the degree of Doctor of Philosophy.

Michael C. Zerner
Professor of Chemistry

This dissertation was submitted to the Graduate Faculty of the Department of Physics in the Collage of Liberal Arts and Sciences and to the Graduate School and was accepted as partial fulfillment of the requirements for the degree of Doctor of Philosophy.

December 1988

Dean, Graduate School